

Sliding Mesh Applications Using the LAVA Curvilinear Solver

Luis S. Fernandes, M.Sc.

&

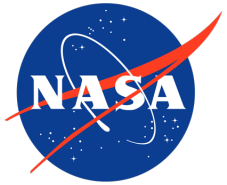
Ercan Dumlupinar, Ph.D.

Computational Aerosciences Branch, NASA Ames Research Center, Moffett Field, CA

Advanced Modeling & Simulation (AMS) Seminar Series

NASA Ames Research Center, June 29th, 2023

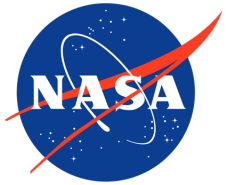
Motivation



Problem

- Dynamic overset meshing, commonly used for simulations involving rotating equipment in propulsion systems, can be computationally demanding due to the frequent requirement of hole-cutting and updating connectivity between different parts of the grid system. These operations can significantly increase the computational cost of such simulations.

Motivation



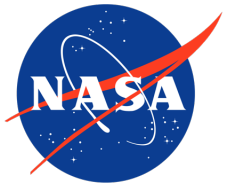
Problem

- Dynamic overset meshing, commonly used for simulations involving rotating equipment in propulsion systems, can be computationally demanding due to the frequent requirement of hole-cutting and updating connectivity between different parts of the grid system. These operations can significantly increase the computational cost of such simulations.

Challenge

- The objective is to investigate the aerodynamic and aeroacoustic behavior of the NASA Source Diagnostic Test (SDT) model fan, as well as the Contra-Rotating Open Rotor (CROR) system. The goal is to conduct these analyses efficiently and in a manner that allows for detailed parametric studies.

Motivation



Problem

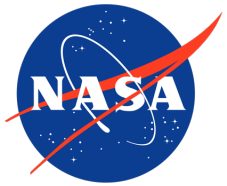
- Dynamic overset meshing, commonly used for simulations involving rotating equipment in propulsion systems, can be computationally demanding due to the frequent requirement of hole-cutting and updating connectivity between different parts of the grid system. These operations can significantly increase the computational cost of such simulations.

Challenge

- The objective is to investigate the aerodynamic and aeroacoustic behavior of the NASA Source Diagnostic Test (SDT) model fan, as well as the Contra-Rotating Open Rotor (CROR) system. The goal is to conduct these analyses efficiently and in a manner that allows for detailed parametric studies.

Approach

- Both of the aforementioned problems exhibit constant rotational mesh motion, which makes them highly compatible with the sliding mesh approach. This approach is commonly employed in the simulation of rotating machinery, given its ability to handle such motion effectively. Therefore, the sliding mesh approach was implemented in the LAVA Curvilinear solver and validated using well-recognized experimental data.



NASA Source Diagnostic Test

Fan Noise Predictions of the NASA Source Diagnostic Test using Unsteady Simulations with LAVA Part I: Near-Field Aerodynamics and Turbulence

Luis S Fernandes, Jeffrey A Housman, Gaetan K Kenway, Gerrit-Daniel Stich, Cetin C Kiris

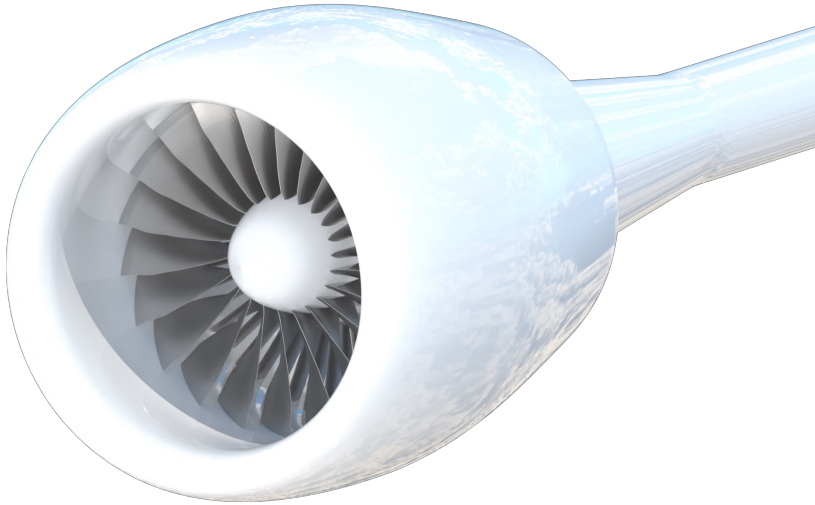
doi.org/10.2514/6.2023-0793

Speaker: Luis S. Fernandes

Introduction

- Trends in commercial aviation turbofan efficiency still favor the development of **ultra-high bypass ratio turbofan engines** as a near-term solution to tackle low-noise demands in urban traffic areas

- This leads to **higher fan-to-jet noise ratios during take-off and approach**, motivating work towards characterizing the noise signature of rotating fan rigs
  - ➢ Turbomachinery applications
  - ➢ Fan noise predictions

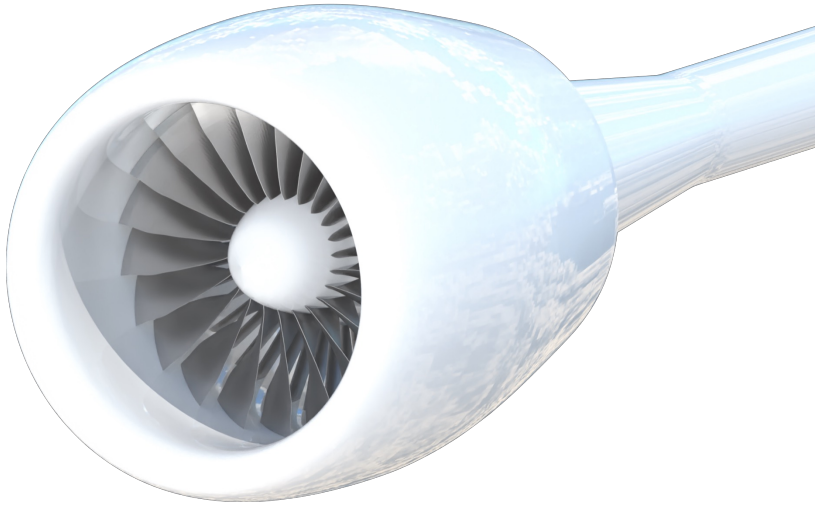


Render of NASA SDT baseline geometry

Introduction

- Trends in commercial aviation turbofan efficiency still favor the development of **ultra-high bypass ratio turbofan engines** as a near-term solution to tackle low-noise demands in urban traffic areas

- This leads to **higher fan-to-jet noise ratios during take-off and approach**, motivating work towards characterizing the noise signature of rotating fan rigs
  - ➢ Turbomachinery applications
  - ➢ Fan noise predictions



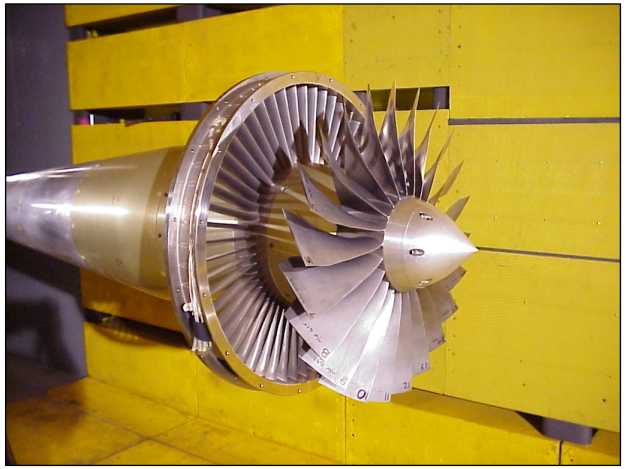
Render of NASA SDT baseline geometry

Goals

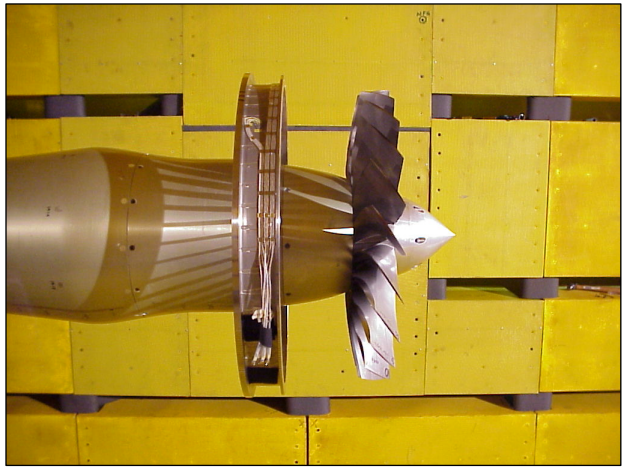
- Understand noise signature during take-off and landing, and its impact on neighborhoods surrounding airports
- Predictive ability during the design phase can help reduce development cost and time to flight
- Improve fuel efficiency by having access to better tools during the design phase

Source Diagnostic Test Overview

- 22” fan rig mounted on the 9x15 ft. Low Speed anechoic Wind Tunnel (LSWT)
- 22 fan blades + 54 Outlet Guide Vane (OGV) blades (baseline)
- Low-speed 7808 RPM (**approach**) + high-speed 12657 RPM (**take-off**) conditions
- Comprehensive experimental dataset:
  - Fan and stage performance metrics
  - Mean and turbulent interstage flow characterization - Hot-wire + Laser Doppler Velocimetry (LDV) measurements
  - Acoustic Sound Pressure Level (SPL) measurements along a sideline microphone array



Rotor-only configuration in the LSWT tunnel



Rotor-only configuration in the LSWT tunnel



Full configuration in the LSWT tunnel

Image credit: C. Hughes (NASA GRC)

Source Diagnostic Test Overview

Stage Metrics

- Mass flow rate through the duct
- Total pressure and total temperature ratios across the duct

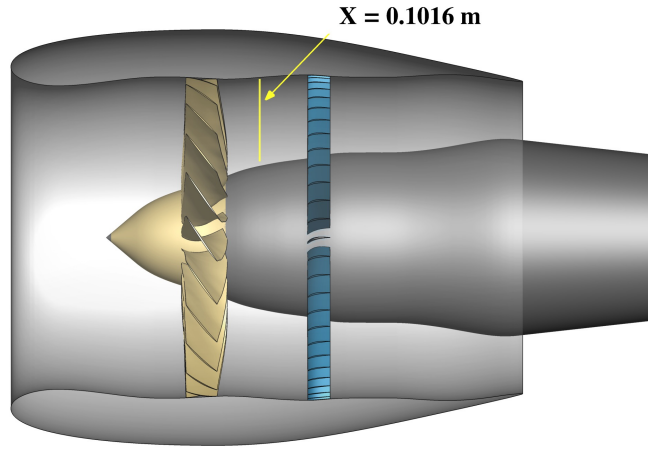
Source Diagnostic Test Overview

Stage Metrics

- Mass flow rate through the duct
- Total pressure and total temperature ratios across the duct

Interstage Flow Characterization

- Mean velocity and Root-Mean-Square (RMS) velocity fluctuation profiles
- Velocity spectra (low-speed condition only)
- Hot-wire probe and LDV measurements available



Hot wire station 1 location

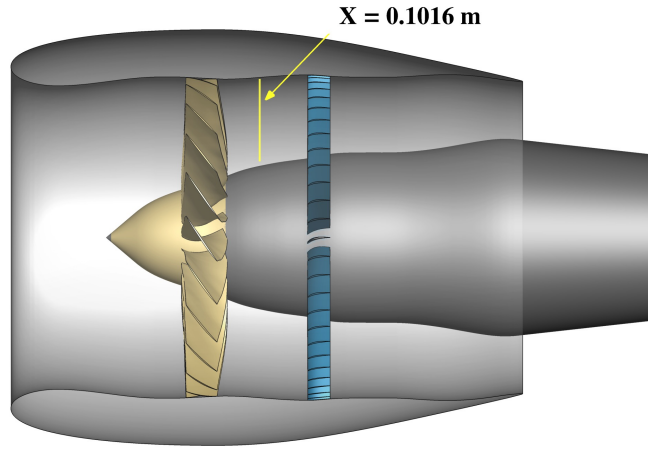
Source Diagnostic Test Overview

Stage Metrics

- Mass flow rate through the duct
- Total pressure and total temperature ratios across the duct

Interstage Flow Characterization

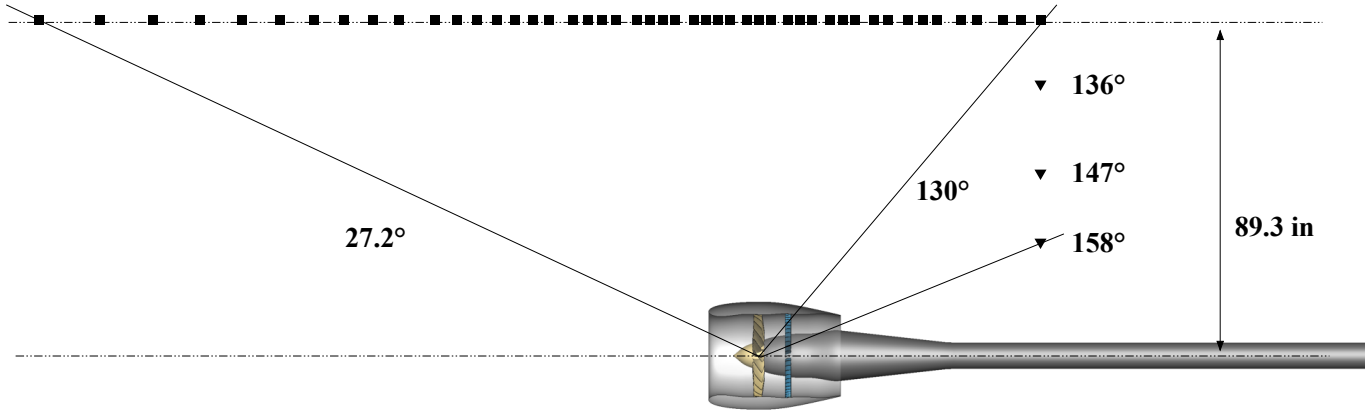
- Mean velocity and Root-Mean-Square (RMS) velocity fluctuation profiles
- Velocity spectra (low-speed condition only)
- Hot-wire probe and LDV measurements available



Hot wire station 1 location

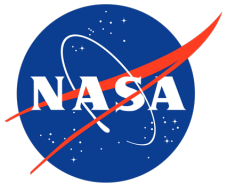
Sideline Microphone Array

- SPL values at each point
- Overall SPL (OASPL) along sideline



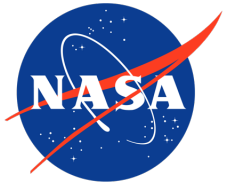
Sideline array microphone locations

Numerical Discretization



- Launch, Ascent, and Vehicle Aerodynamics (**LAVA**) Curvilinear Solver Framework
- Structured overset grid paradigm with block-to-block point-matched grid capabilities
- Conservative finite-difference formulation applied to the strong conservation law form of the flow equations in curvilinear coordinates
- **Time-stepping**: 2nd order Backwards Differencing Formula (BDF2)
- **Convective fluxes**: 2nd order discretization
  - Modified Roe scheme
  - Blended 3rd order upwind and 4th order central left/right state interpolation/reconstruction operators
    - **URANS** blending factor 1% upwind everywhere
    - **HRLES** blending factor 1% upwind in LES regions ($f_d > 0.8$), pure upwind in RANS regions

Turbulence Model Closures



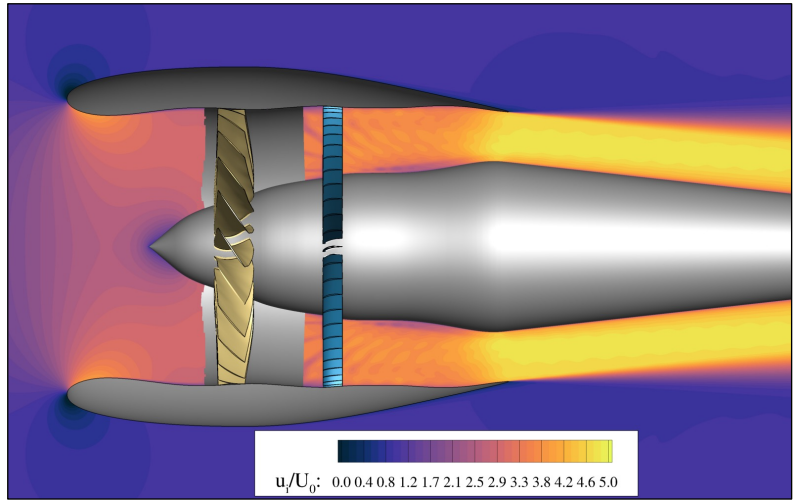
Unsteady Reynolds-Averaged Navier Stokes (URANS)

- Favre-averaged RANS equations
- Spalart-Allmaras (SA) turbulence model
  - Baseline (**SA**)
  - Baseline w/ Rotation/Curvature correction (**SA-RC**)
  - Baseline w/ Quadratic Constitutive Relation, version 2000 (**SA-QCR**)
  - Baseline w/ RC + QCR corrections (**SA-RC-QCR**)
  - Baseline w/ mixing layer Compressibility Correction (**SA-CC**)

Turbulence Model Closures

Unsteady Reynolds-Averaged Navier Stokes (URANS)

- Favre-averaged RANS equations
- Spalart-Allmaras (SA) turbulence model
  - Baseline (**SA**)
  - Baseline w/ Rotation/Curvature correction (**SA-RC**)
  - Baseline w/ Quadratic Constitutive Relation, version 2000 (**SA-QCR**)
  - Baseline w/ RC + QCR corrections (**SA-RC-QCR**)
  - Baseline w/ mixing layer Compressibility Correction (**SA-CC**)



URANS instantaneous flow field

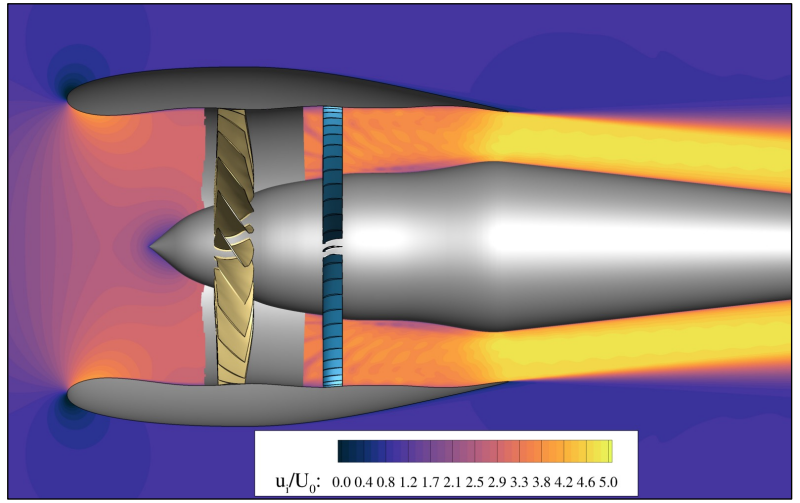
Turbulence Model Closures

Unsteady Reynolds-Averaged Navier Stokes (URANS)

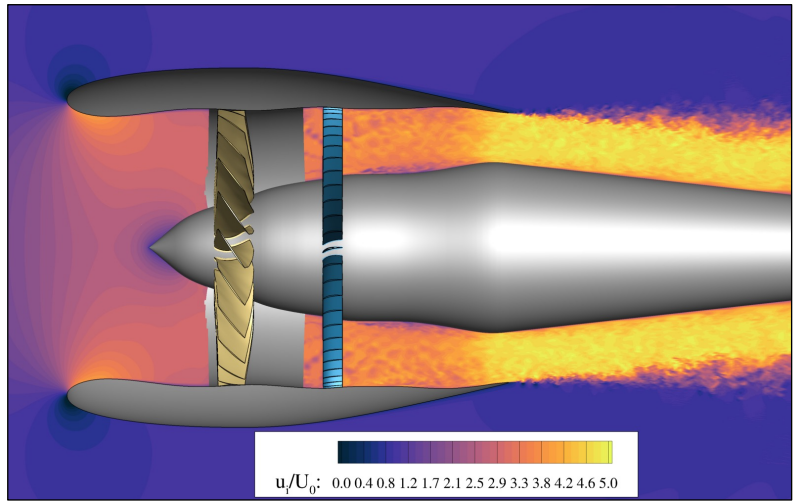
- Favre-averaged RANS equations
- Spalart-Allmaras (SA) turbulence model
  - Baseline (**SA**)
  - Baseline w/ Rotation/Curvature correction (**SA-RC**)
  - Baseline w/ Quadratic Constitutive Relation, version 2000 (**SA-QCR**)
  - Baseline w/ RC + QCR corrections (**SA-RC-QCR**)
  - Baseline w/ mixing layer Compressibility Correction (**SA-CC**)

Hybrid RANS/Large Eddy Simulation (HRLES)

- Zonal Detached Eddy Simulation (ZDES)
- Shielding function protects attached boundary layers from LES mode
- ZDES2020-Mode2-EP – Enhanced Protection model by Deck & Renard [1]
- Baseline SA closure used in RANS mode



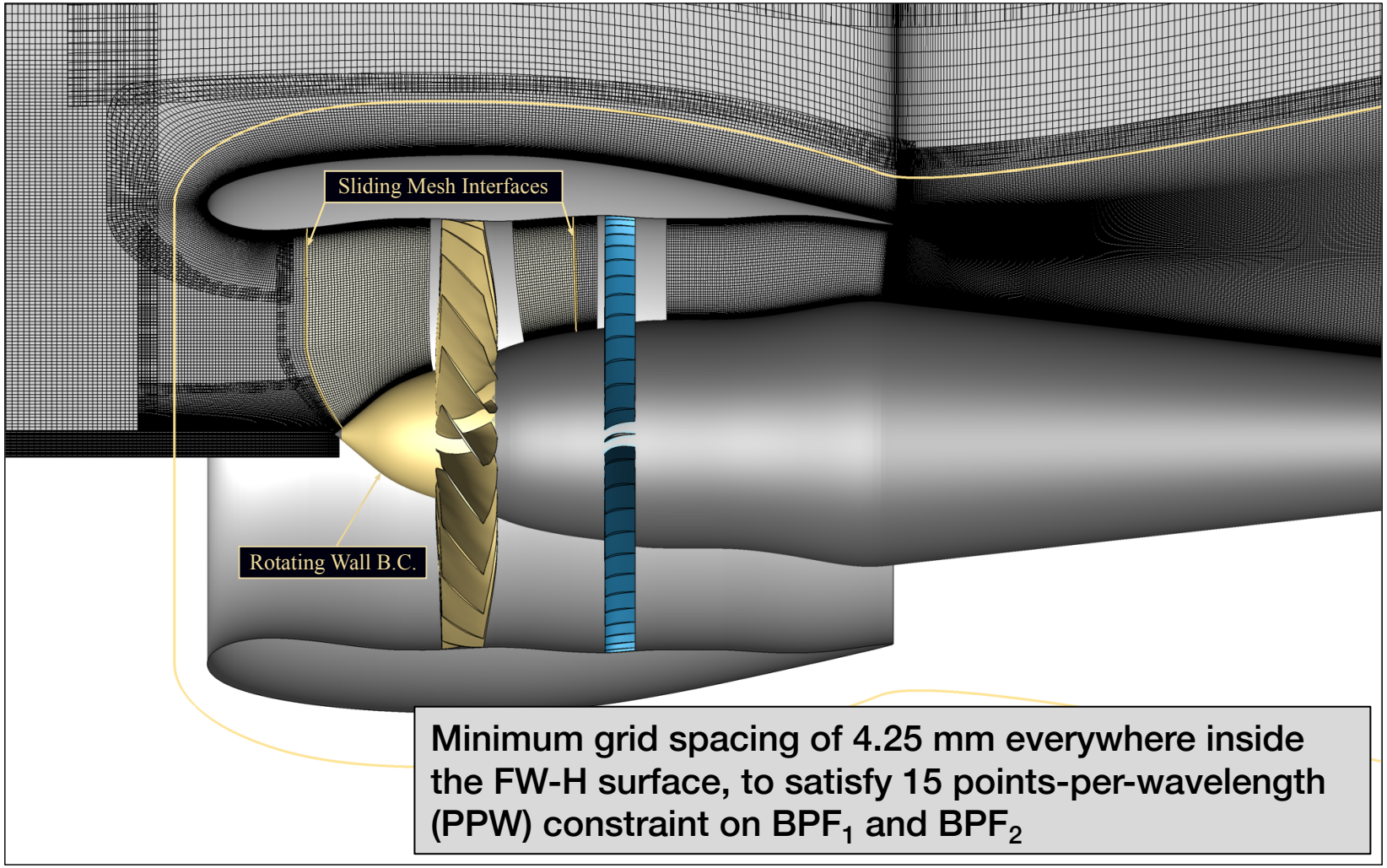
URANS instantaneous flow field



HRLES instantaneous flow field

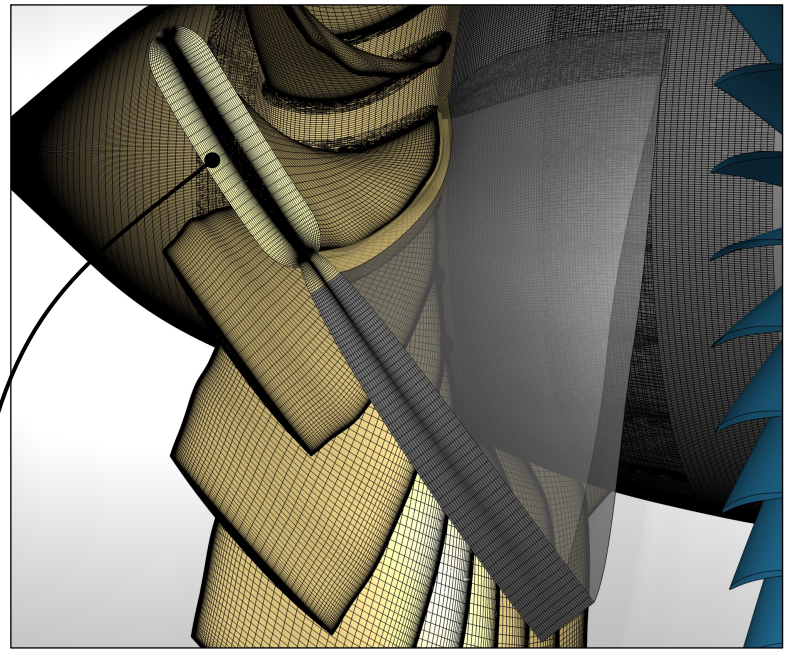
[1] Deck, S., *Recent improvements in the Zonal Detached Eddy Simulation (ZDES) formulation* Theoretical and Computational Fluid Dynamics, 2012

Overset Grid Topologies



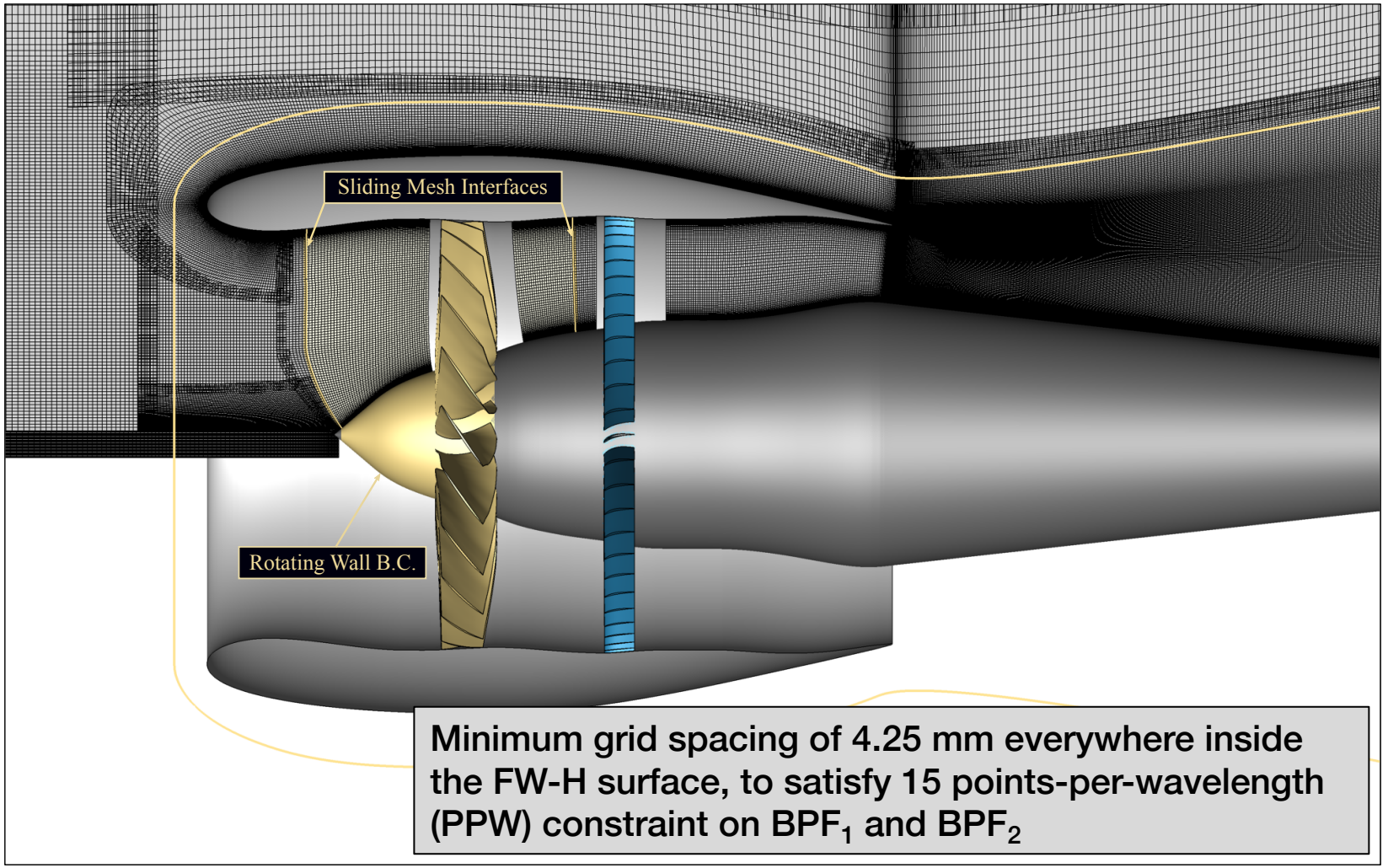
Grid slice along the Y = 0 plane, showing grid topologies utilized around nacelle and exhaust regions of the computational domain

Overset Grid Topologies



O-grid topologies utilized around fan blades, and localized refinement applied to each fan blade wake to properly resolve the small scale fluctuations that develop along the wake.

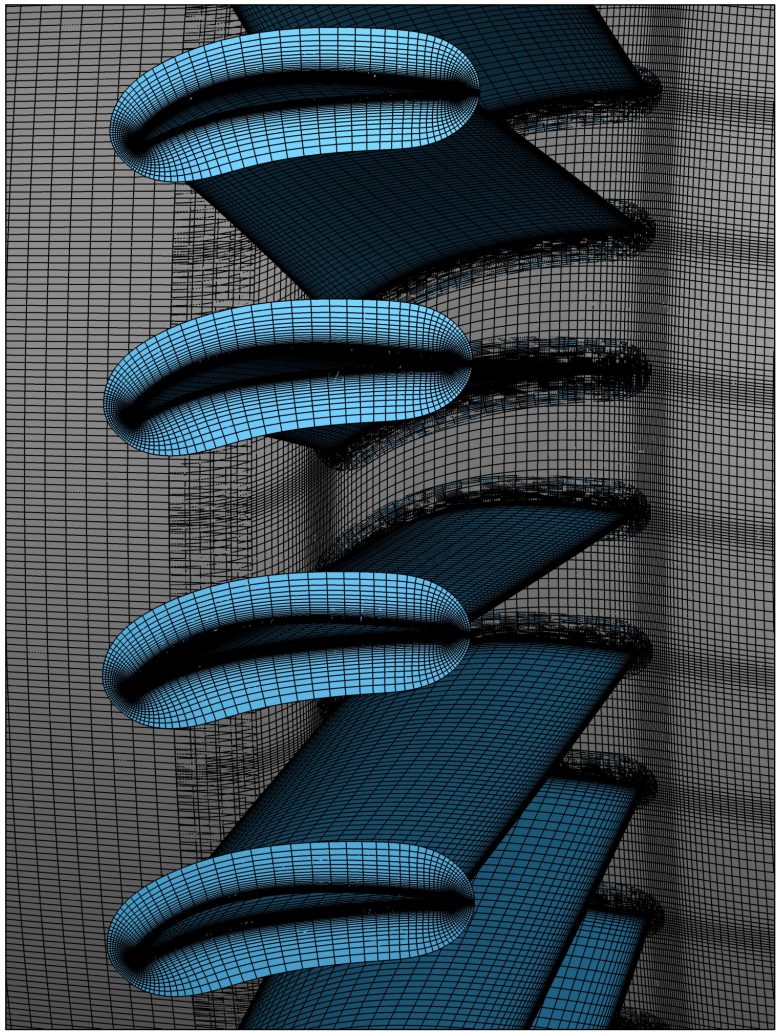
0.5 mm blade tip gap is fully meshed



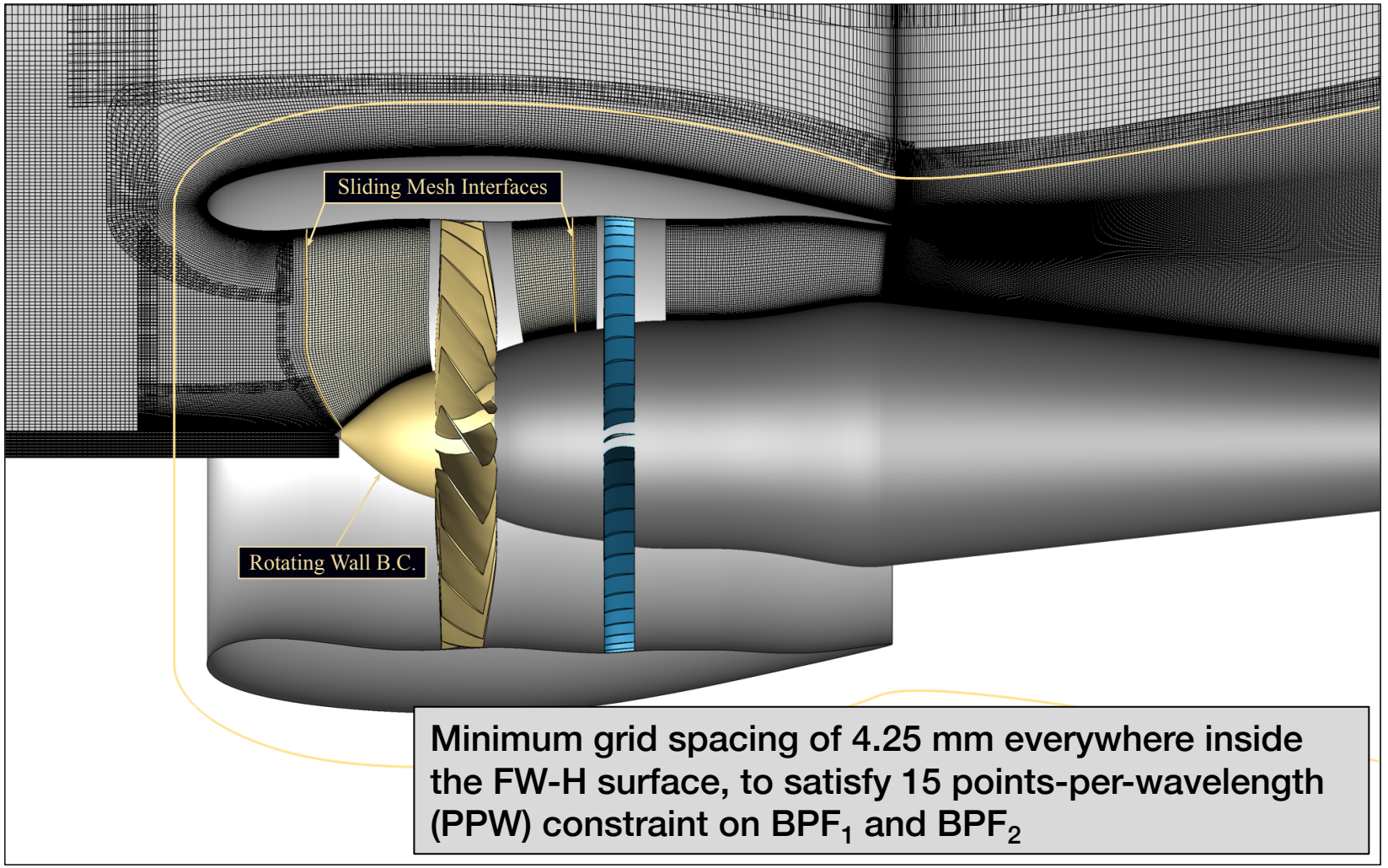
Minimum grid spacing of 4.25 mm everywhere inside the FW-H surface, to satisfy 15 points-per-wavelength (PPW) constraint on BPF_1 and BPF_2

Grid slice along the Y = 0 plane, showing grid topologies utilized around nacelle and exhaust regions of the computational domain

Overset Grid Topologies



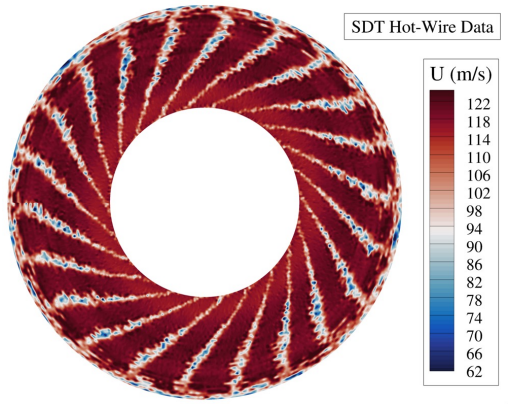
O-grid topologies utilized around OGV blades.

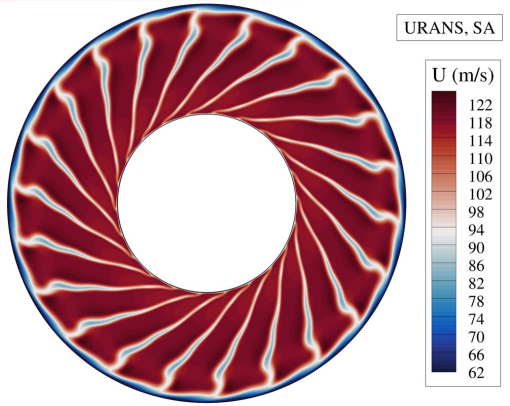


Grid slice along the Y = 0 plane, showing grid topologies utilized around nacelle and exhaust regions of the computational domain

Turbulence Model Sensitivity

- Performed initial assessment of turbulence model sensitivity using URANS
- **Baseline SA** model instantaneous axial velocity shows good qualitative agreement with experiment in the interstage flow field

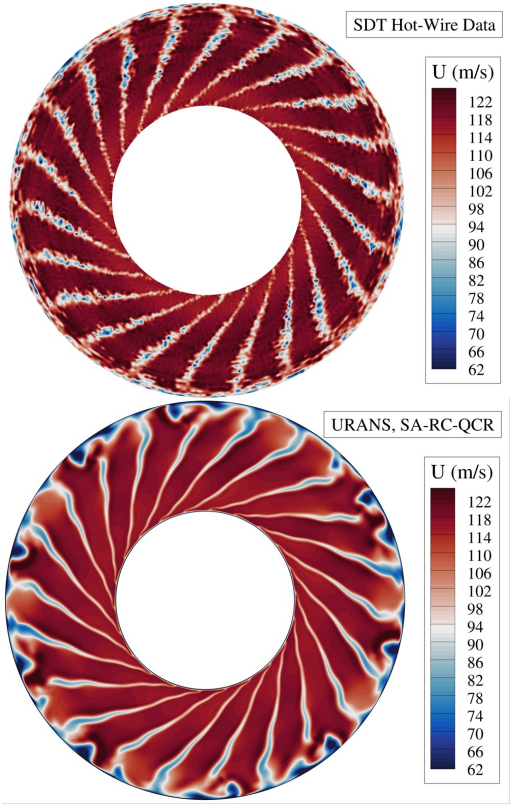


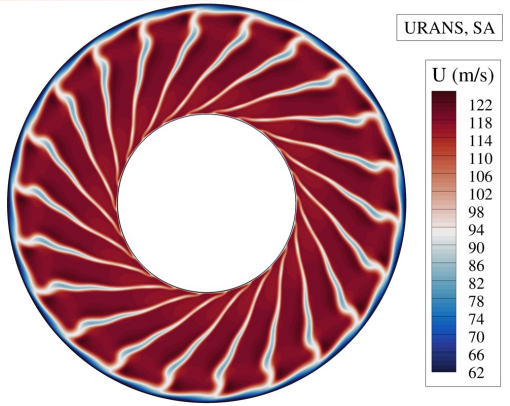


Instantaneous axial velocity at hot-wire station 1

Turbulence Model Sensitivity

- Performed initial assessment of turbulence model sensitivity using URANS
- **Baseline SA** model instantaneous axial velocity shows good qualitative agreement with experiment in the interstage flow field
- **Baseline SA with RC and QCR corrections** shows the presence of large-scale unsteady vortical features in the blade tip region, not present in the experimental data

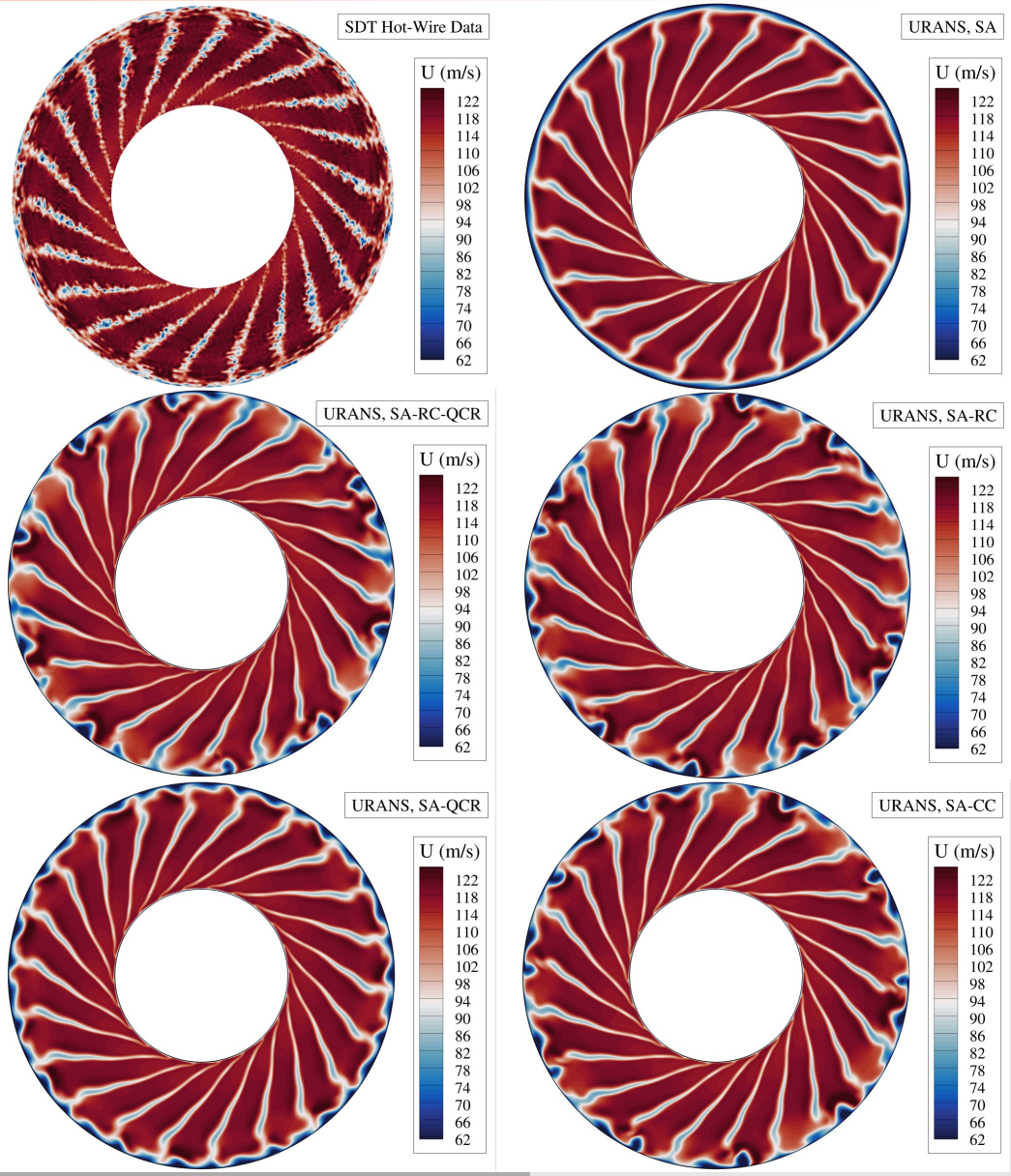




Instantaneous axial velocity at hot-wire station 1

Turbulence Model Sensitivity

- Performed initial assessment of turbulence model sensitivity using URANS
- **Baseline SA** model instantaneous axial velocity shows good qualitative agreement with experiment in the interstage flow field
- **Baseline SA with RC and QCR corrections** shows the presence of large-scale unsteady vortical features in the blade tip region, not present in the experimental data
- Other SA variants also show a subset of these features
- Therefore, we used the **baseline SA turbulence model for the production runs**



Instantaneous axial **velocity** at hot-wire station 1

Grid Refinement Sensitivity

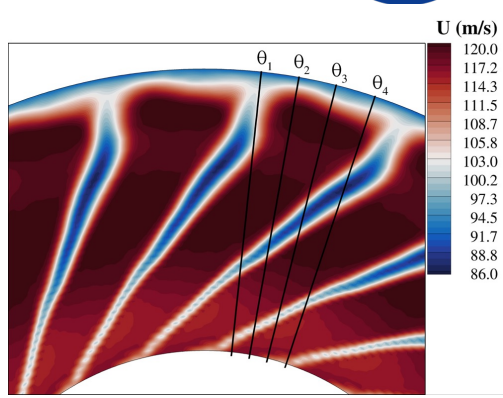
Refinement Level		Coarse	Medium	Fine
Refinement Ratio R_f		0.8	1.0	1.25
Viscous Wall Spacing (m)		6.25×10^{-6}	5.0×10^{-6}	4.0×10^{-6}
Grid Point Counts	Total Points	236,500,101	447,776,278	801,581,618
	Blanked Points	12,930,218	25,008,354	44,924,390
	Fringe Points	24,308,381	37,709,931	50,964,856
	Solution Points	199,261,502	385,057,993	705,692,372
Azimuthal Point Counts N_ϕ	Nacelle	529	661	837
	Inlet	419	506	639
	Rotor	639	793	969
	Interstage	639	793	991
	OGV	1,189	1,297	1,567
	OGV Exit	811	973	1,243
	Exhaust †	441	551	703

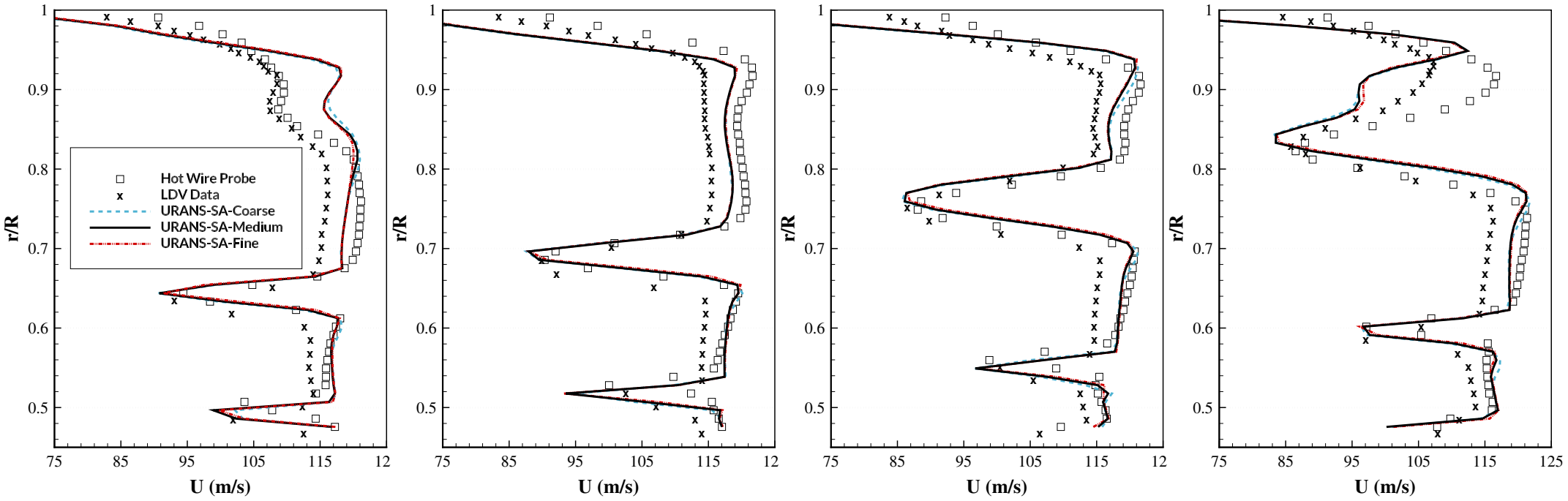
Details on the grids used for the grid refinement study

Grid Refinement Sensitivity

Radial line extractions of velocity profiles

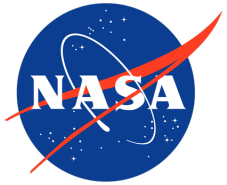
- Little sensitivity observed with grid refinement on the interstage flow field characteristics
- Medium grid level (385M) was chosen for the production runs





Mean Axial Velocity at hot-wire station 1

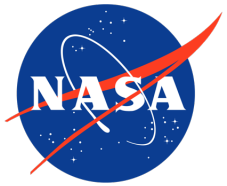
Evaluation of Performance Metrics



- Results for **low-speed** condition show good agreement between URANS and HRLES, within 1% of the experimental data performance metrics

Case	Mass Flow Rate		Fan Stage Total Pressure Ratio		Fan Stage Total Temperature Ratio	
	Value [kg/s]	Δ	Value	Δ	Value	Δ
Approach Condition (Low speed)						
SDT Data	**26.535**	-	**1.154**	-	**1.049**	-
URANS (SA)	26.779	+0.92 %	1.160	+0.6 %	1.050	+0.1 %
HRLES	26.780	+0.92 %	1.161	+0.6 %	1.050	+0.1 %

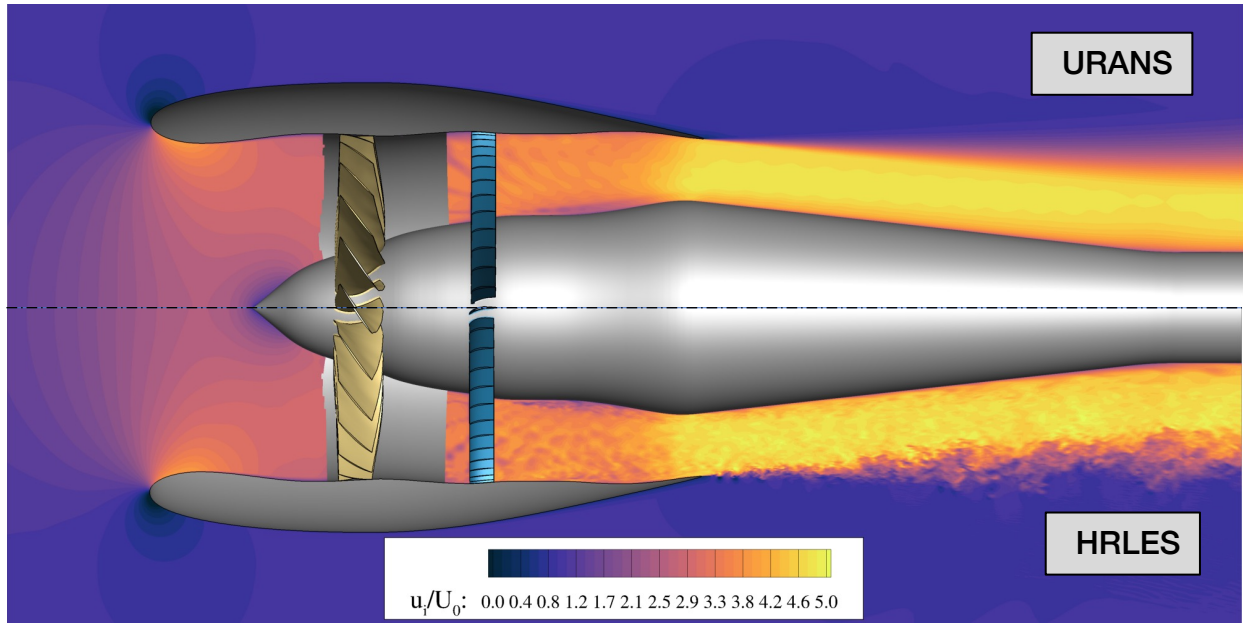
Evaluation of Performance Metrics



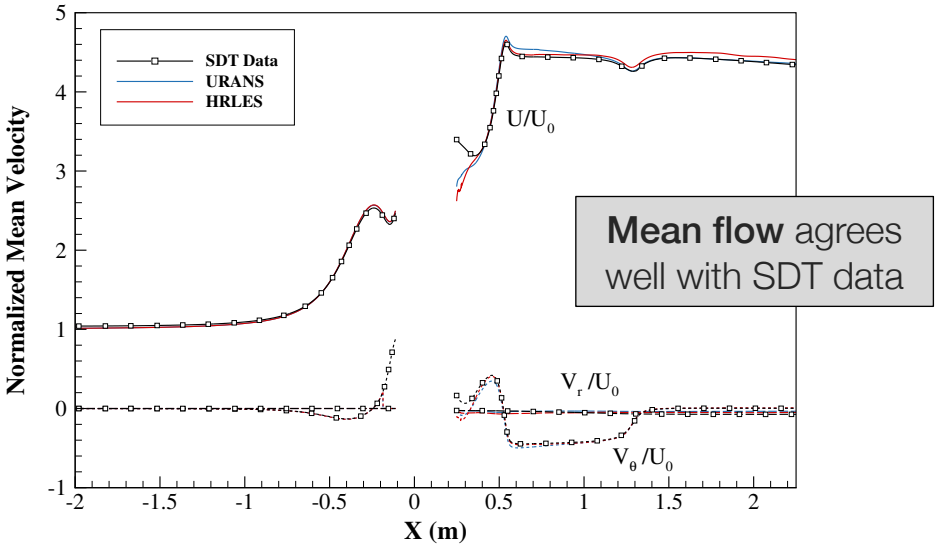
- Results for **low-speed** condition show good agreement between URANS and HRLES, within 1% of the experimental data performance metrics
- **High-speed** results slightly favor the use of HRLES, although the difference is still within 2% of the experimental data for both turbulence treatment options

Case	Mass Flow Rate		Fan Stage Total Pressure Ratio		Fan Stage Total Temperature Ratio	
	Value [kg/s]	Δ	Value	Δ	Value	Δ
Approach Condition (Low speed)						
SDT Data	**26.535**	-	**1.154**	-	**1.049**	-
URANS (SA)	26.779	+0.92 %	1.160	+0.6 %	1.050	+0.1 %
HRLES	26.780	+0.92 %	1.161	+0.6 %	1.050	+0.1 %
Take-off Condition (High speed)						
SDT Data	**43.998**	-	**1.490**	-	**1.137**	-
URANS (SA)	44.787	+1.79 %	1.497	+0.47 %	1.136	+0.09 %
HRLES-L	44.523	+1.19 %	1.492	+0.13 %	1.135	-0.18 %

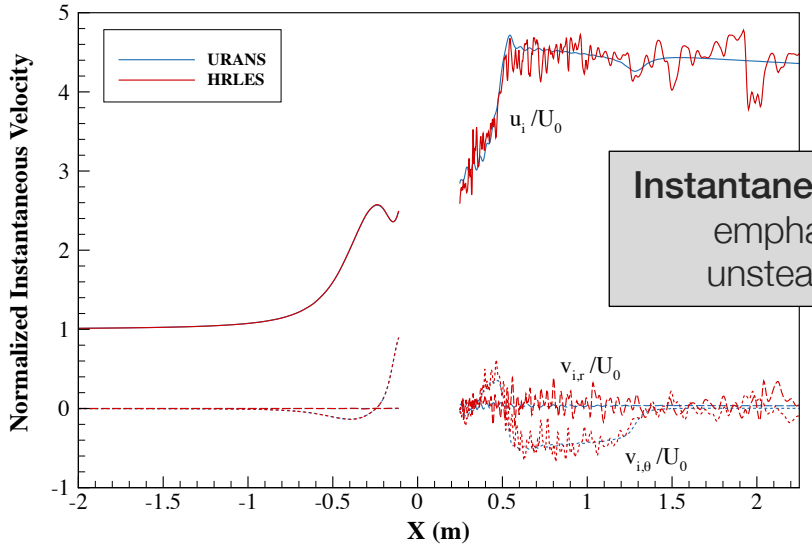
Low-Speed Condition Results



Instantaneous Axial Velocity contour

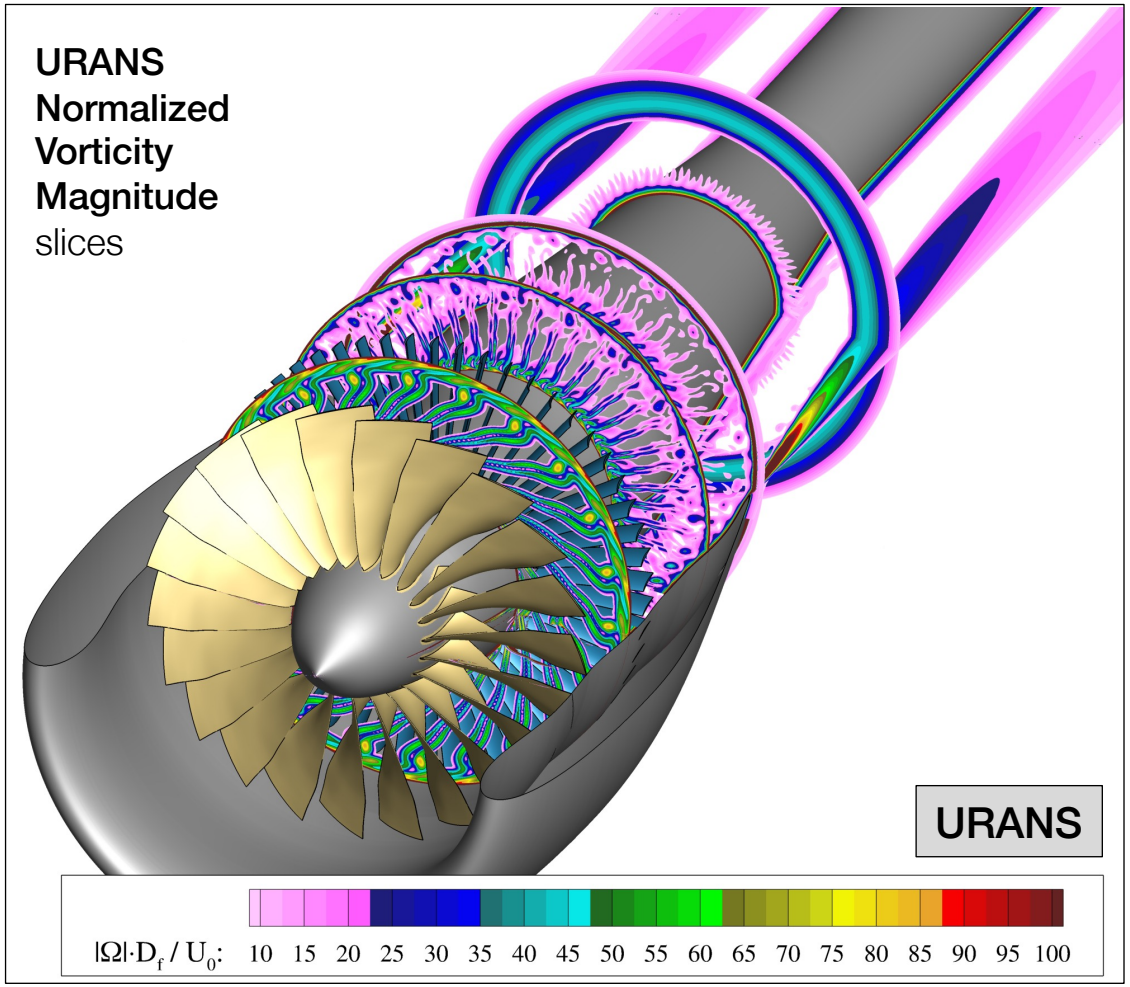


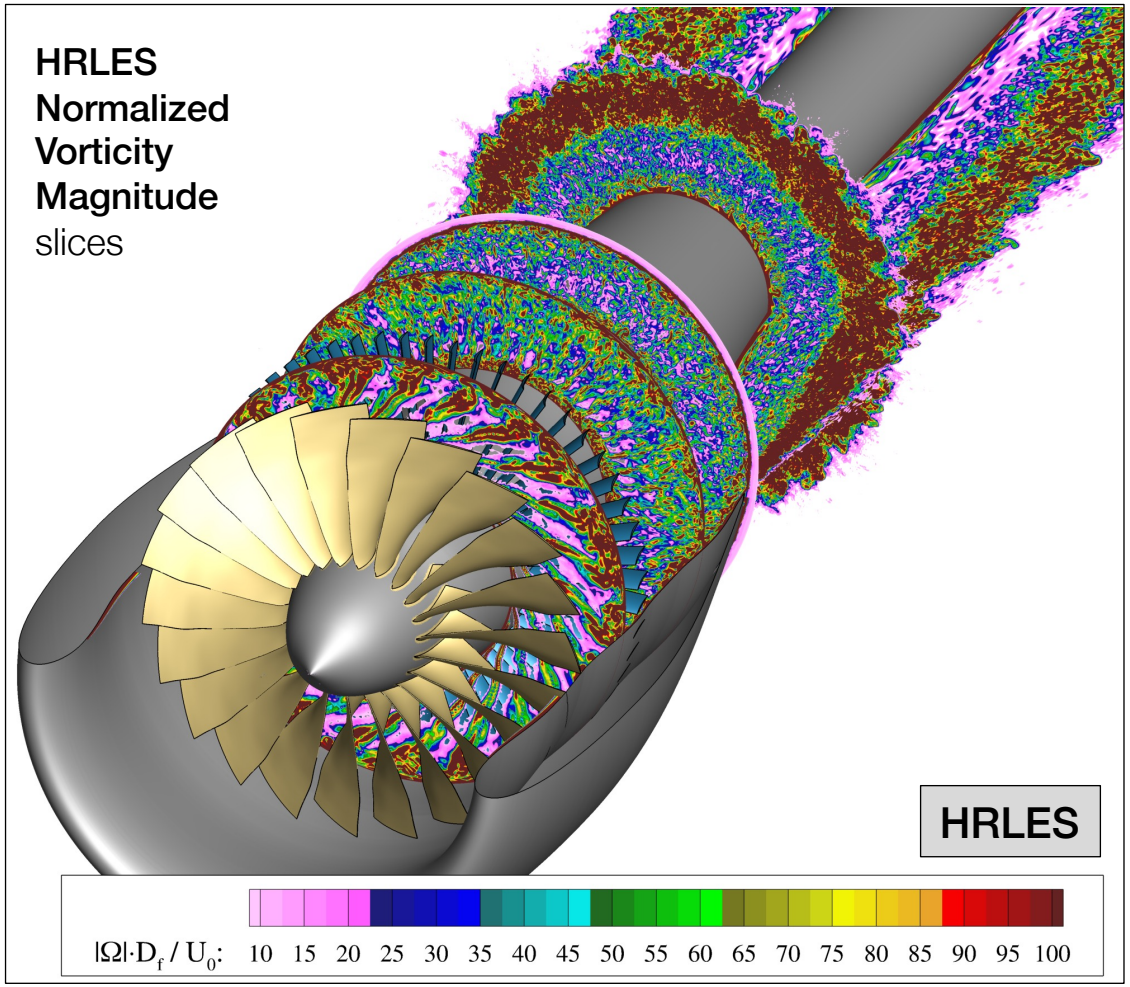
Mean flow agrees well with SDT data



Instantaneous velocity profiles emphasize small-scale unsteadiness in HRLES

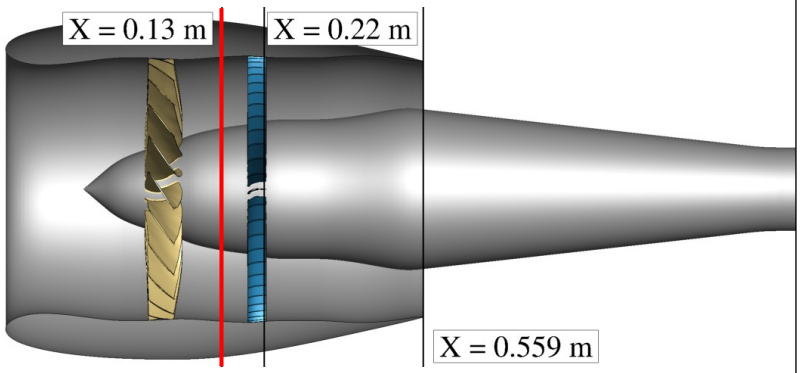
Low-Speed Condition Results



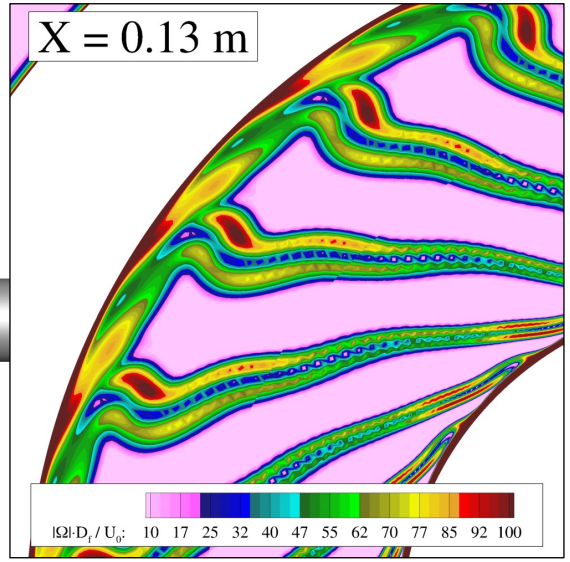


Significant differences in **small-scale turbulent content** predicted by the two models

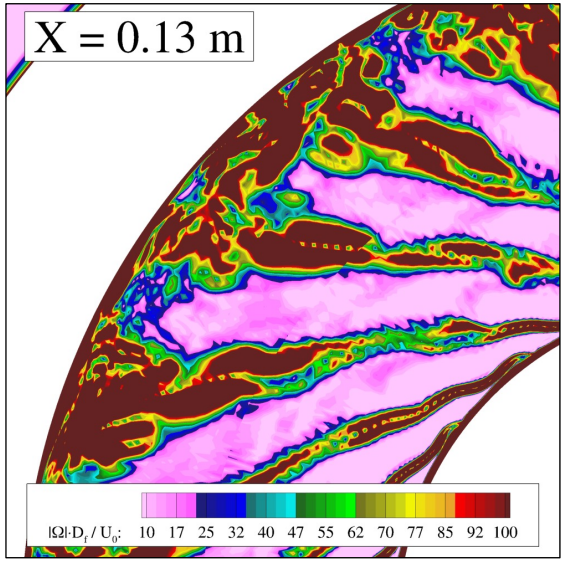
Low-Speed Condition Results



URANS

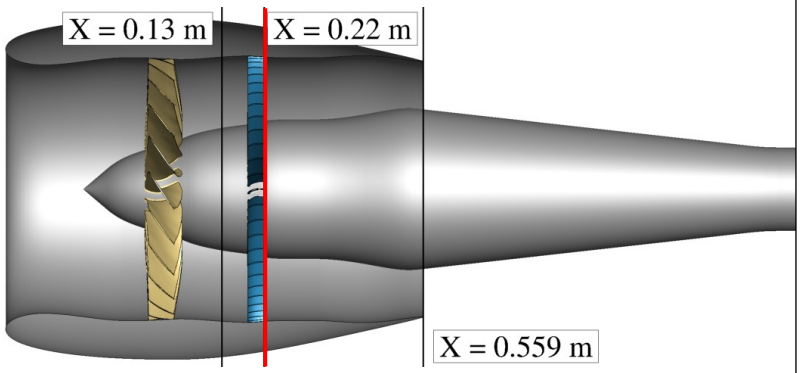


HRLES

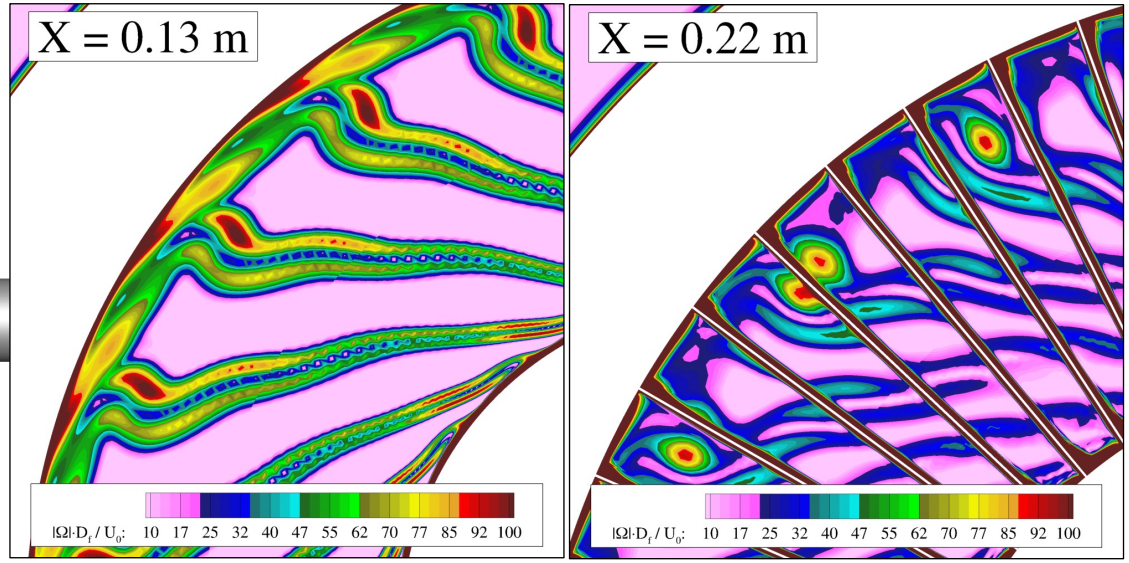


Normalized vorticity magnitude slices
for URANS (top) and HRLES (bottom)

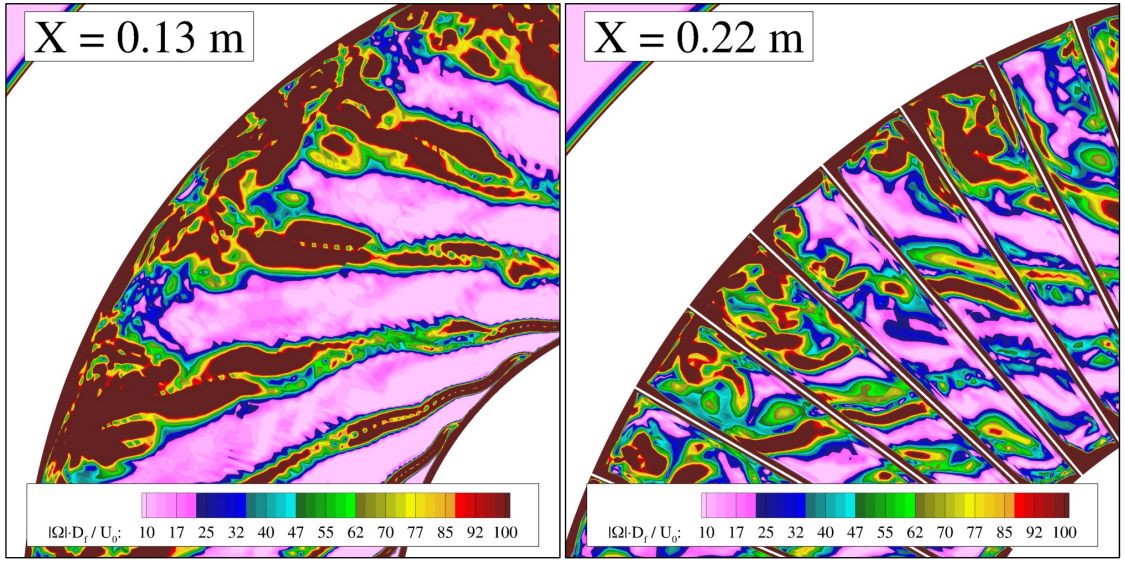
Low-Speed Condition Results



URANS

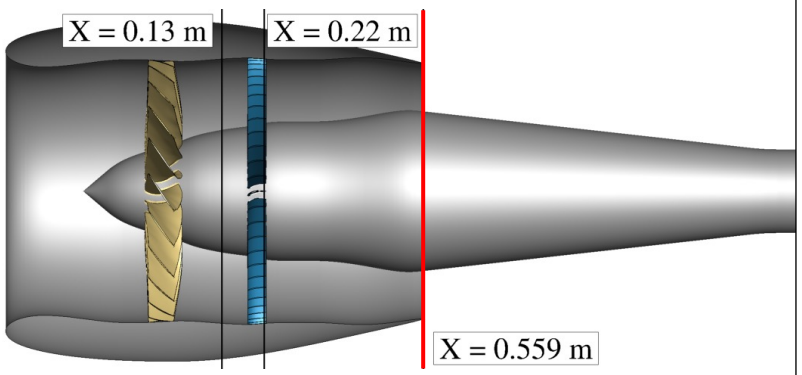


HRLES

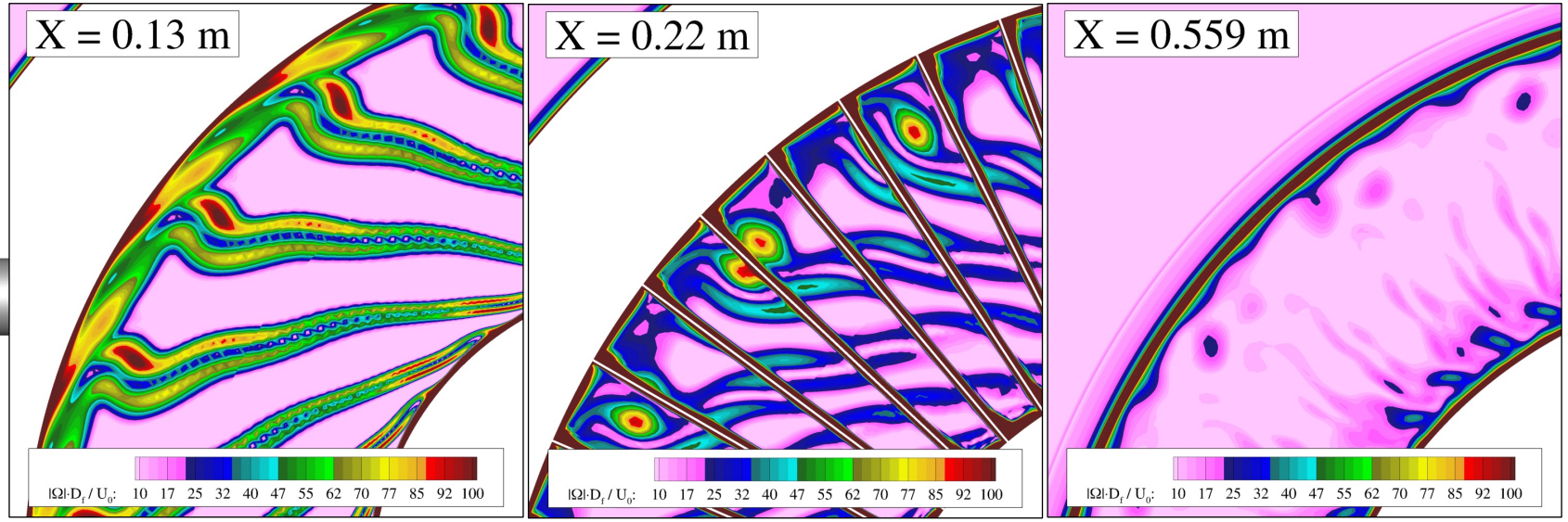


Normalized vorticity magnitude slices
for URANS (top) and HRLES (bottom)

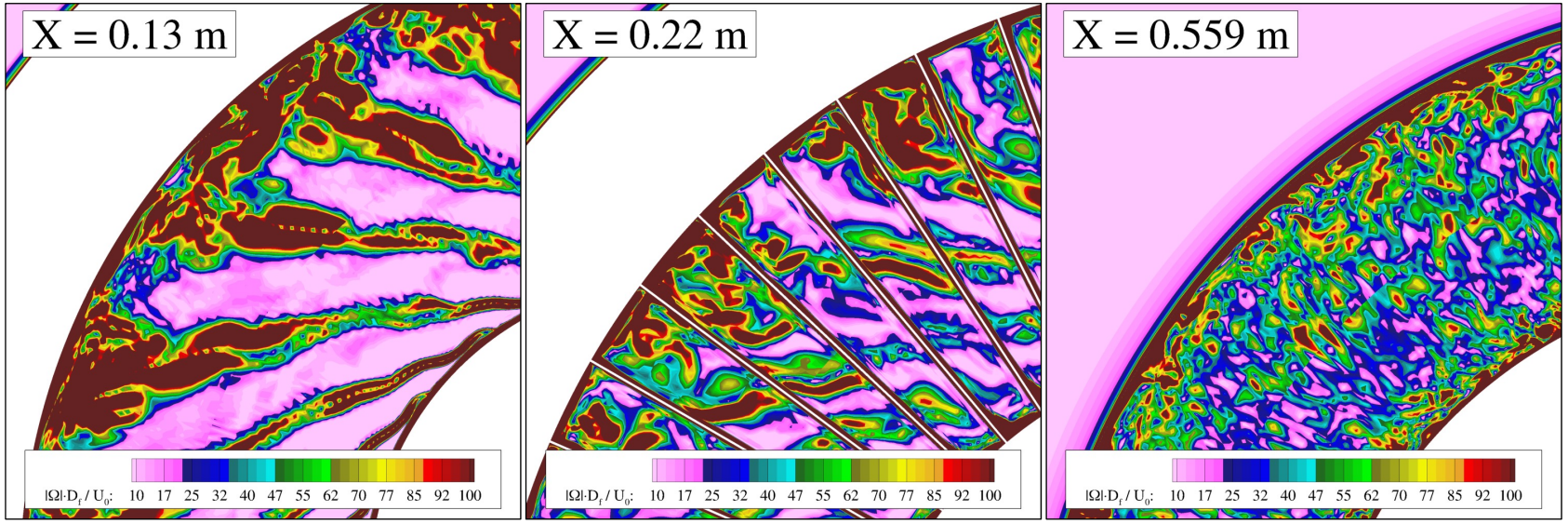
Low-Speed Condition Results



URANS

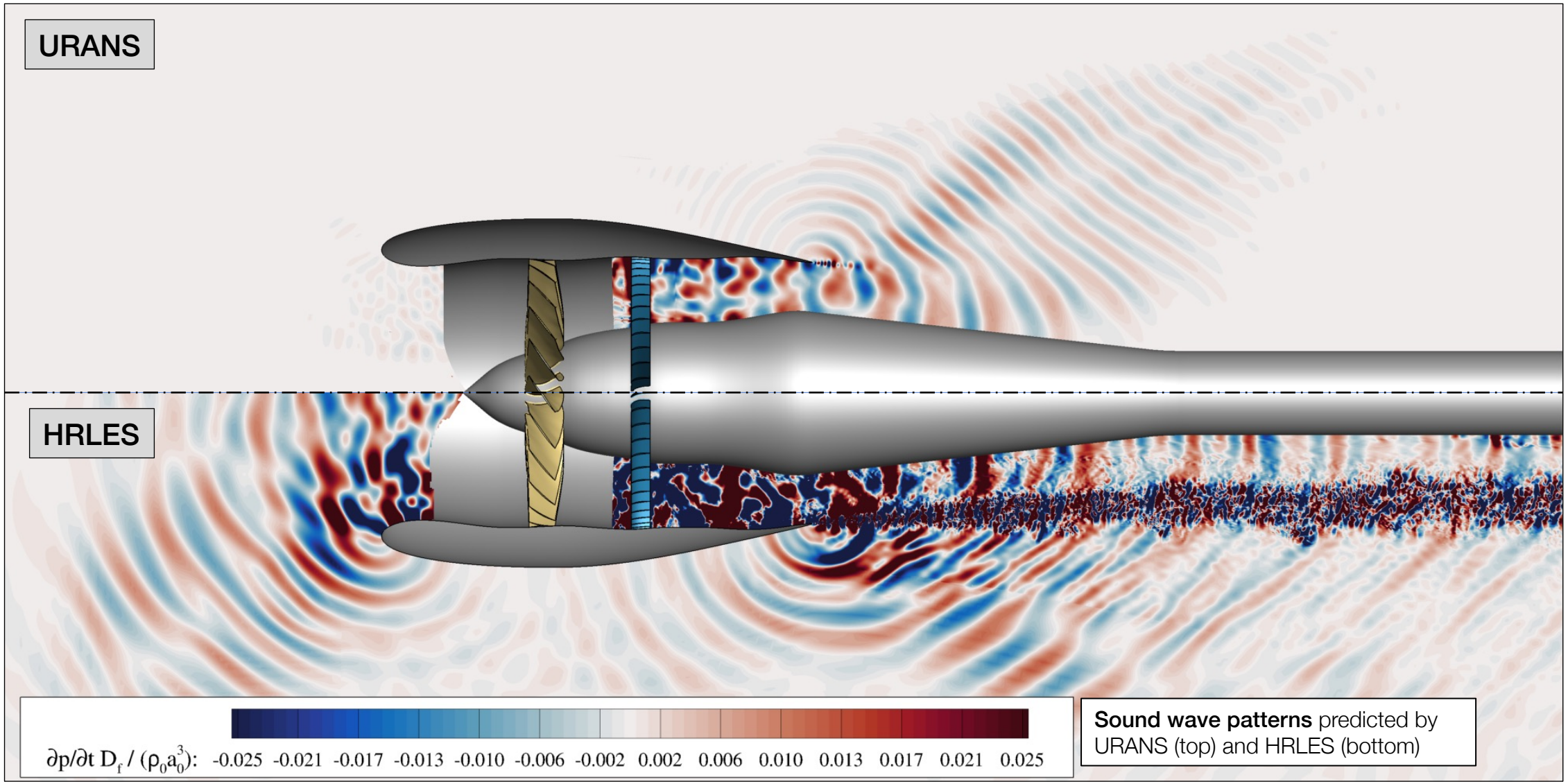


HRLES



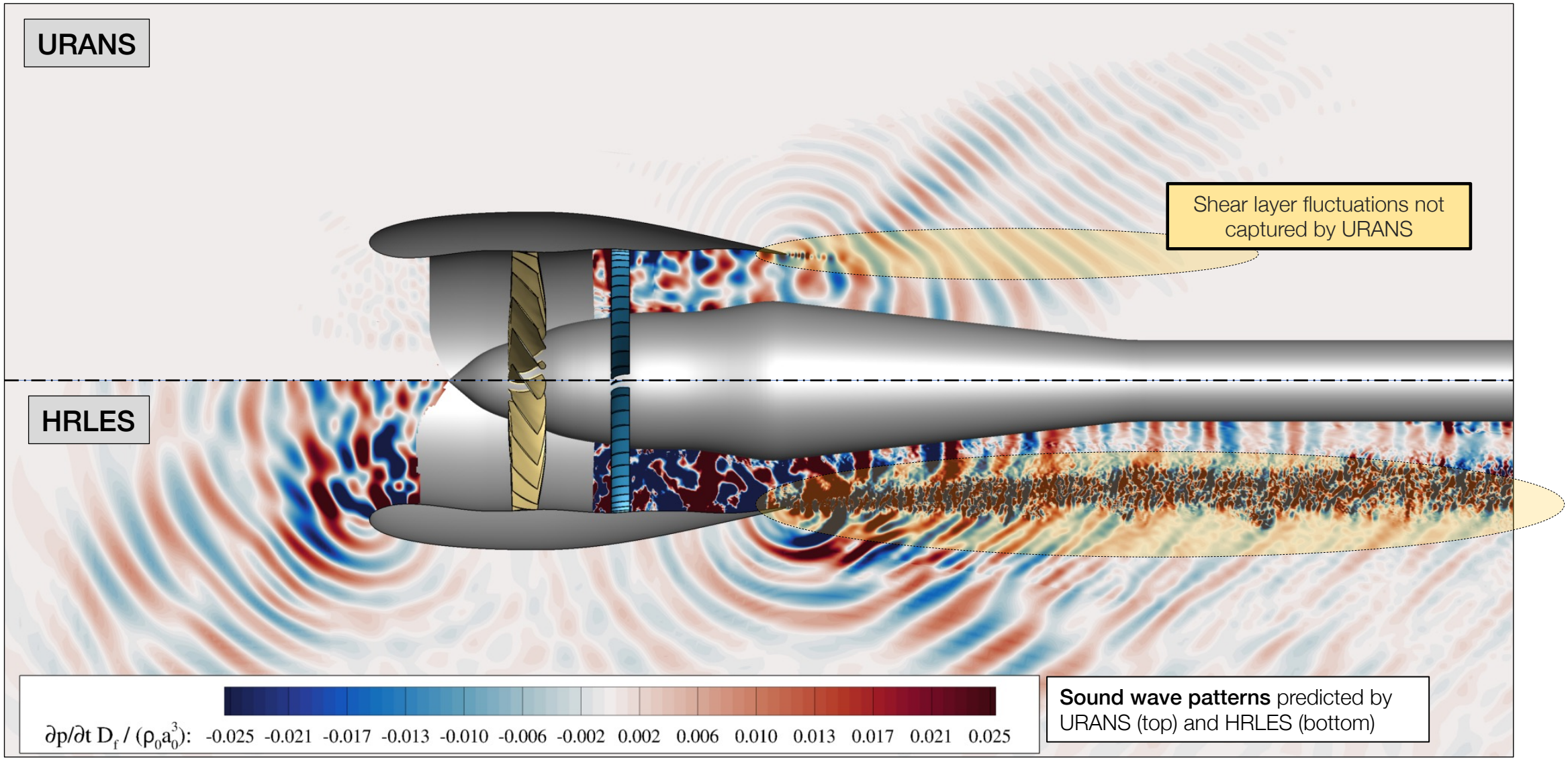
Normalized vorticity magnitude slices
for URANS (top) and HRLES (bottom)

Low-Speed Condition Results



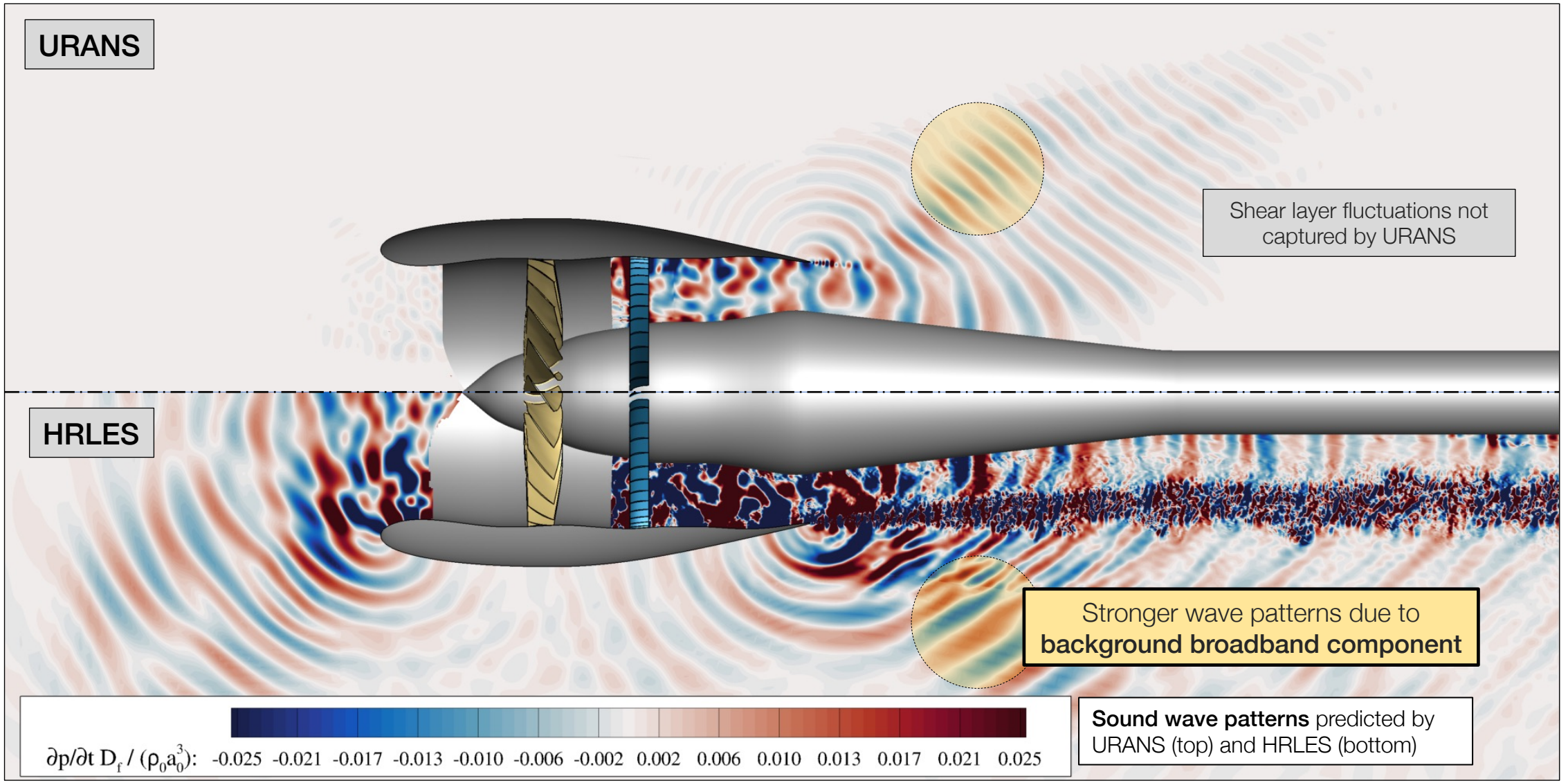
Sound wave patterns predicted by URANS (top) and HRLES (bottom)

Low-Speed Condition Results



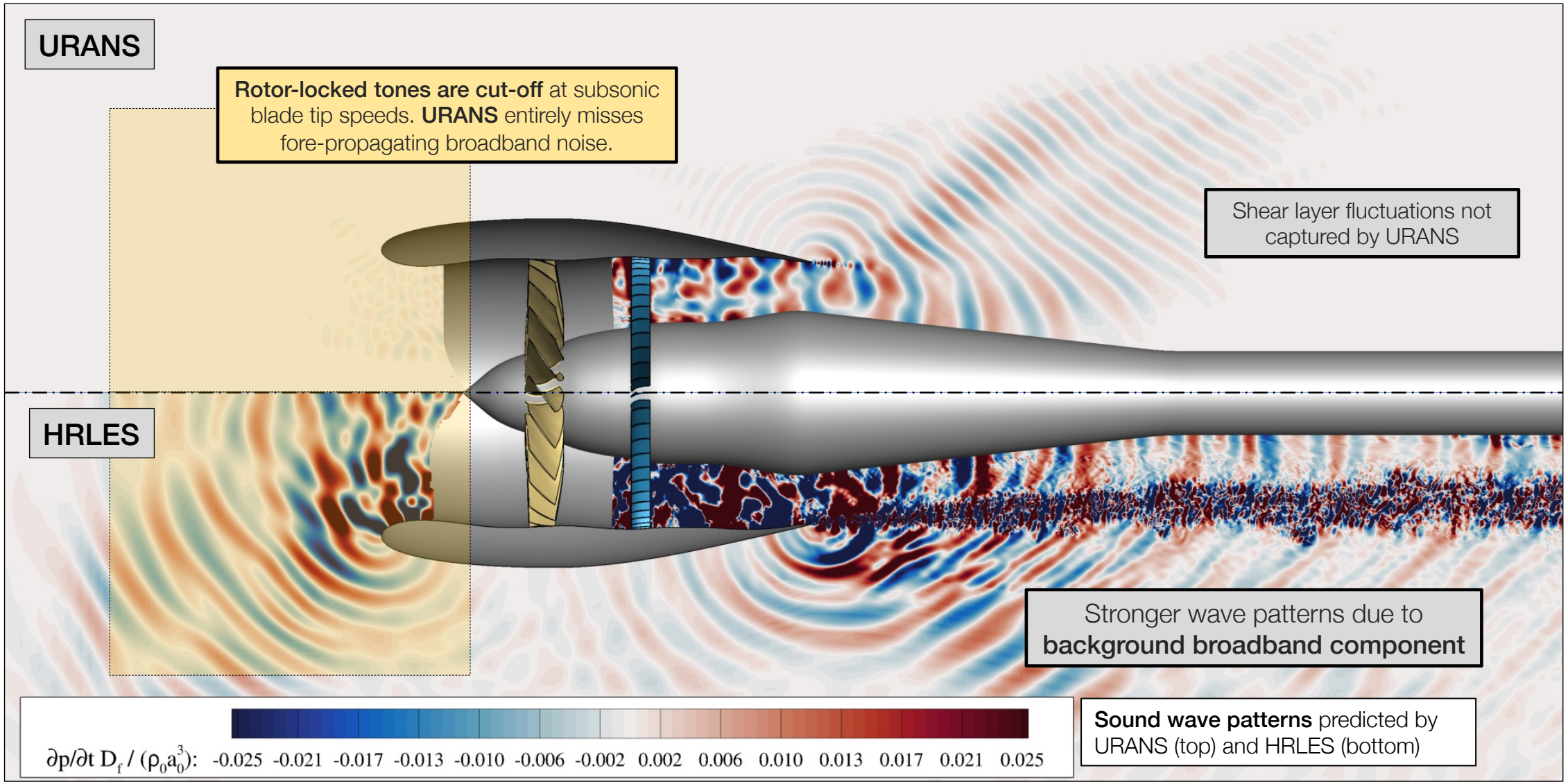
Sound wave patterns predicted by URANS (top) and HRLES (bottom)

Low-Speed Condition Results



Sound wave patterns predicted by URANS (top) and HRLES (bottom)

Low-Speed Condition Results

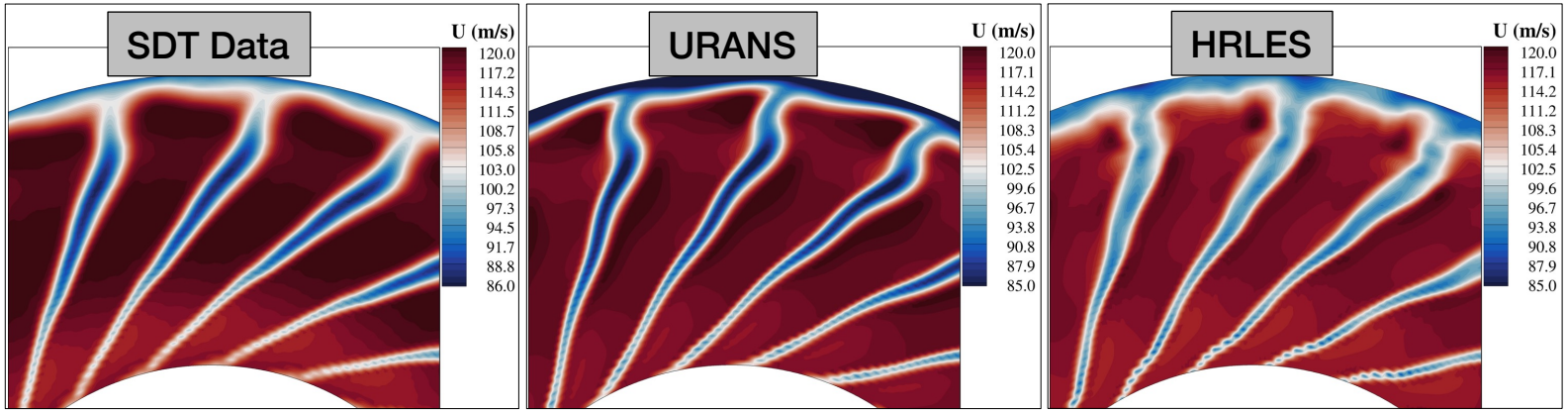


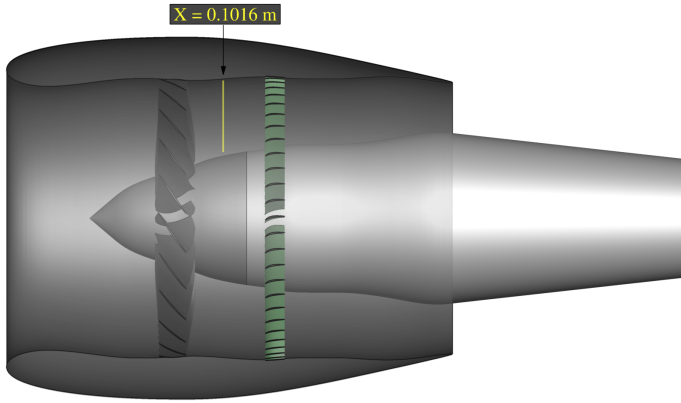
Low-Speed Condition Results

Qualitative interstage flow field comparisons

- Wake shape and size compare well with experiment
- **URANS** shows S-shaped wake downstream of blade tip
- **HRLES** underpredicts velocity deficit inside wake

Mean Axial Velocity



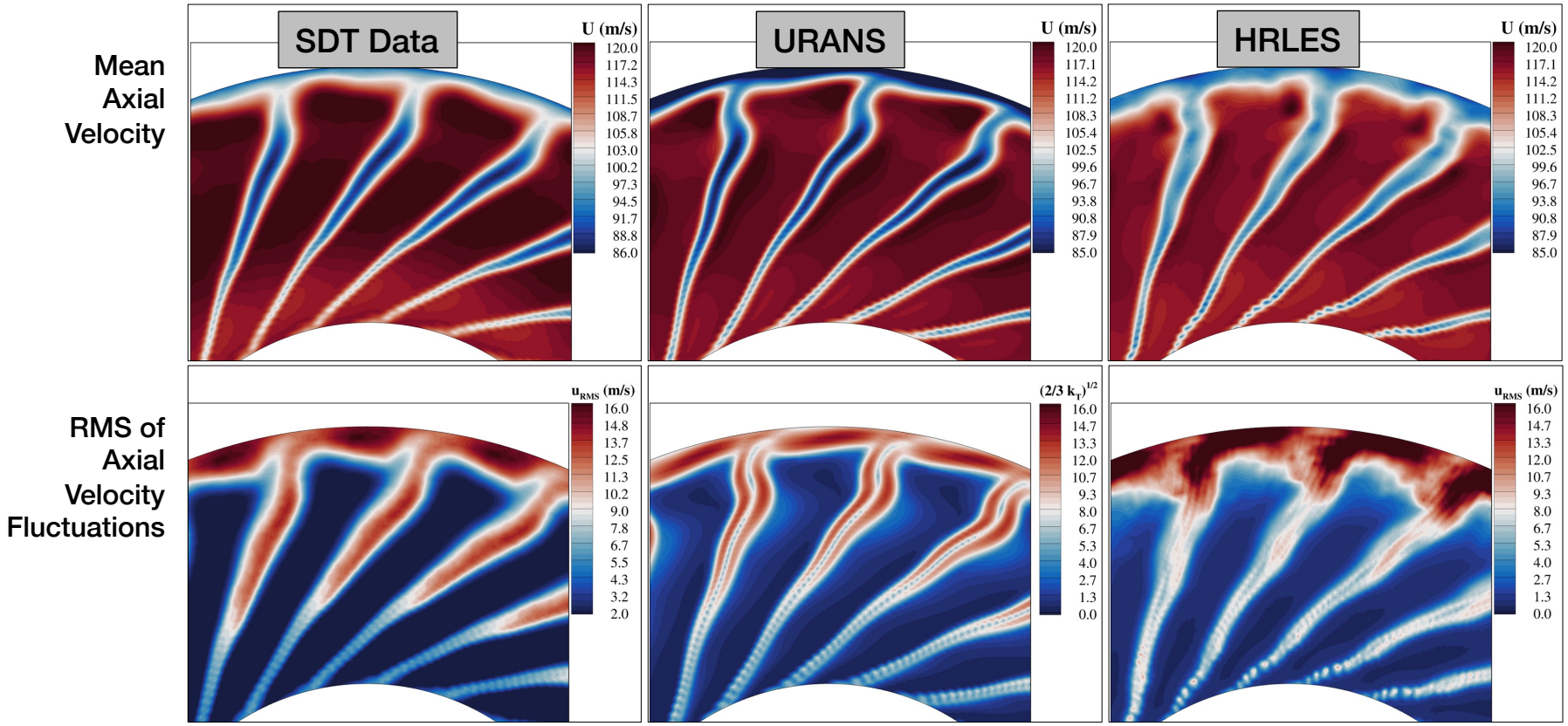


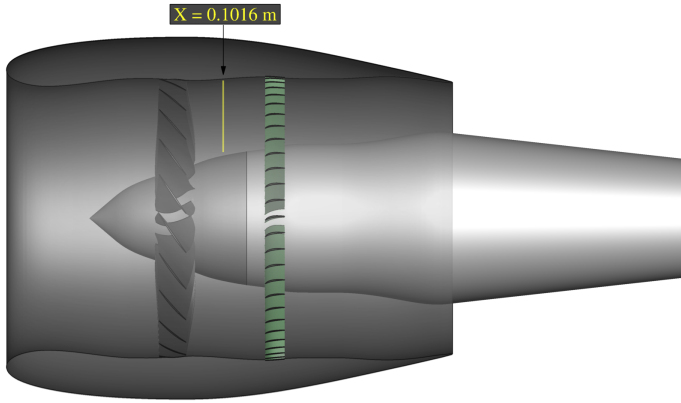
Hot-wire probe station 1 location in interstage region

Low-Speed Condition Results

Qualitative interstage flow field comparisons

- Wake shape and size compare well with experiment
- **URANS** shows S-shaped wake downstream of blade tip
- **HRLES** underpredicts velocity deficit inside wake



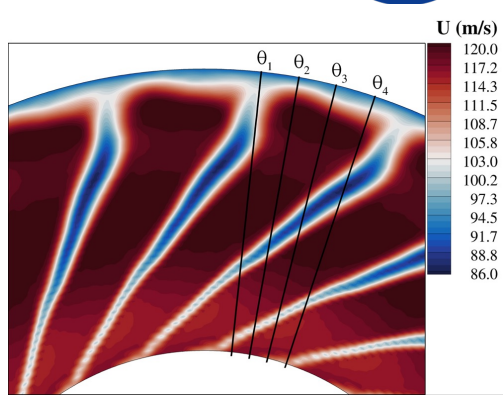


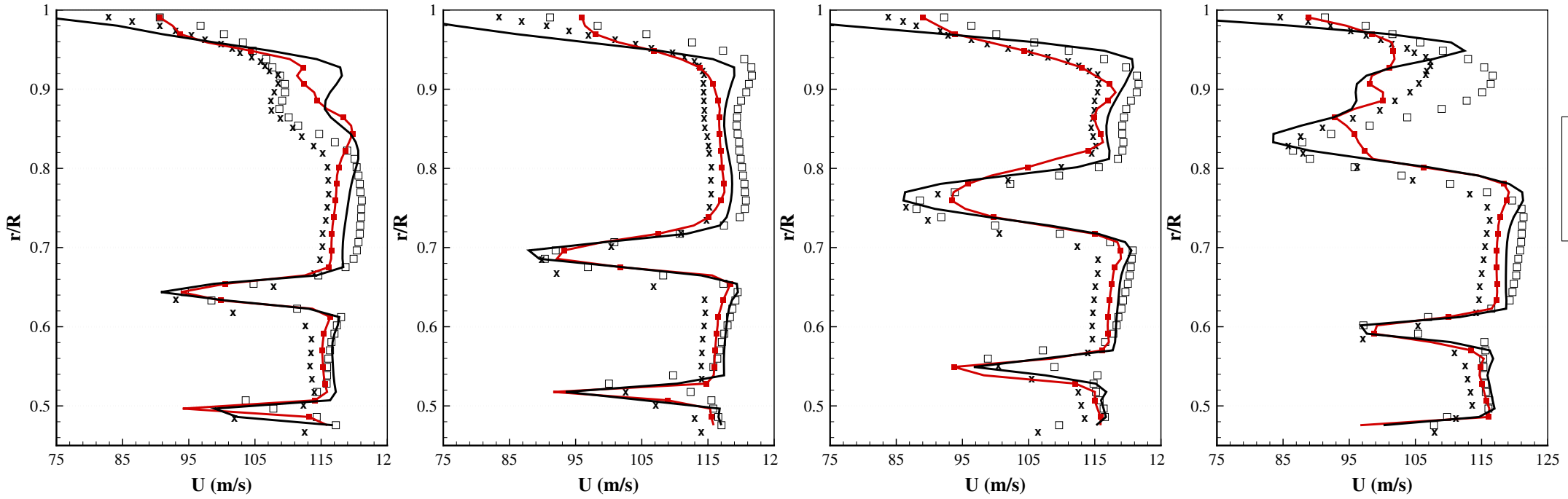
Hot-wire probe station 1 location in interstage region

Low-Speed Condition Results

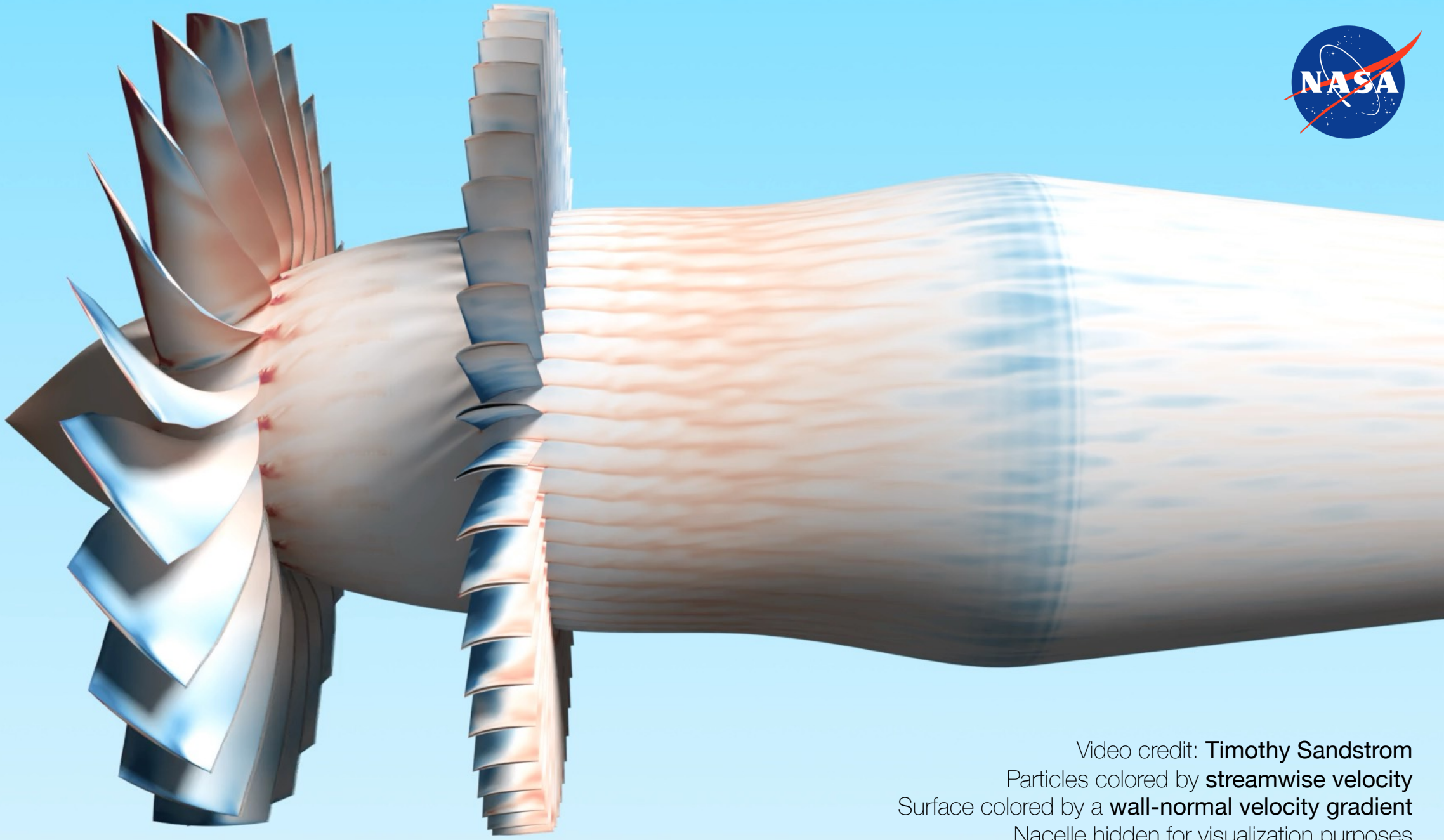
Radial line extractions of velocity profiles

- Both URANS and HRLES show streamwise velocities between the hot-wire probe and LDV data measured in experiment away from blade tip
- Region of highest variability is the blade tip region, where **HRLES outperforms URANS**
- HRLES, however, slightly **underpredicts blade wake velocity deficits**



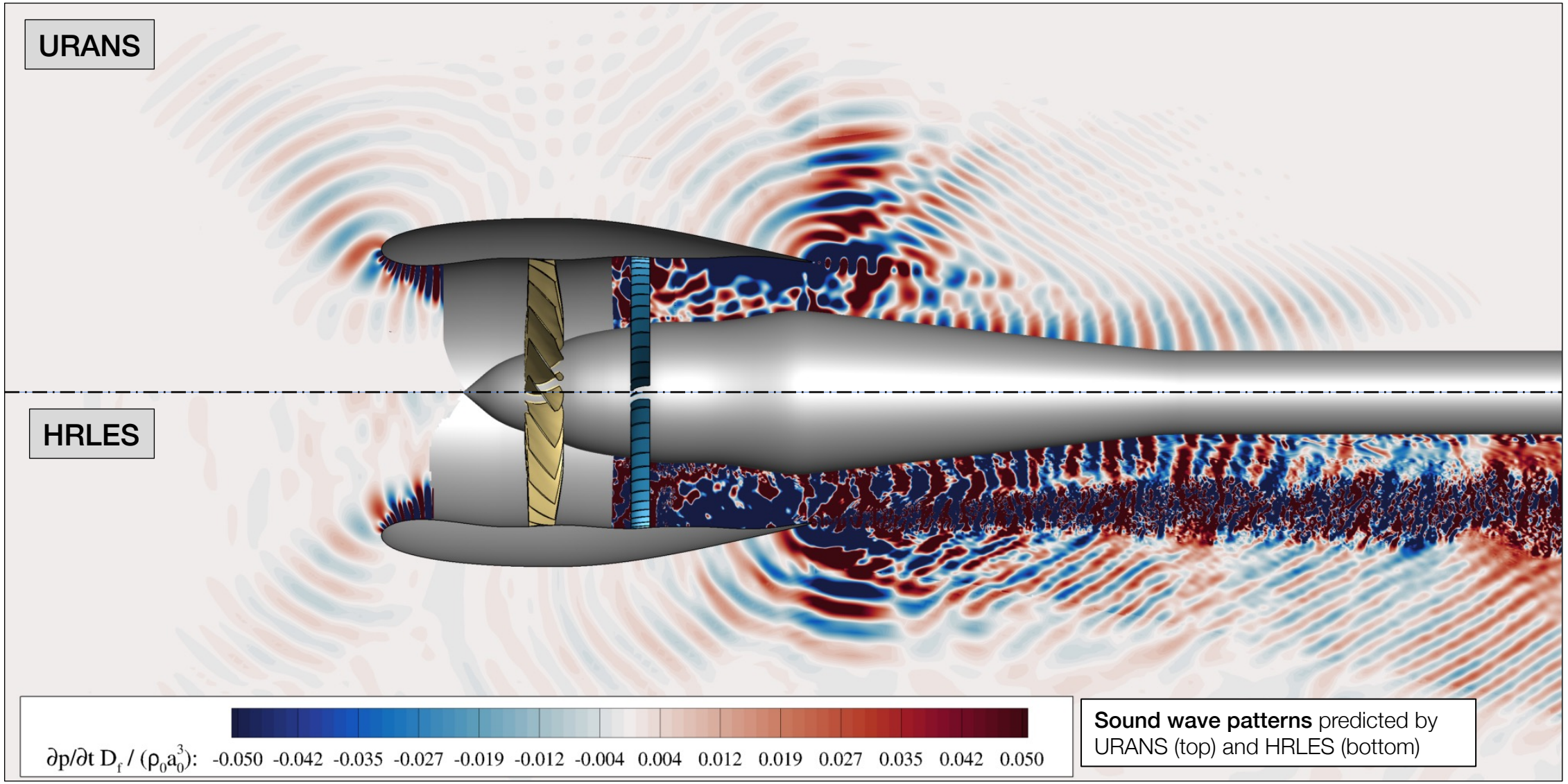


HRLES
7808 RPM
22” R4 Rotor
Baseline OGV



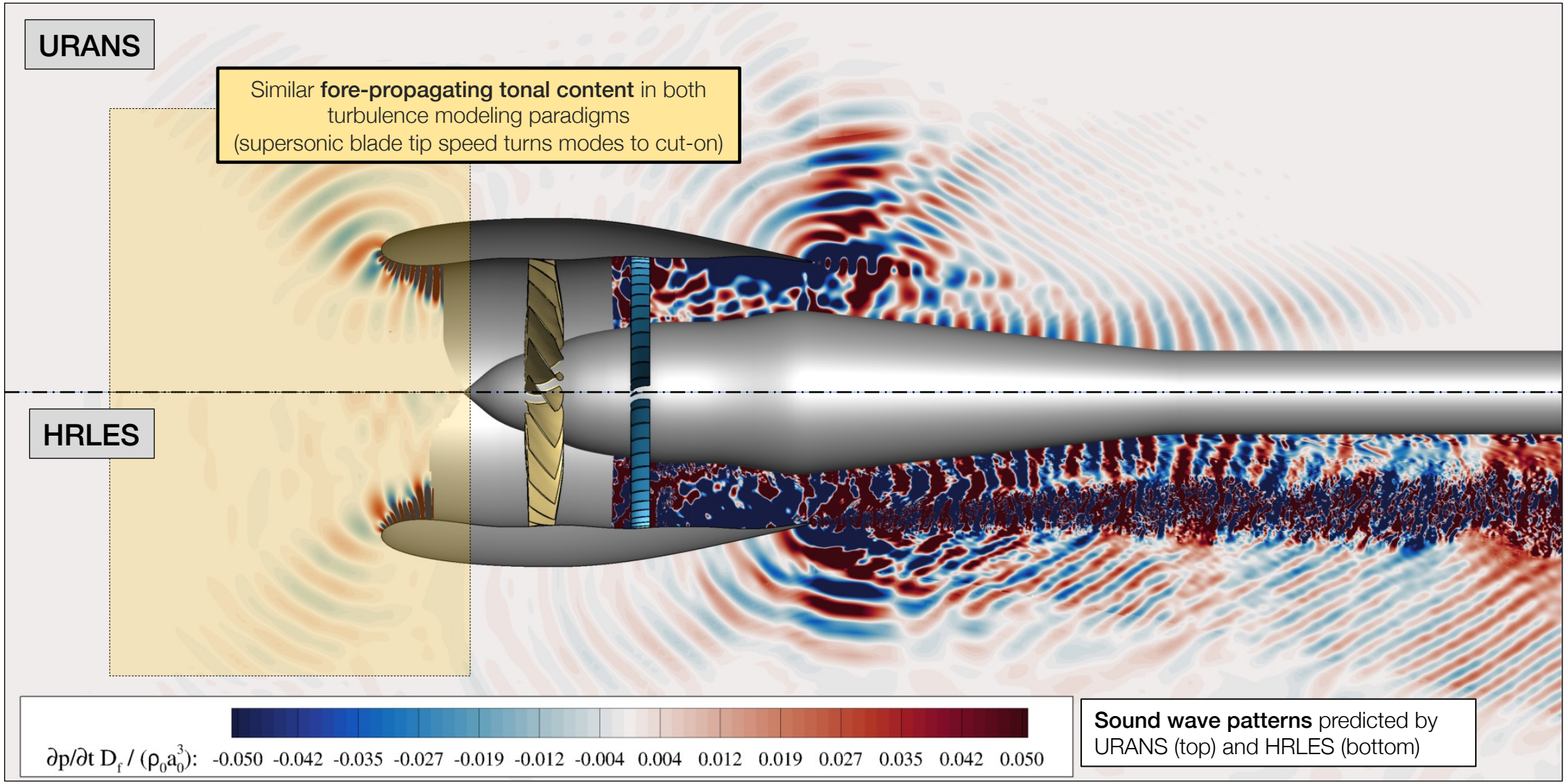
Video credit: **Timothy Sandstrom**
Particles colored by **streamwise velocity**
Surface colored by a **wall-normal velocity gradient**
Nacelle hidden for visualization purposes

High-Speed Condition Results

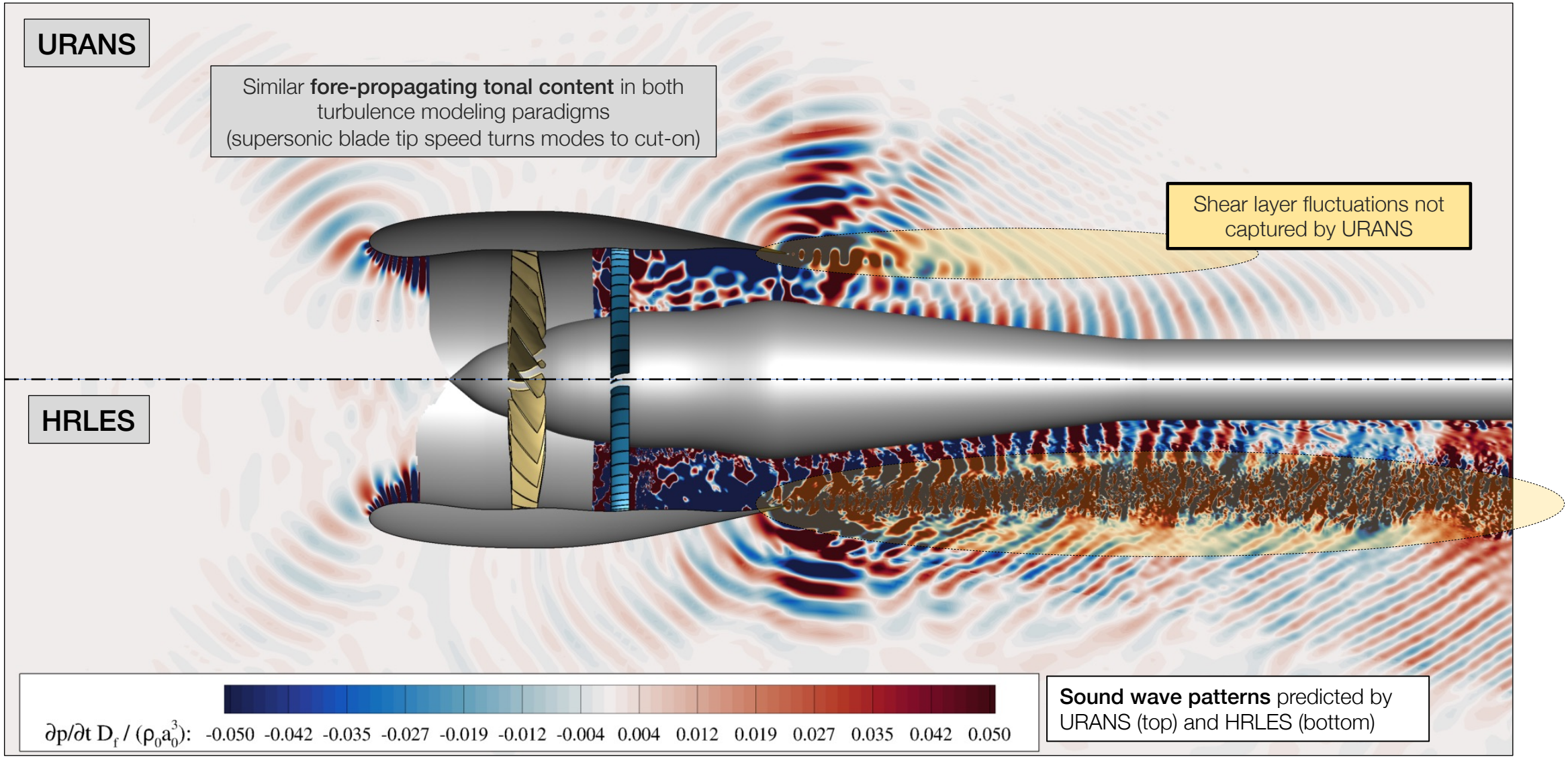


Sound wave patterns predicted by URANS (top) and HRLES (bottom)

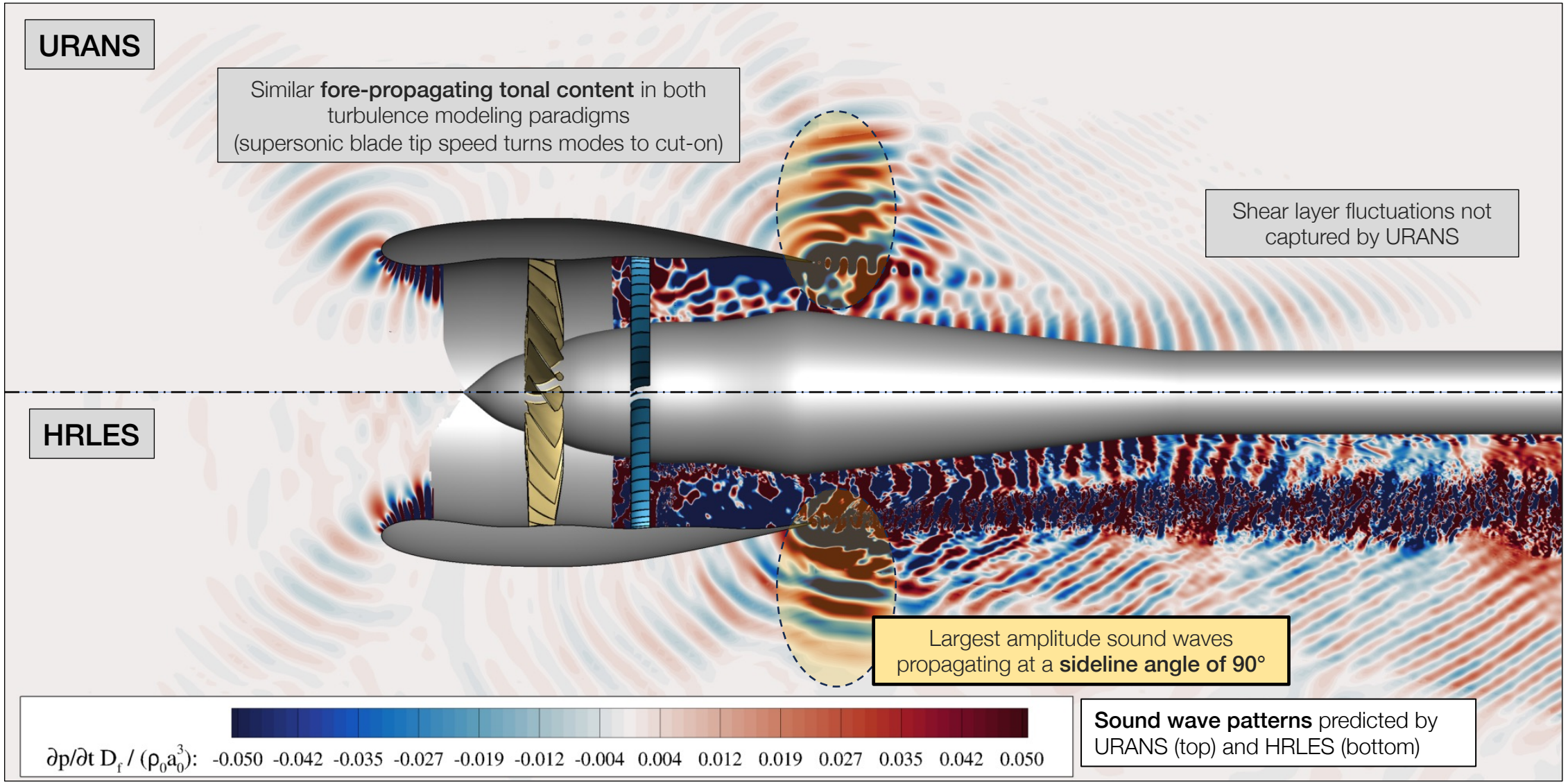
High-Speed Condition Results



High-Speed Condition Results



High-Speed Condition Results

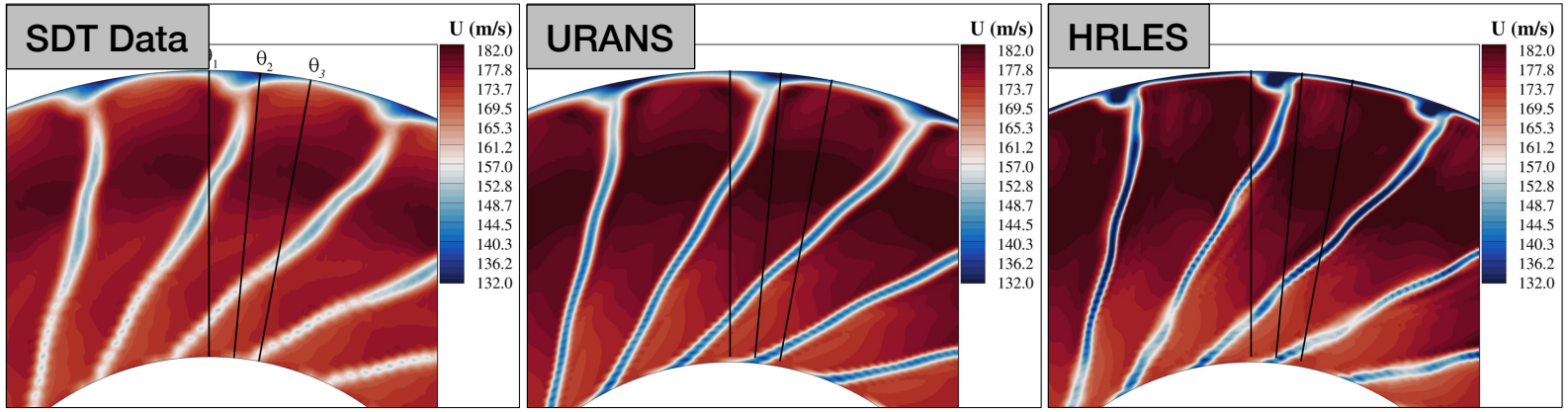


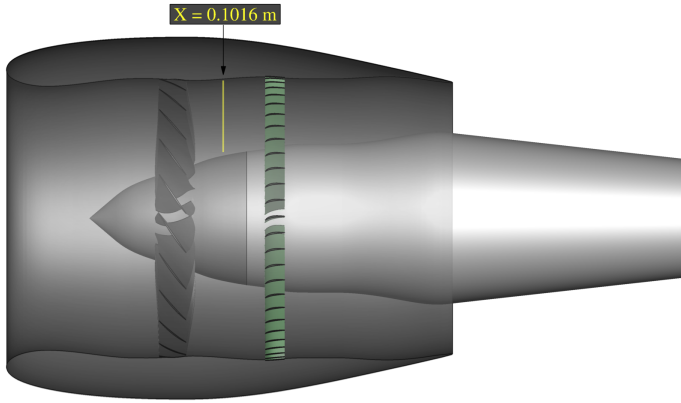
High-Speed Condition Results

Qualitative interstage flow field comparisons

- **URANS** mean velocity shows good agreement in the blade tip
- **HRLES** tip vortex trails behind blade wake, and is confined to a smaller region

Mean Axial Velocity



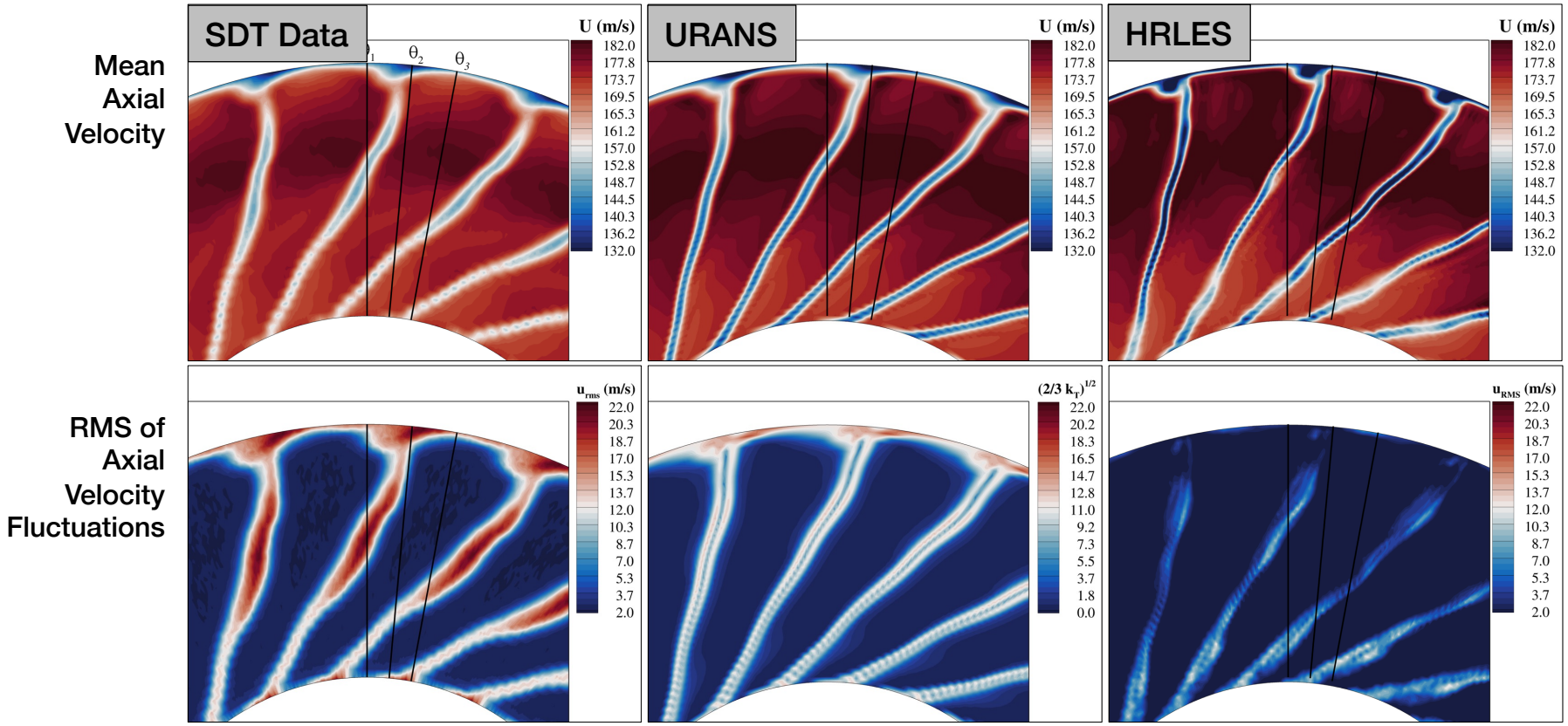


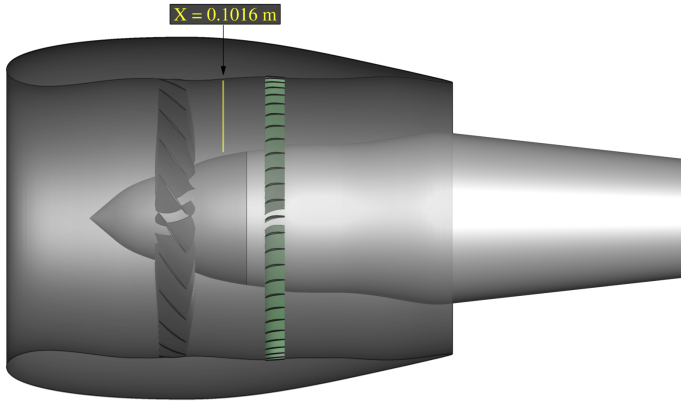
Hot-wire probe station 1 location in interstage region

High-Speed Condition Results

Qualitative interstage flow field comparisons

- **URANS** mean velocity shows good agreement in the blade tip
- **HRLES** tip vortex trails behind blade wake, and is confined to a smaller region
- Both methods unable to capture axial velocity fluctuations in the blade wake



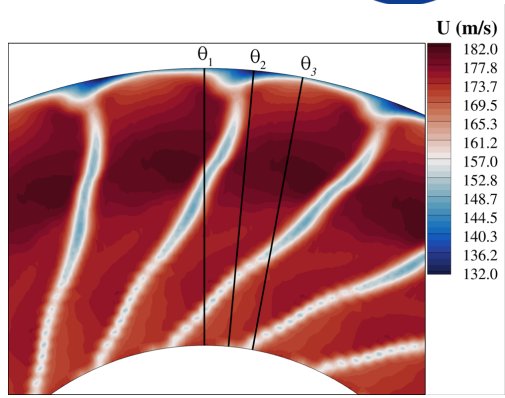


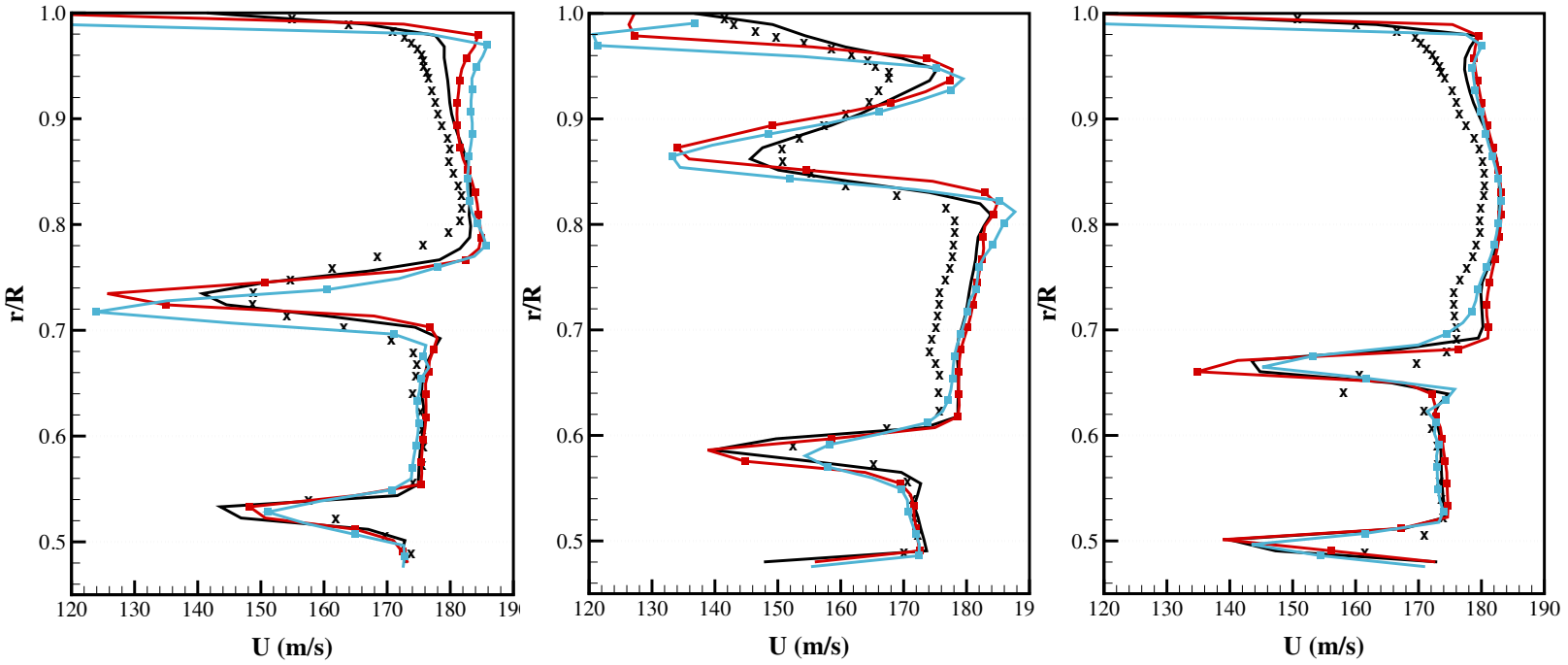
Hot-wire probe station 1 location in interstage region

High-Speed Condition Results

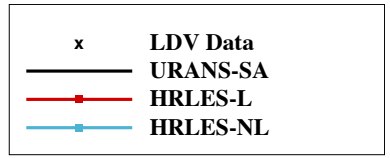
Radial line extractions of velocity profiles

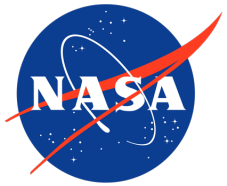
- Velocity profiles follow experimental data trends closely
- Both URANS and HRLES tend to over-predict wake velocity deficit
- Complex blade tip flow is not well captured by either model, but **URANS shows stronger agreement with experimental mean flow**





Mean Axial Velocity at hot-wire station 1





Contra Rotating Open Rotor

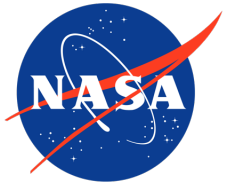
Unsteady RANS and Scale Resolving Simulations of Open Rotor Noise

Ercan Dumlupinar, Jeffrey A Housman, Gaetan K Kenway, Cetin C Kiris

doi.org/10.2514/6.2023-0028

Speaker: Ercan Dumlupinar

Outline



The following is an outline of this subsection

- Introduction
  - Motivation and Objective
  - Experimental Setup Overview
- Methodology
  - Numerical methods and turbulence treatments
  - Mesh generation, and surface triangulation
- Results
  - Sensitivity study
  - Low-speed condition
  - High-speed condition

Finally, the conclusion and acknowledgements

Introduction

Open rotor propulsion system is a potential candidate for future commercial transport aircraft

- Offering substantial improvements in fuel efficiency
- Significant reduction of CO_2 emission

NASA's aeronautics vision for aviation in the 21st century encompasses subsonic transport

- Targeting the next-generation propulsor development for a 5 to 10% fuel burn reduction and a 4 EPNdB noise reduction

The biggest drawback is the noise emission

  - The directional noise may increase up to 30 dB

The goal of the present work is to investigate the complex noise generation mechanisms using LAVA with a computationally efficient sliding mesh approach



CROR installed in 9 by 15 ft Low Speed Acoustic Wind Tunnel(*)

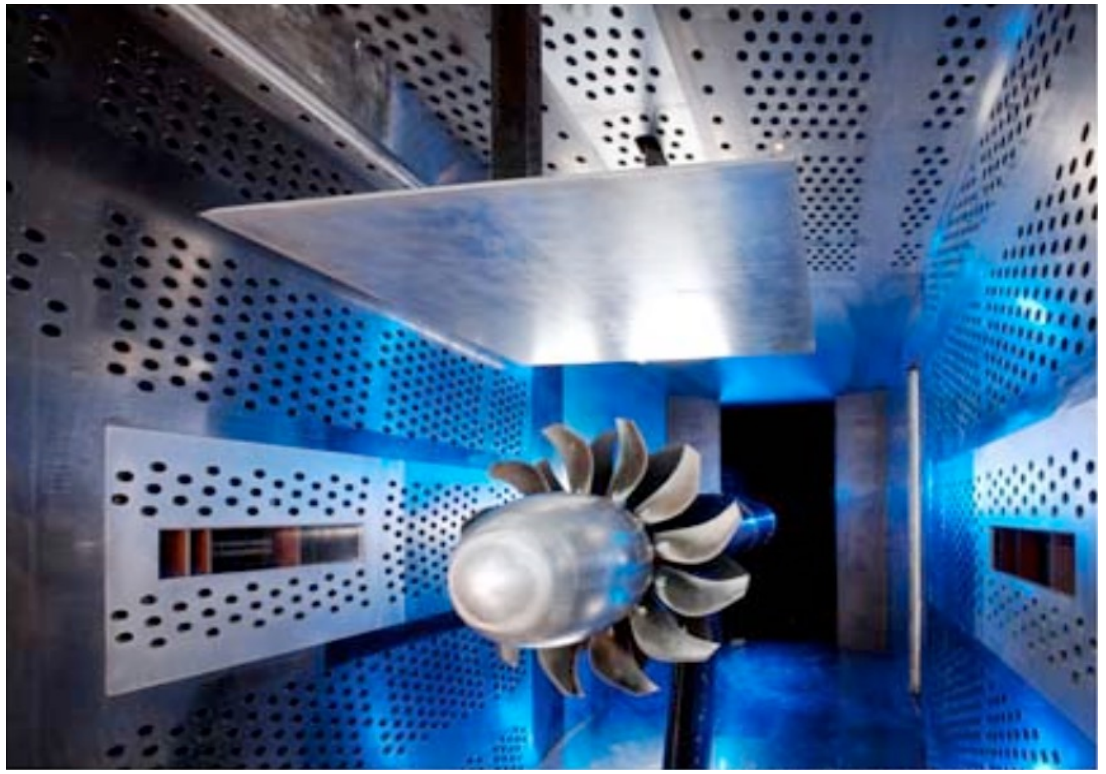
(*)Stephens, D. B., "*Data Summary Report for The Open Rotor Propulsion Rig Equipped with F31/A31 Rotor Blades*", NASA/TM-2014-216676, 2014.

Experimental Setup for both Low- and High-Speed Conditions



CROR installed in 9 by 15 ft Low Speed Acoustic Wind Tunnel(*)

- Blade pitch angles are 40.1 & 40.8 degrees
- Mach 0.2, rotating at a constant 6303 RPM (corrected RPM)
- All data recorded sound pressure spectral densities (PSDs)
- Total 18 microphone stations, 1.52 m radially away from CROR center

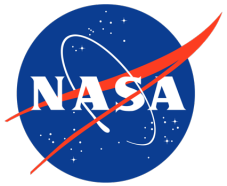


CROR installed in 8 by 6 ft SWT with Kulite plate above (*)

- Blade pitch angles are 64.4 & 61.8 degrees
- Mach 0.78, rotating at a constant 6848 RPM (corrected RPM)
- All recorded data were processed into narrowband sound pressure level
- Total of 17 Kulite at five different vertical stations

(*)Stephens, D. B., "*Data Summary Report for The Open Rotor Propulsion Rig Equipped with F31/A31 Rotor Blades*", NASA/TM-2014-216676, 2014.

Numerical Schemes

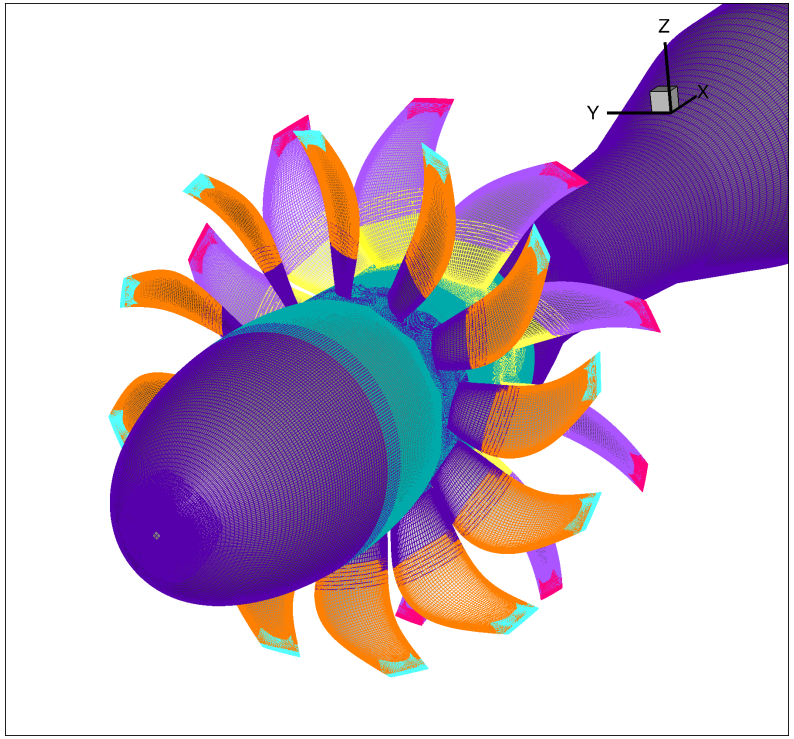


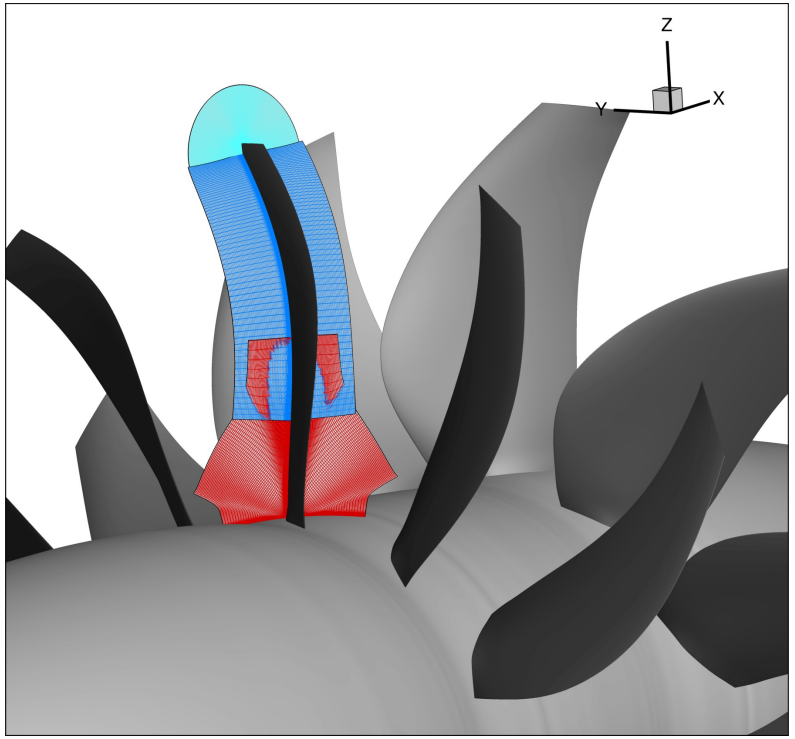
The Launch, Ascent, and Vehicle Aerodynamics (LAVA) computational framework is used for all computational studies shown in this work

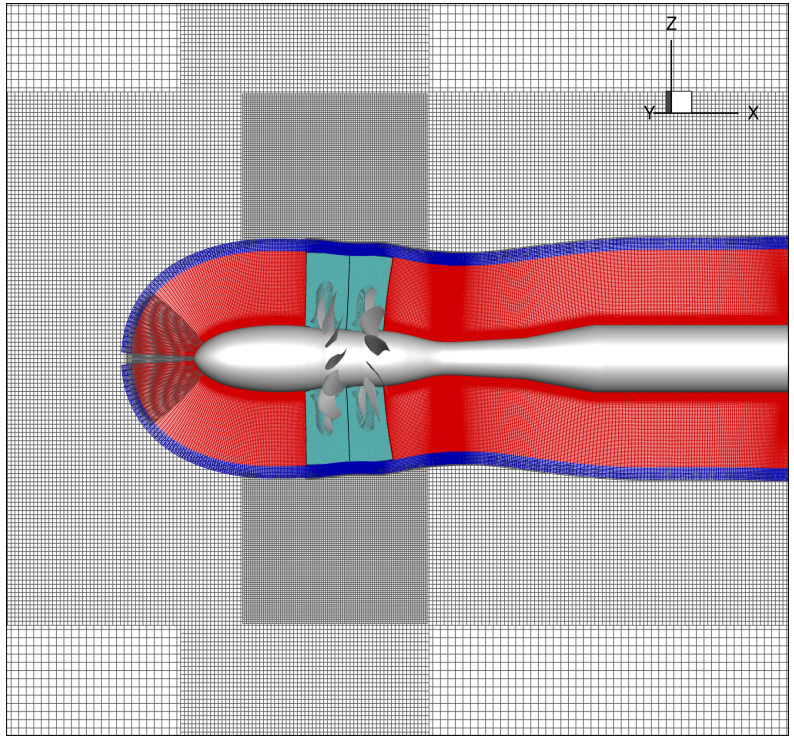
- Structured curvilinear overset grid solver
- A third-order modified Roe scheme for the nominal takeoff condition
- A modified third-order upwind scheme with a local shock sensor based WENO limiter along with the Ducros sensor for the cruise condition
- Two turbulence closure treatments – URANS and HRLES
  - SA-neg with RC and QCR2000 corrections
  - ZDES 2020 with enhanced protection, f_d
- An implicit second-order backward differencing

Overset Grid System

- Near body meshes are generated utilizing Chimera Grid Tools (CGT) using script to build fully automated mesh for various flight conditions
- The octree-based overlapping off-body Cartesian grid is generated using built-in module in the LAVA framework
- Hole cutting and connectivity are performed using the modules within the LAVA framework for the overset grid system

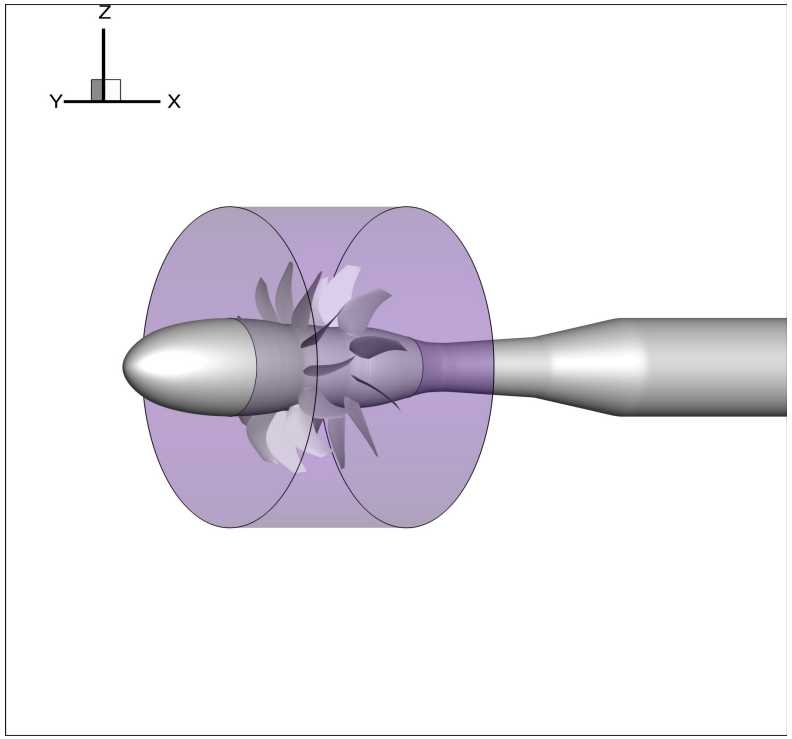


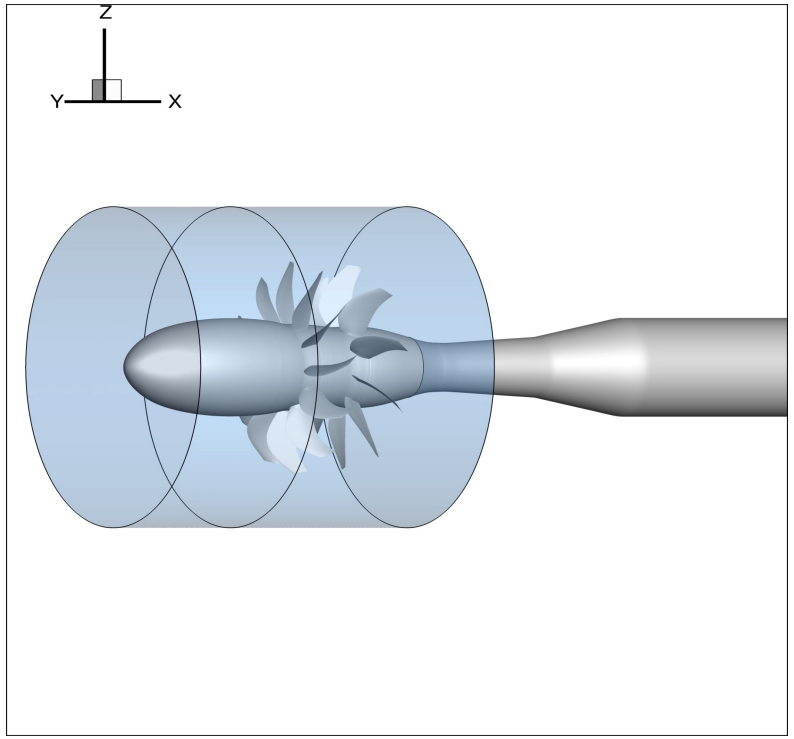


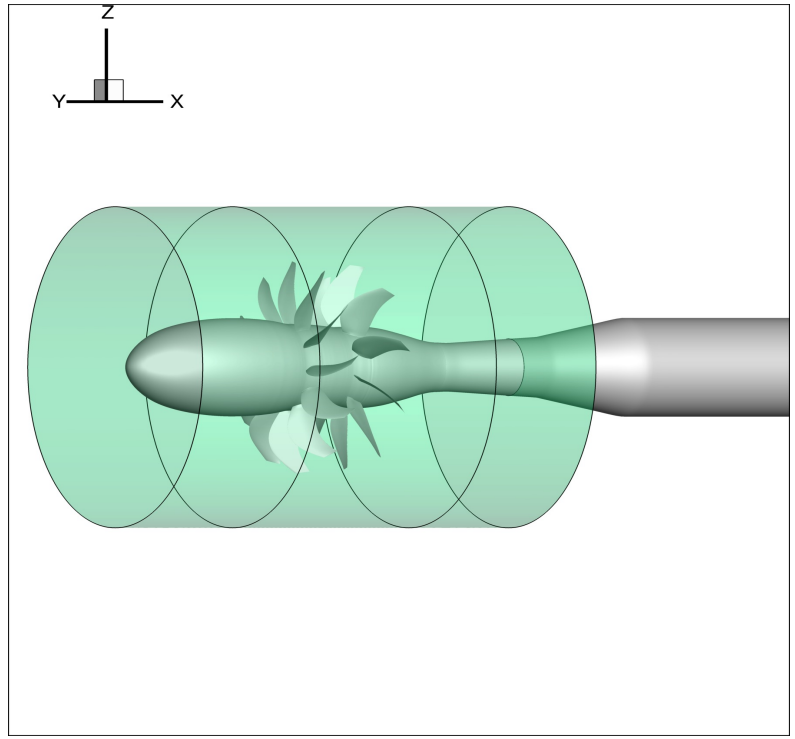


Acoustic Propagation Surfaces

- Three closed surface triangulations are generated to store unsteady CFD data for acoustic propagation sensitivity studies
- An edge length of 12 mm is used
- Triangulation is labeled with component IDs allowing various combinations of surfaces to be included in propagation







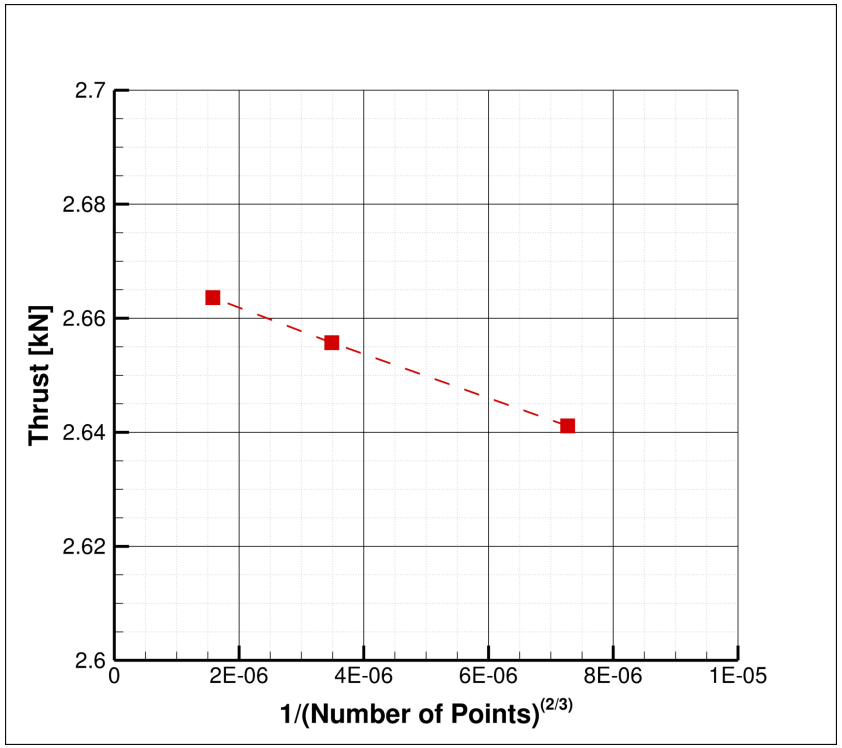
Grid Sensitivity Study using URANS

- A grid sensitivity study is conducted using a set of RANS (Reynolds-Averaged Navier-Stokes) based structured overset meshes, specifically 51M, 154M, and 502M meshes, under the nominal takeoff condition
- The asymptotic range has been reached
- For detailed aerodynamic and aeroacoustics comparisons the medium-level grid system is used with modifications

Grid Level	Grid Metric		
	Refinement Factor	Stretching Ratio	Viscous Wall Spacing [m]
Coarse	1.00	1.25	3.00E-6
Medium	1.50	1.15	2.00E-6
Fine	2.25	1.09	1.33E-6

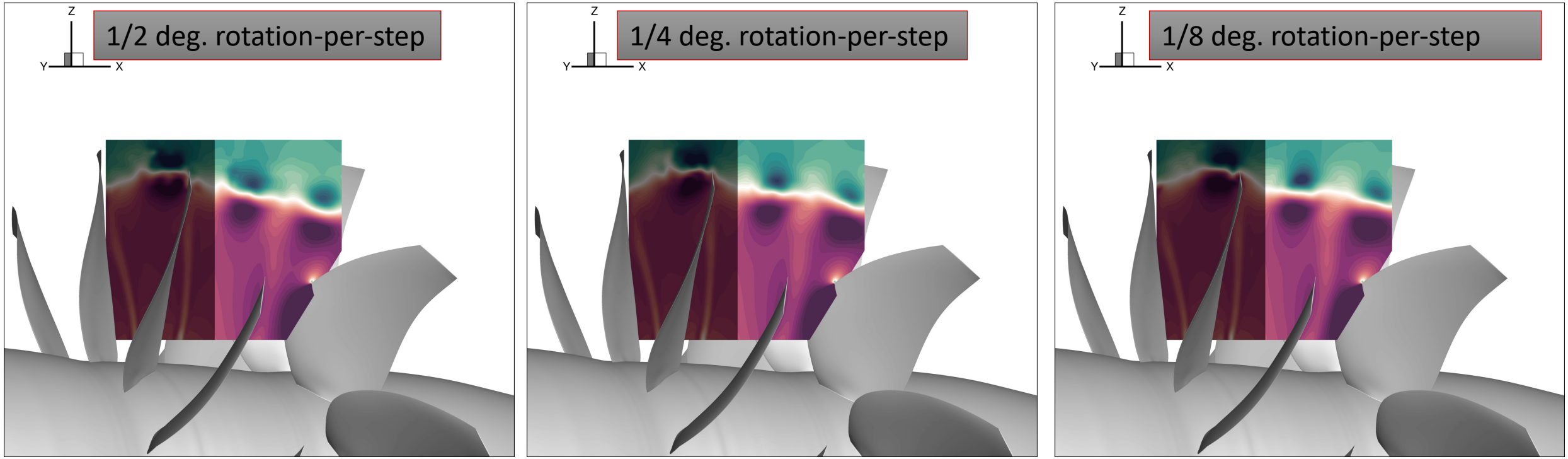
Apparent Order, P	Approx. Error [%]	Extrap. Error [%]	GCI_{12} [%]	GCI_{23} [%]	Ratio $\frac{GCI_{23}}{r^P * GCI_{12}}$
1.785	0.296	0.289	0.362	0.734	1.003

Convergence properties of total thrust for low-speed configuration



Time Sensitivity Study using HRLES

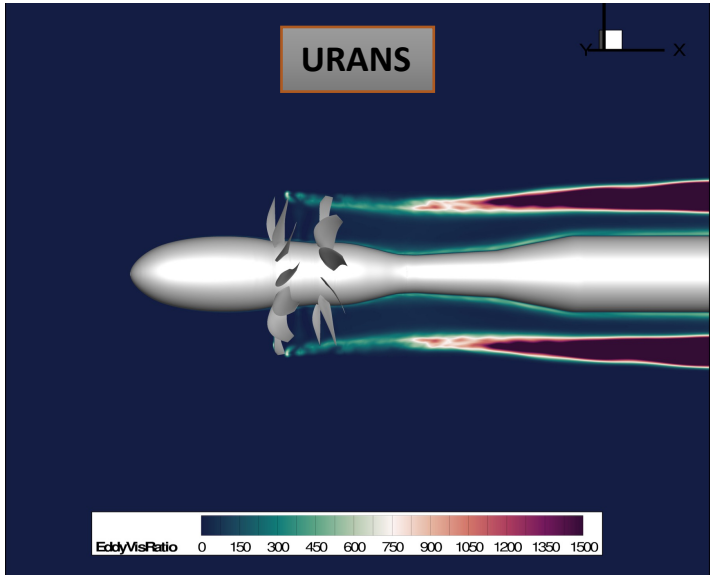
- In order to identify the optimal physical time-step, a thorough time-step sensitivity study for HRLES is conducted, employing a modified version of the medium level mesh, and examines time-steps associated with 1/2, 1/4, and 1/8 degrees rotation-per-step

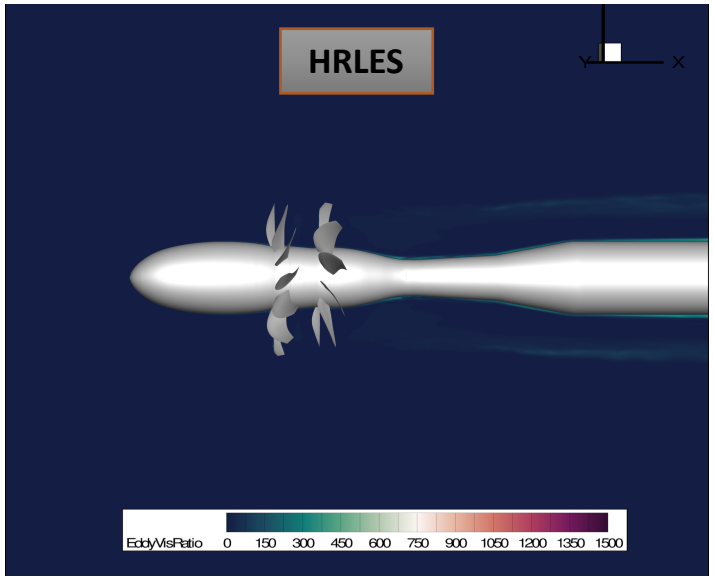


Side by side comparison of velocity magnitude contours at constant axial and circumferential cut-planes

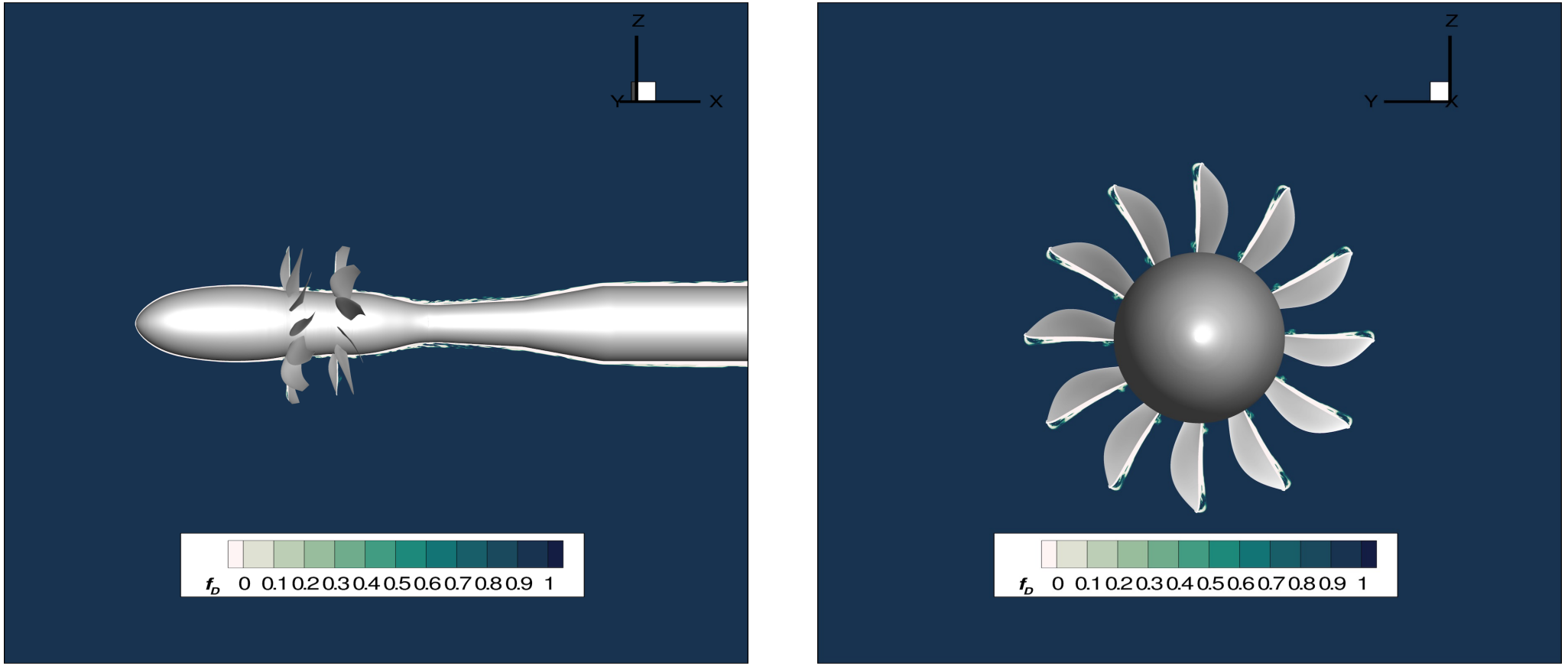
Nominal Take-off Condition

- The grid system has 321 zones, containing approximately 192 million grid points
- A third-order modified Roe scheme, with an implicit second-order backward differencing
- Two turbulence closure treatments – URANS and HRLES
  - **SA-neg** with **RC** and **QCR2000** corrections
  - **ZDES 2020** with enhanced protection
- Zonal Detached Eddy Simulation (ZDES) 2020 Enhanced Protection, f_d
  - RANS mode when $f_d \sim 0$, LES mode when $f_d \sim 1$
- The time-averaged thrust load using URANS and HRLES are 4.6 and 6.1 percent larger than the measured thrust in the experiment. These discrepancies may be attributed to differences between the "as-built" rig and the CAD





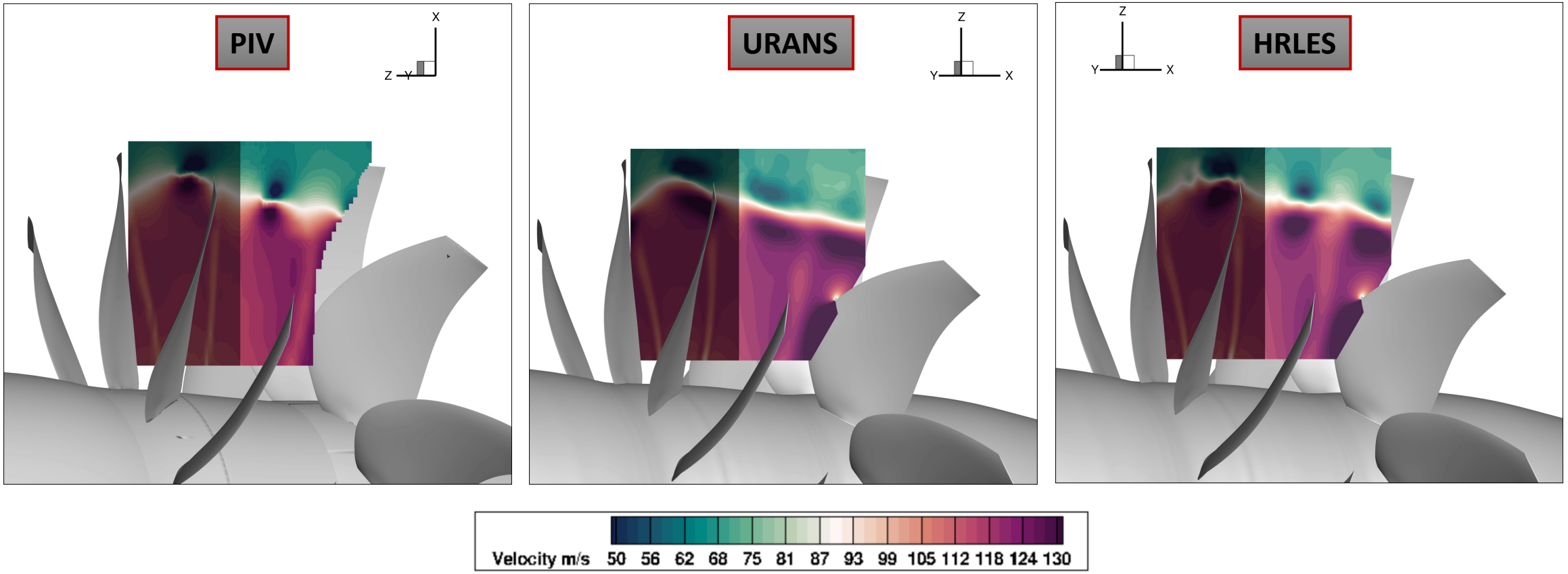
Nominal Take-off Condition



Contour plots of shielding function employed in HRLES, f_D, on constant a) y = 0 m, and b) x = 4.85 m

- The contour plots indicate that a RANS closure is employed inside the boundary layer around the hub and spanwise direction over the suction side of the blade, where f_d is approximately 0.0
- The LES mode is activated, f_d = 1.0, away from the boundary layer without an observable spurious switching back to URANS mode

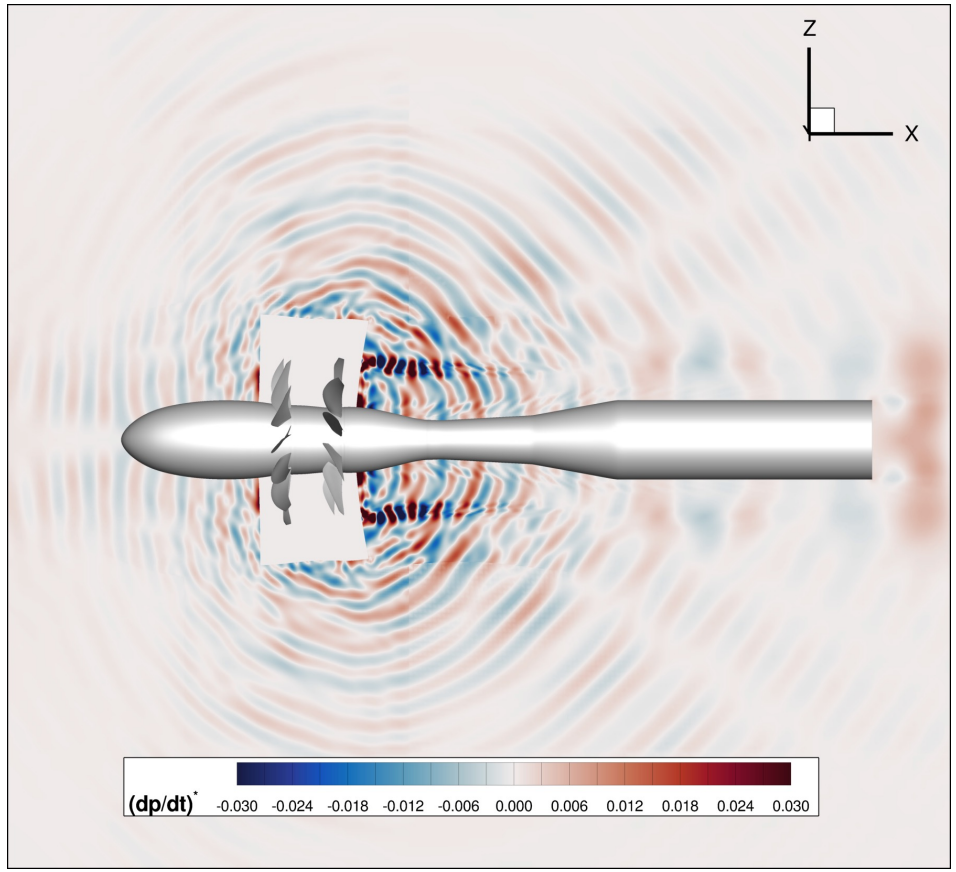
Nominal Take-off Condition

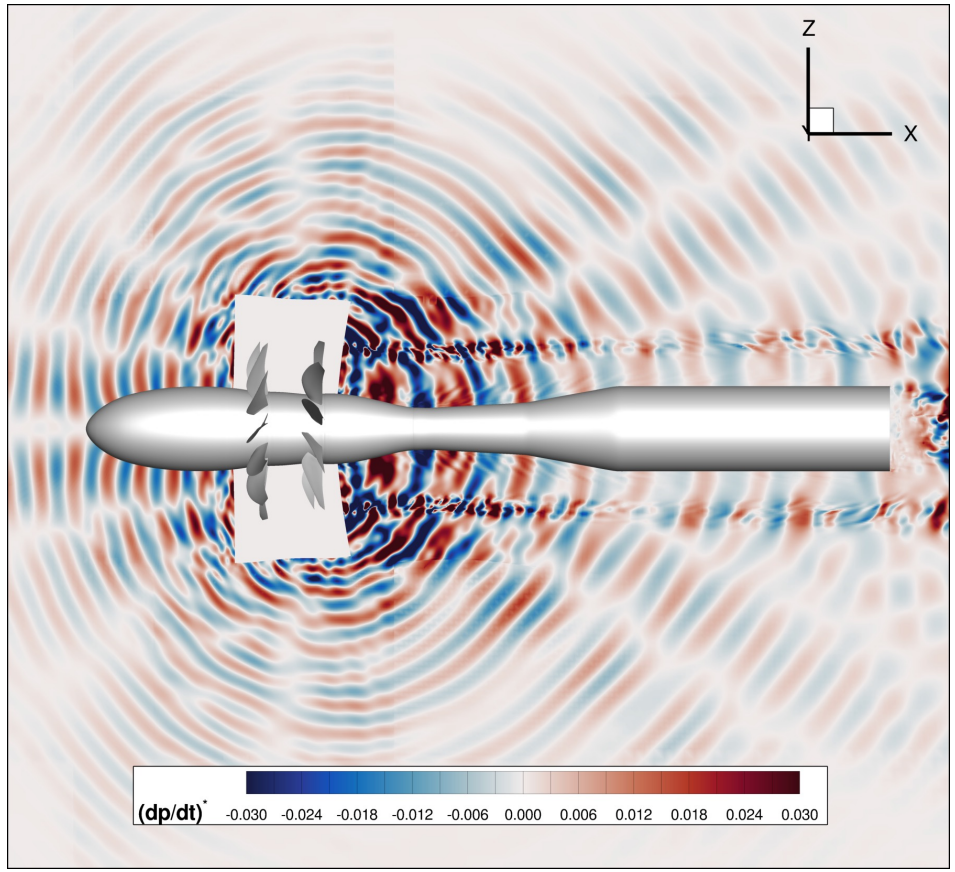


Side by side comparison of velocity magnitude contours at constant axial and circumferential cut-planes

- The location and strain of tip vortices and wake from the forward blades are well captured with the Hybrid RANS/LES compared to URANS

Nominal Take-off Condition



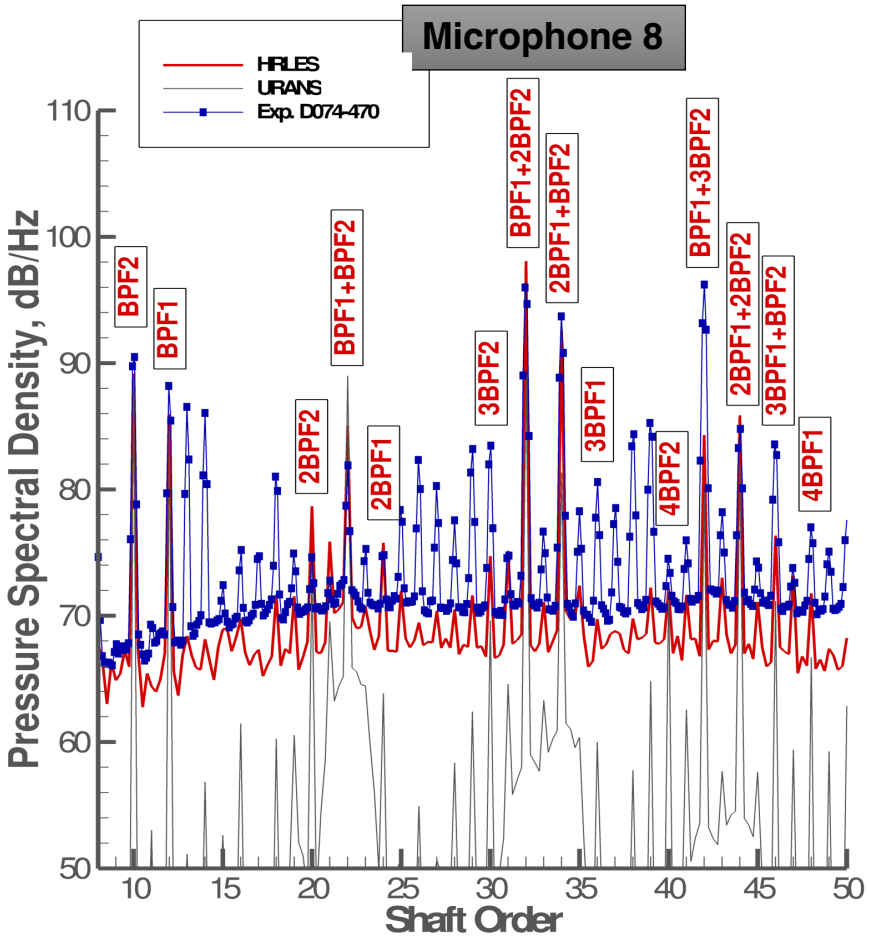


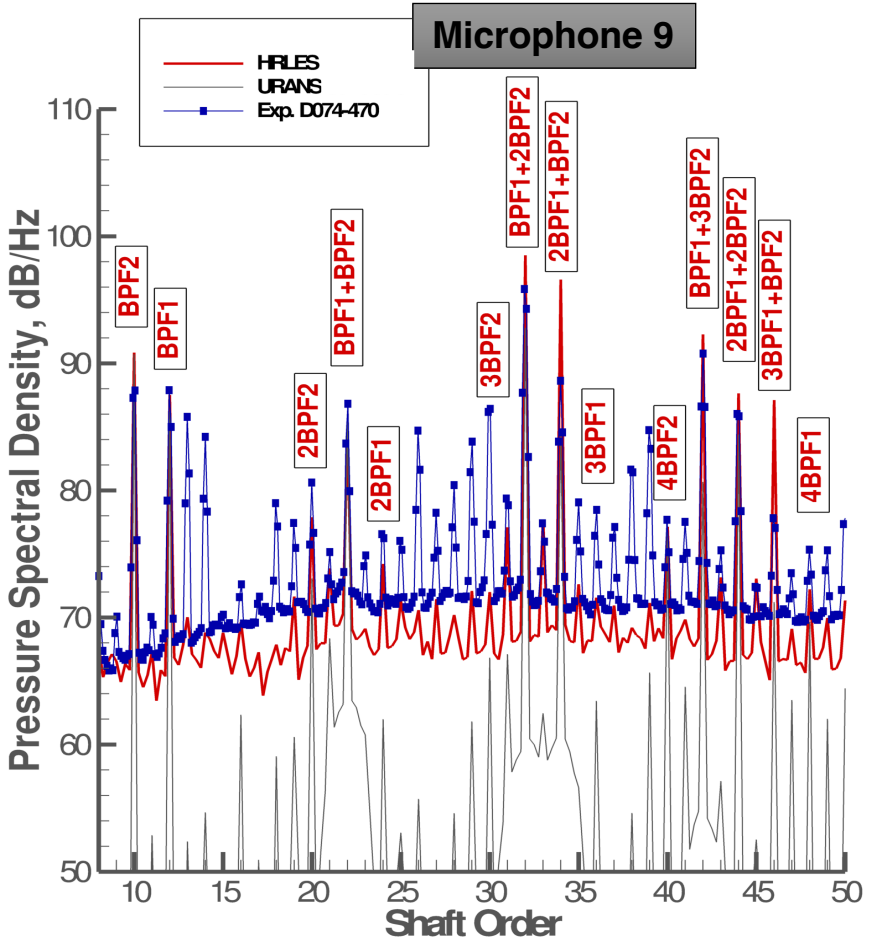
Figures present the time derivative of the normalized pressure field in a y = 0 cutting plane, using URANS (left) and HRLES (right) simulations

- There is a notable distinction between the two turbulence closure treatments in terms of their predictions of acoustic waves
- The limitations of URANS simulations become more evident when comparing narrow-band spectra

Nominal Take-off Condition

Microphone 8 and 9 are located 1.52 m radially away from the center of the aft and forward blade rows





Nominal Take-off Condition

Acoustic microphone geometric angles are from 17.6 to 140 degrees, positioned upstream to downstream of the propulsor at 18 stations

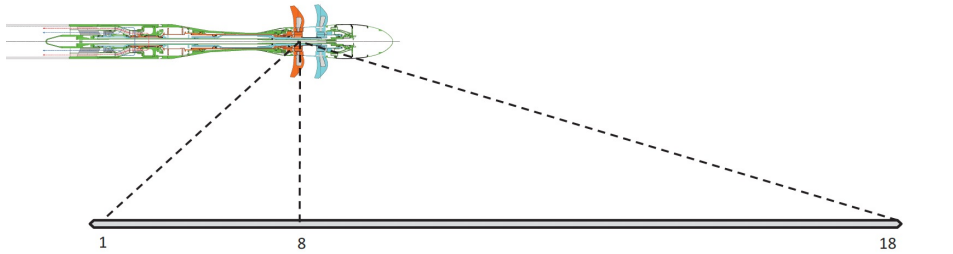
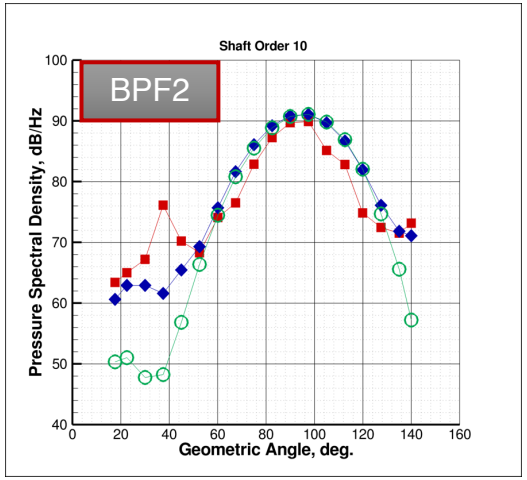
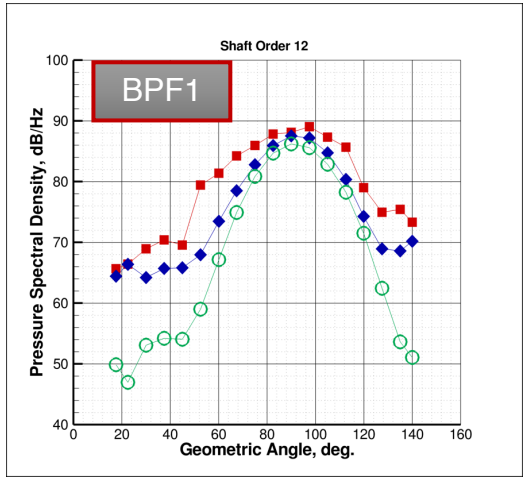
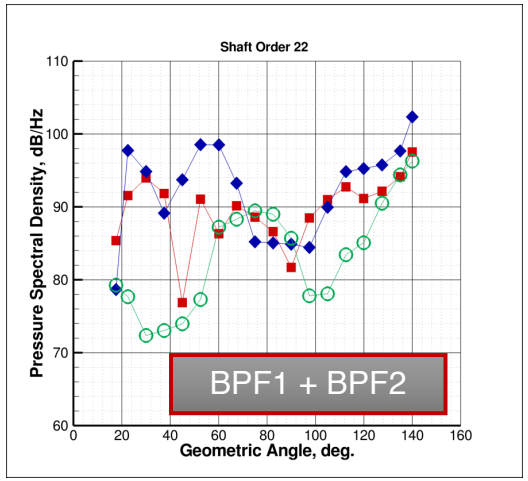


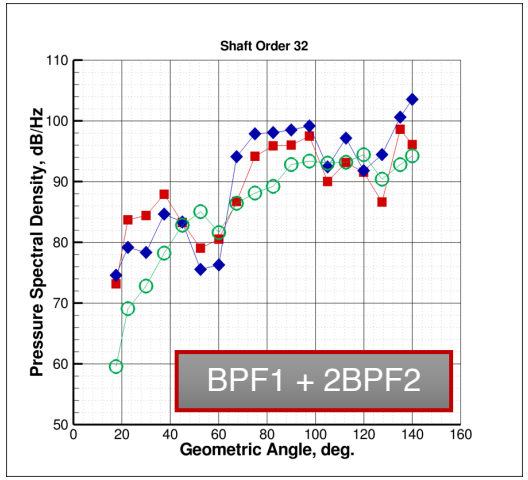
Diagram of microphone locations and respective geometric angles in the 9- by 15-ft LSWT

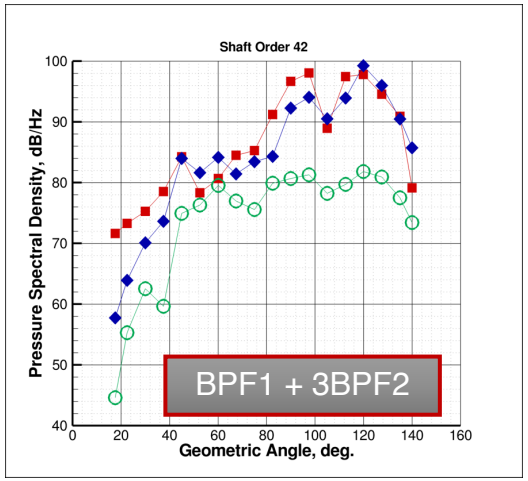






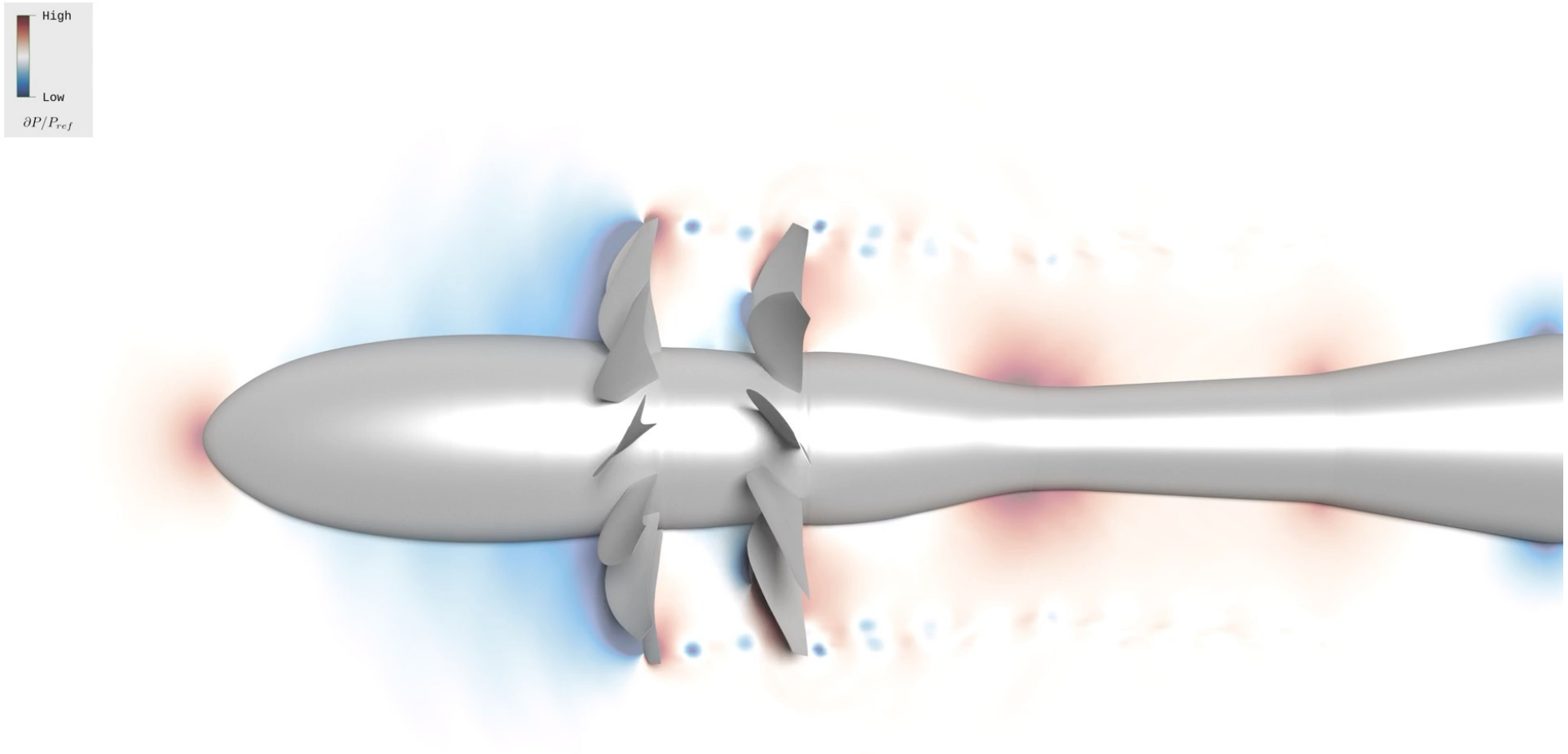






(*)Stephens, D. B., "*Data Summary Report for The Open Rotor Propulsion Rig Equipped with F31/A31 Rotor Blades*", NASA/TM-2014-216676, 2014.

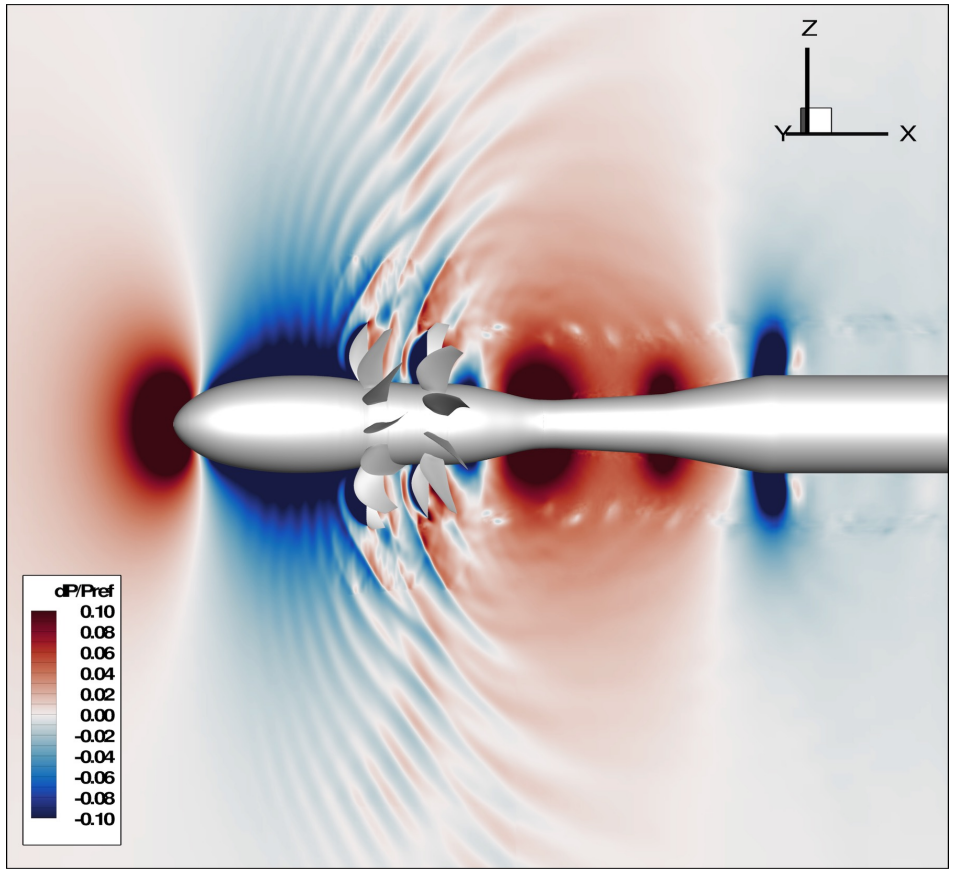
Nominal Take-off Condition



Video credit: **Timothy Sandstrom**

Cruise Condition

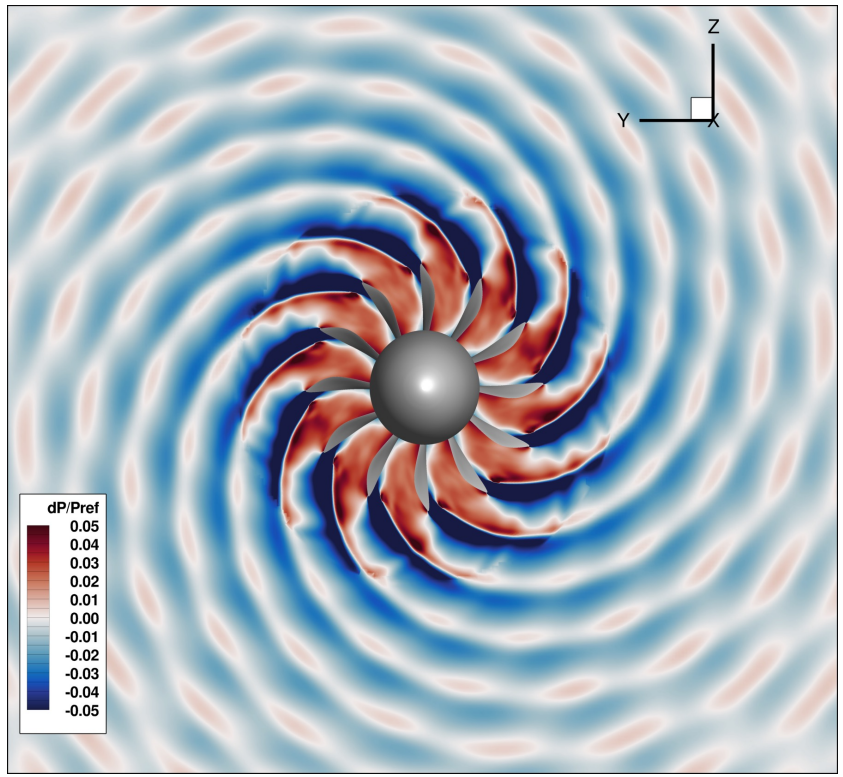
- The high-speed case has forward, and aft blade pitch angles of 64.4 and 61.8 degrees, rotating at a constant 6848 RPM at an inflow Mach number of 0.78
- The modified grid system has 321 zones, containing approx. 202 million grid points
- The time-averaged thrust load using URANS and HRLES are both 6.9 percent larger than the measured thrust in the experiment. As highlighted before, these discrepancies may be attributed to differences between the actual constructed rig and the Computer-Aided Design (CAD) representation



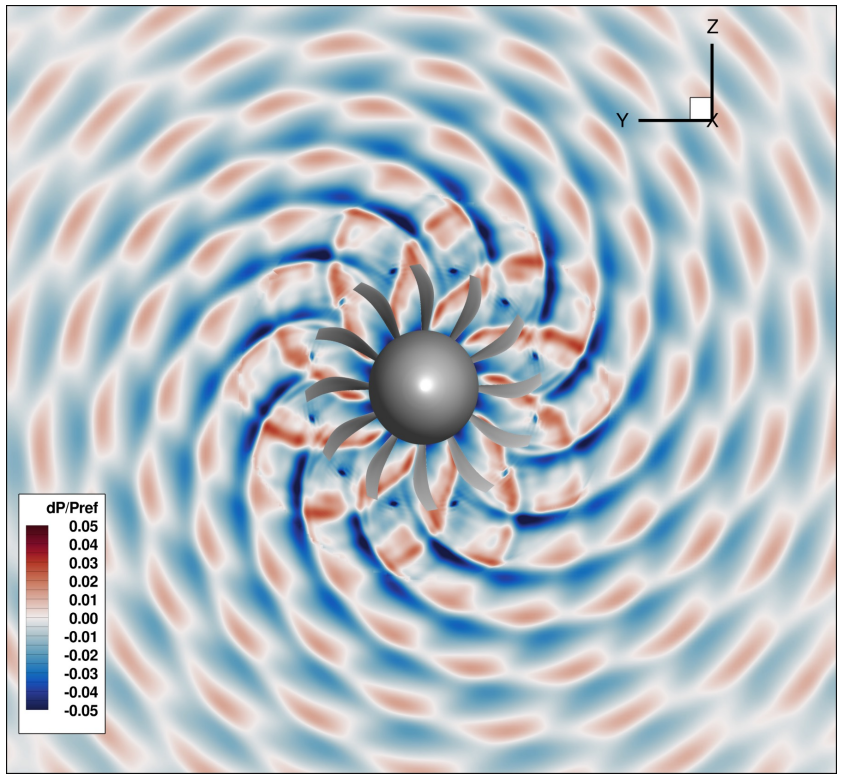
Normalized pressure contour plot for the cruise flight condition on a slice through the centerline of the hub

Cruise Condition

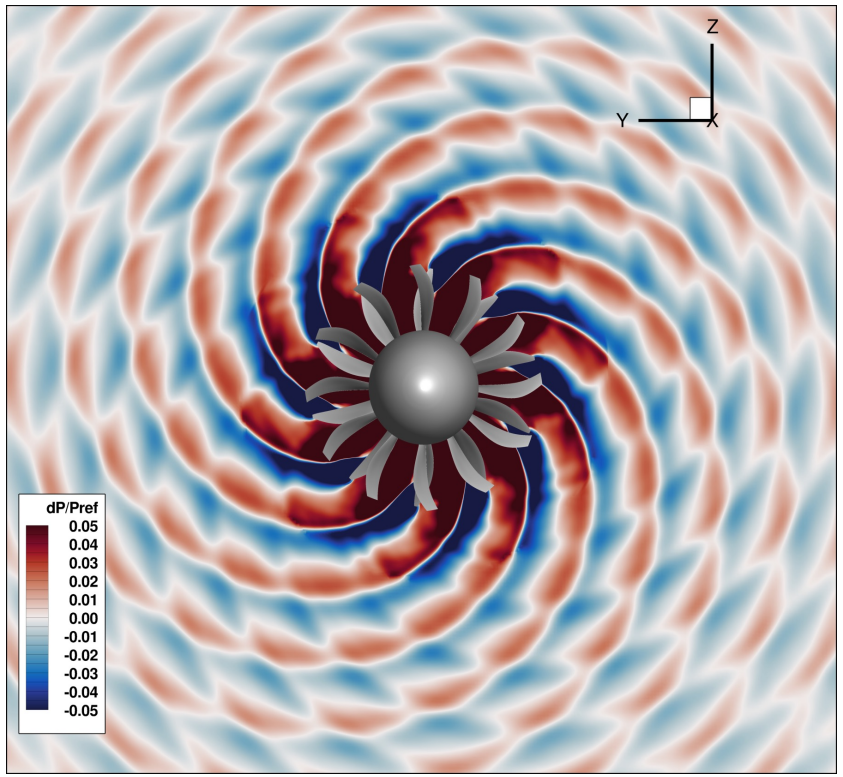
- The figures depict contour plots of the normalized pressure generated by HRLES on constant stream-wise slices through the forward rotor, between the two rotor rows, and the aft rotor, respectively
- The wave pattern through the forward blade set is dominated by clockwise rotation, while the aft blades exhibit a counter-clockwise rotation. There is a strong interaction observed between the rotor rows



Through the forward rotor row



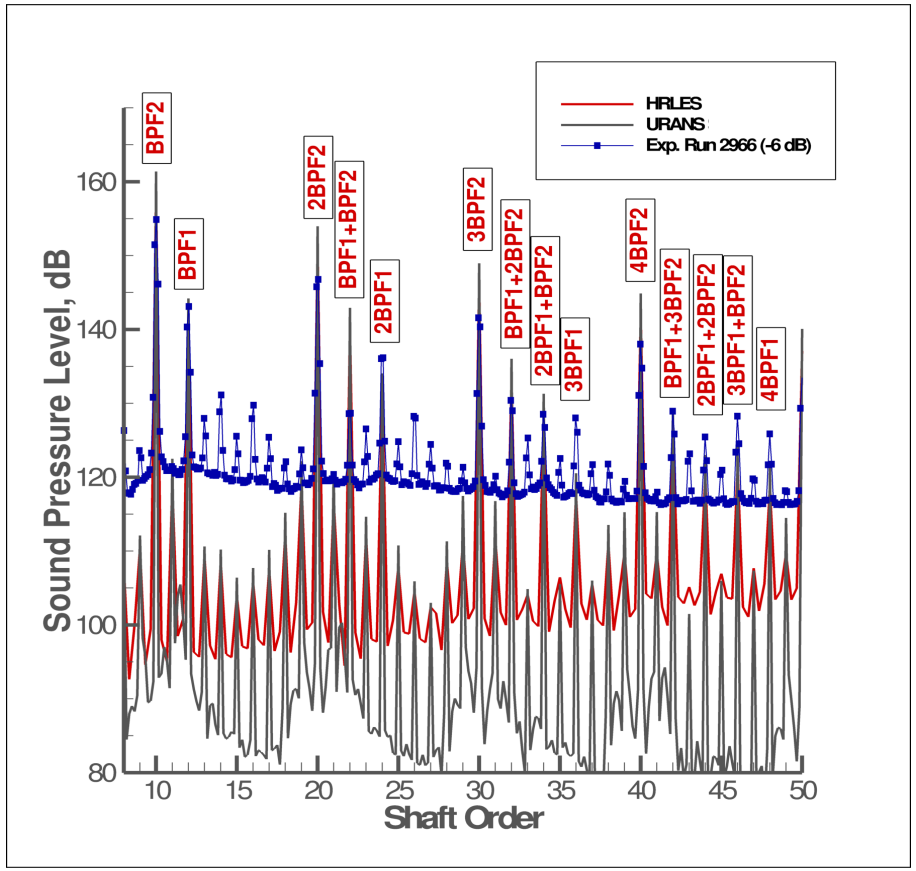
Between the two rotor rows

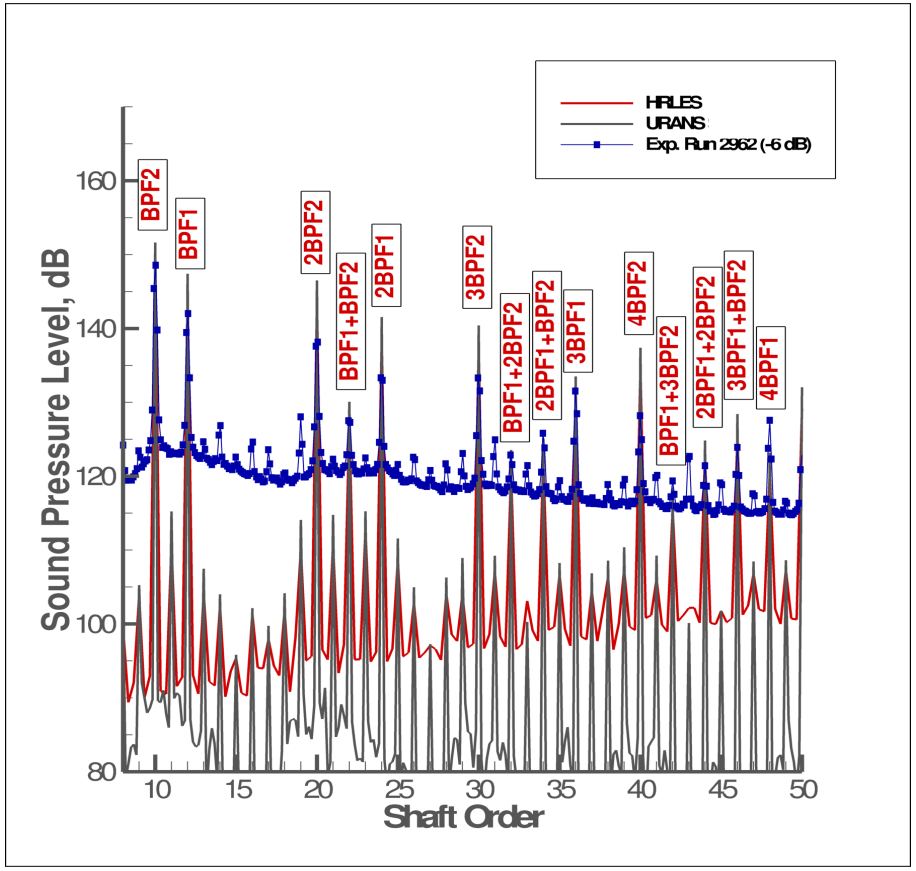


Through the aft rotor row

Cruise Condition

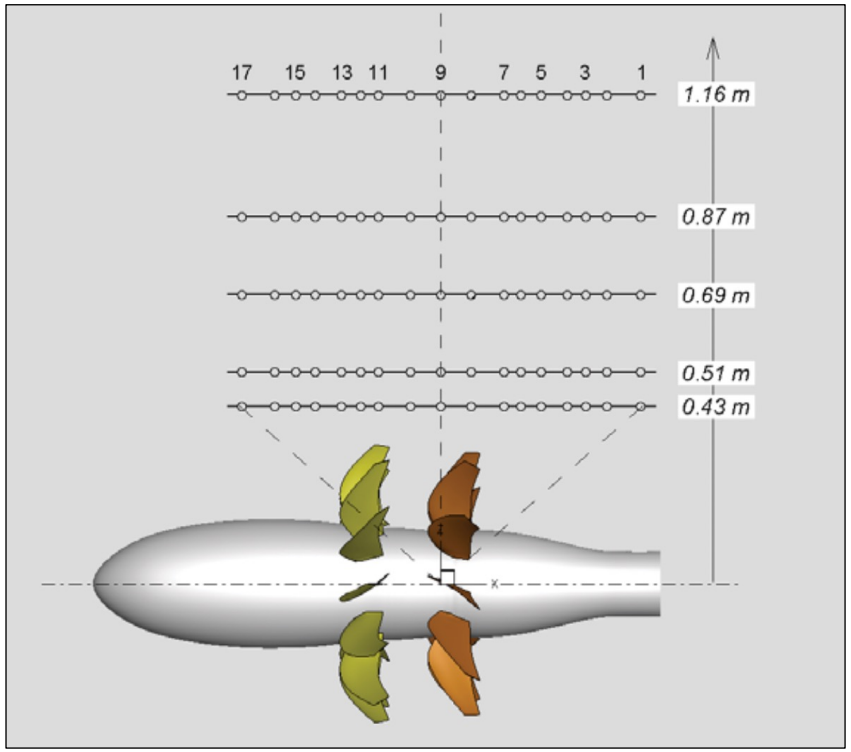
- Sound pressure level (SPL) spectrum at Kulite 9 located above the aft rotor at a vertical distance of 0.51 m (left) and 1.16 m (right)
- The broadband noise level measured in the experiment did not originate primarily from the CROR



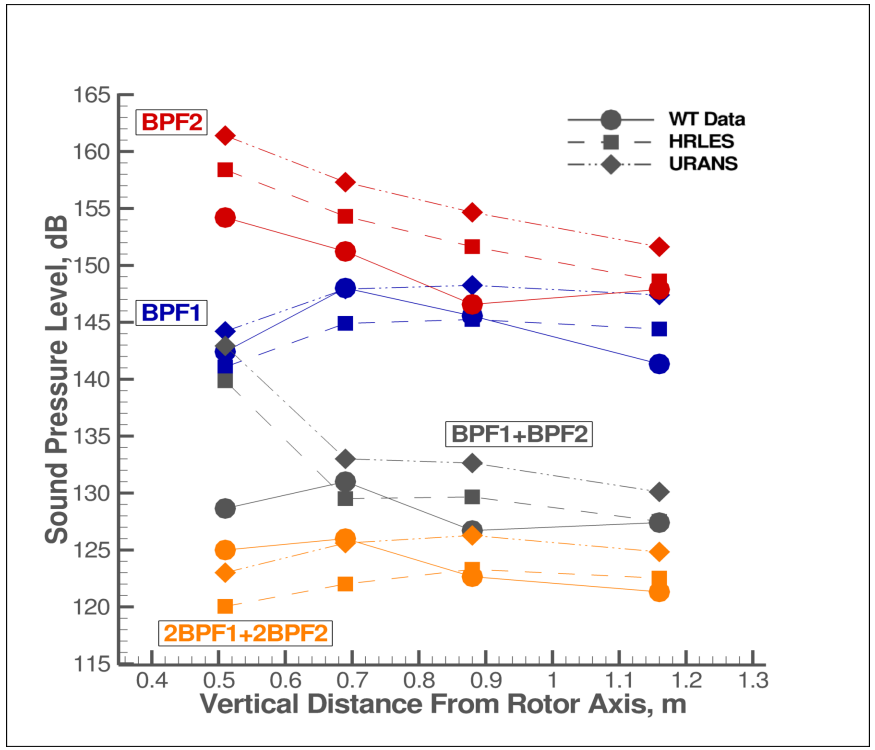


Cruise Condition

Figures show the narrow-band spectrum for the individual and interaction tones, plotted as a function of the vertical distance from the hub centerline, comparing the computational values with the measured values at Kulite 9



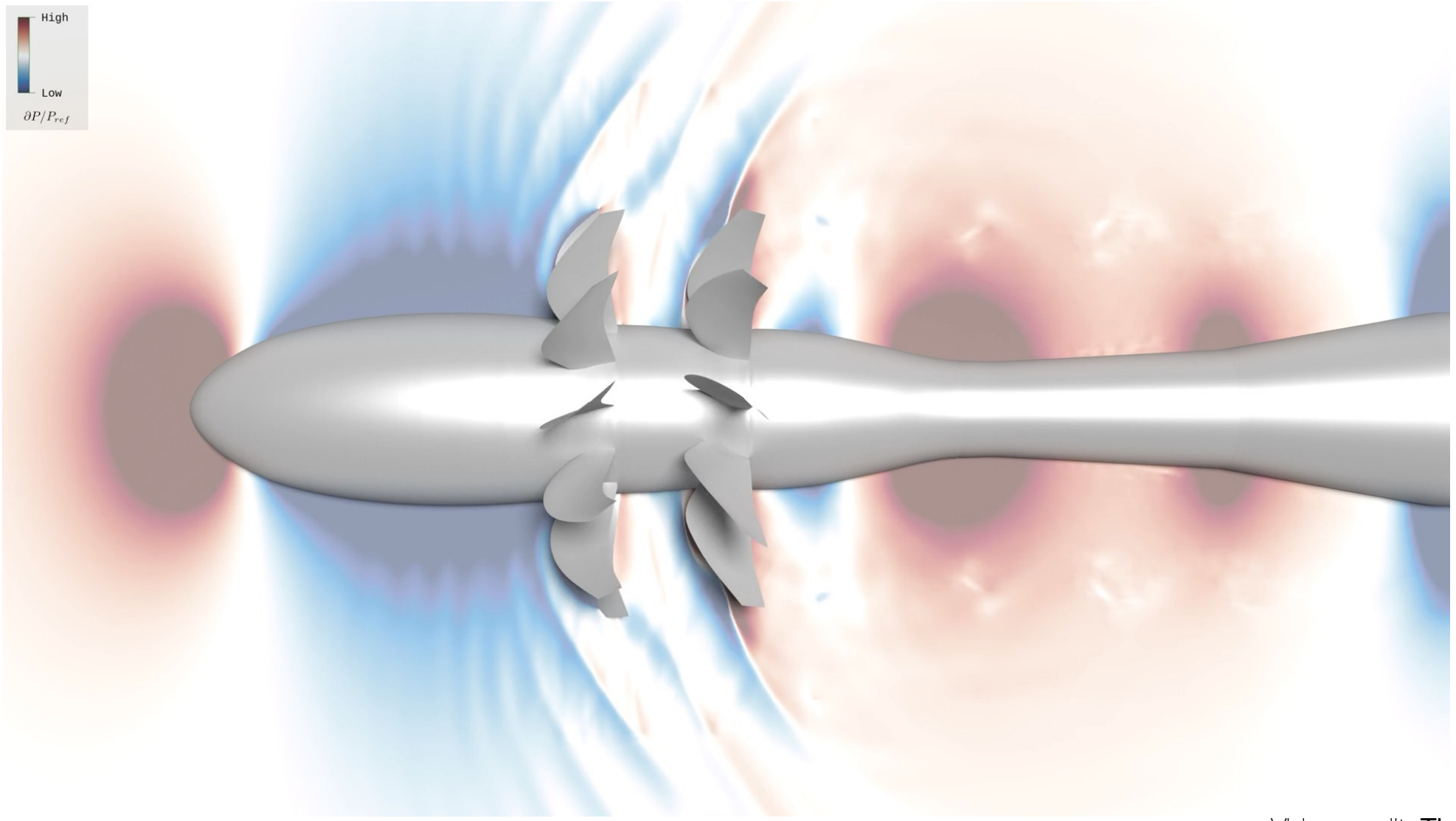
Sketch* showing the vertical position of the acoustic plate relative to the F31/A31 rotational axis



Kulite 9

(*)Envia, E. "*Contra-Rotating Open Rotor Tone Noise Prediction*", AIAA -2014-2606

Cruise Condition



Video credit: **Timothy Sandstrom**

Summary

The Launch, Ascent, and Vehicle Aerodynamics (LAVA) Curvilinear solver has been successfully applied to the prediction of the aerodynamic and acoustic behavior of the flow field generated by two different propulsion systems, using structured overlapping grids with a sliding mesh approach and a coupled CFD/CAA

- HRLES simulations generally exhibit a strong correlation with measured flow field variables for both propulsor systems. Furthermore, scale resolving simulations demonstrate excellent agreement with measured tonal noise for nominal take-off and cruise conditions, specifically for the contra-rotating open rotor system
- URANS simulations typically demonstrate a tendency to either underestimate or overestimate both tonal and broadband noise, as well as their associated acoustic waves, in both applications
- The sliding mesh approach provides a significant increase in computational efficiency, by eliminating additional numerical overheads related to dynamic hole-cutting and connectivity requirements
- Moreover, additional sensitivity studies specifically focusing on aeroacoustics predictions are being conducted

Acknowledgements

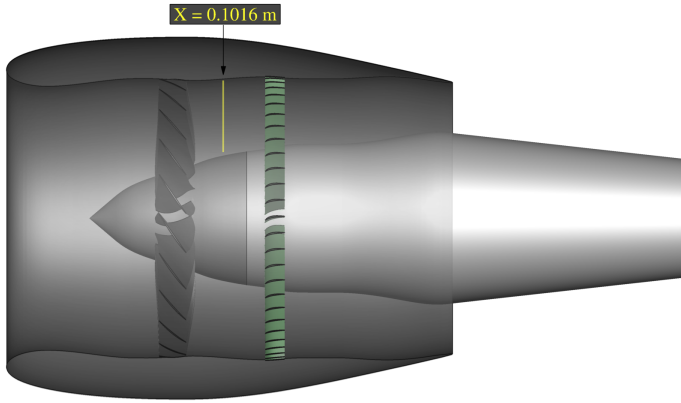
- These works were partially funded by the Advanced Air Transport Technology (AATT) project and the Transformational Tools & Technologies (TTT) project under NASA Aeronautics Research Mission Directorate (ARMD)
- Computer time has been provided by the NASA Advanced Supercomputing (NAS) facility at NASA Ames Research Center
- The authors would like to thank and acknowledge the following teams/individuals
  - Dr. Clifford A. Brown and Dr. Mujeeb R. Malik for their invaluable technical guidance and unwavering support for the duration of this project
  - The LAVA team members for their continued contributions and insightful discussions
  - Former LAVA team members Dr. Gaetan Kenway and Dr. Cetin Kiris for their contributions to this work
  - Dr. Edmane Envia and Dr. David Stephens from NASA Glenn Research Center (GRC) for providing the experimental datasets and valuable insight into the interpretation of the data
  - Timothy Sandstrom for the particle traced rendered visualizations

Backup Slides

Low-Speed Condition Results

Qualitative interstage flow field comparisons

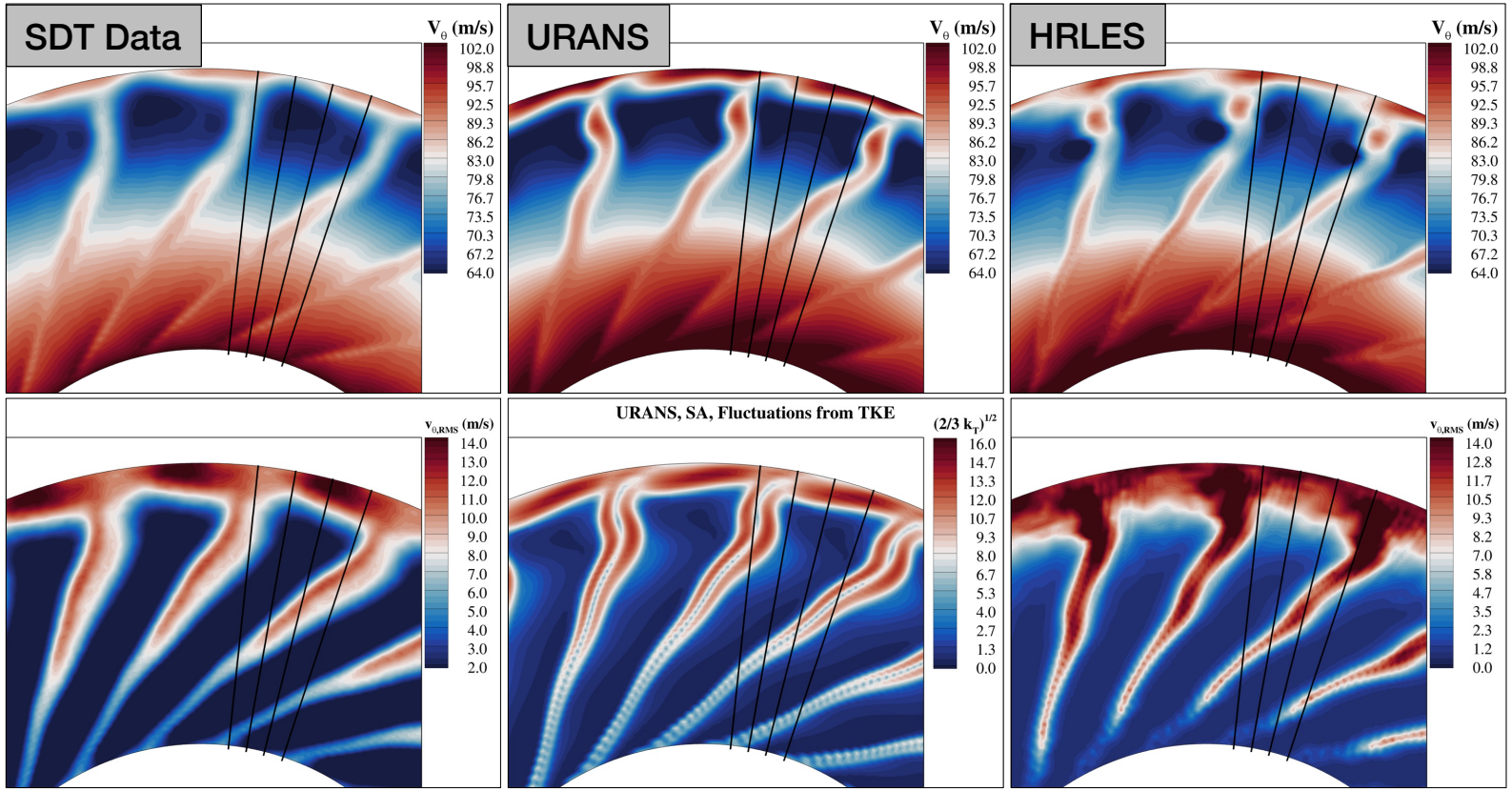
- Wake shape and size compare well with experiment
- **URANS** shows S-shaped wake downstream of blade tip
- **HRLES** underpredicts velocity deficit inside wake



Hot-wire probe station 1 location in interstage region

Mean Tangential Velocity

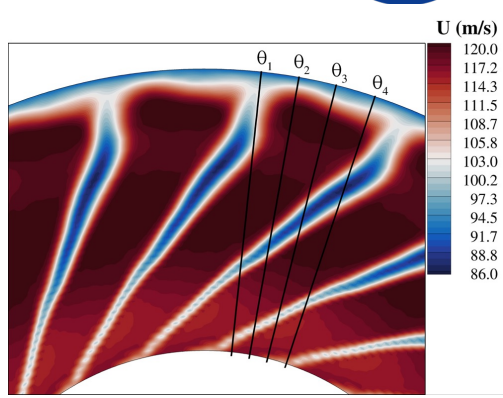
RMS of Tangential Velocity Fluctuations

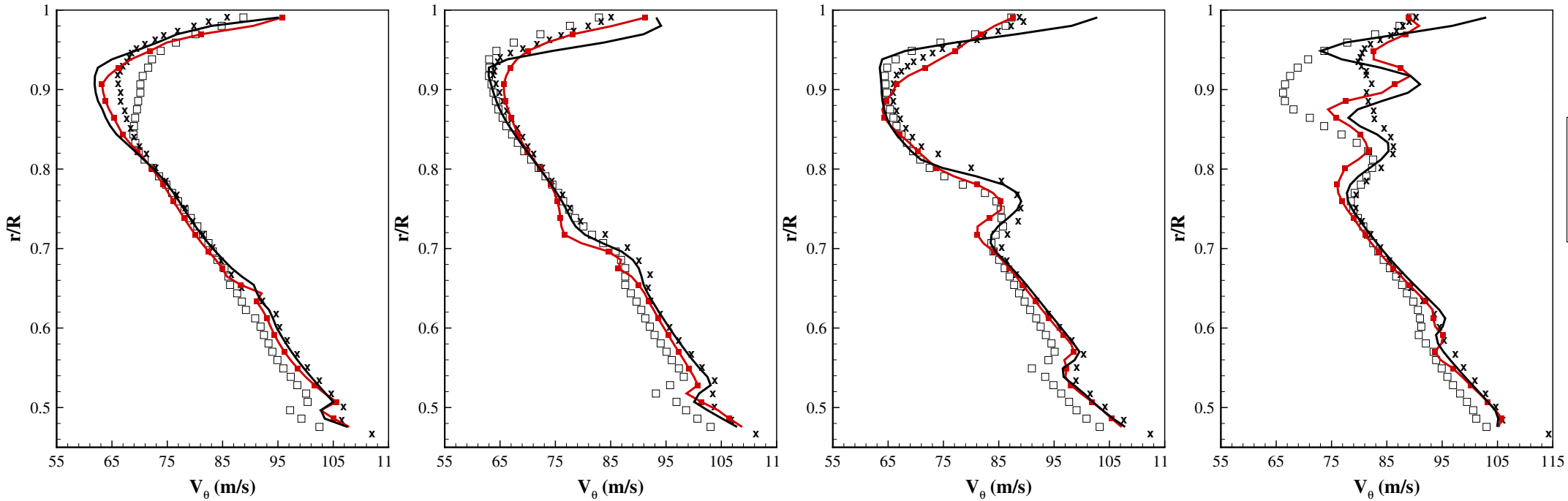


Low-Speed Condition Results

Radial line extractions of velocity profiles

- Both URANS and HRLES show tangential velocities between the hot-wire probe and LDV data measured in experiment away from blade tip
- Region of highest variability is the blade tip region, where **HRLES outperforms URANS**
- HRLES, however, slightly **underpredicts blade wake velocity deficits**

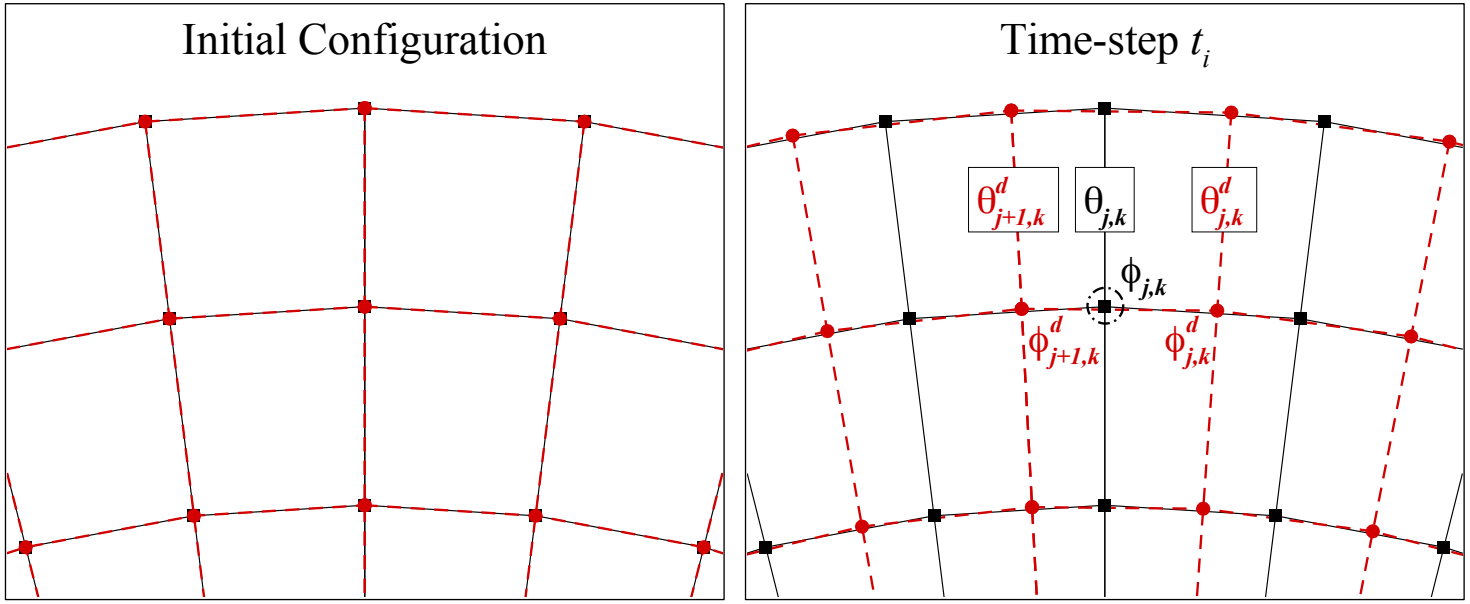




Sliding Mesh Implementation

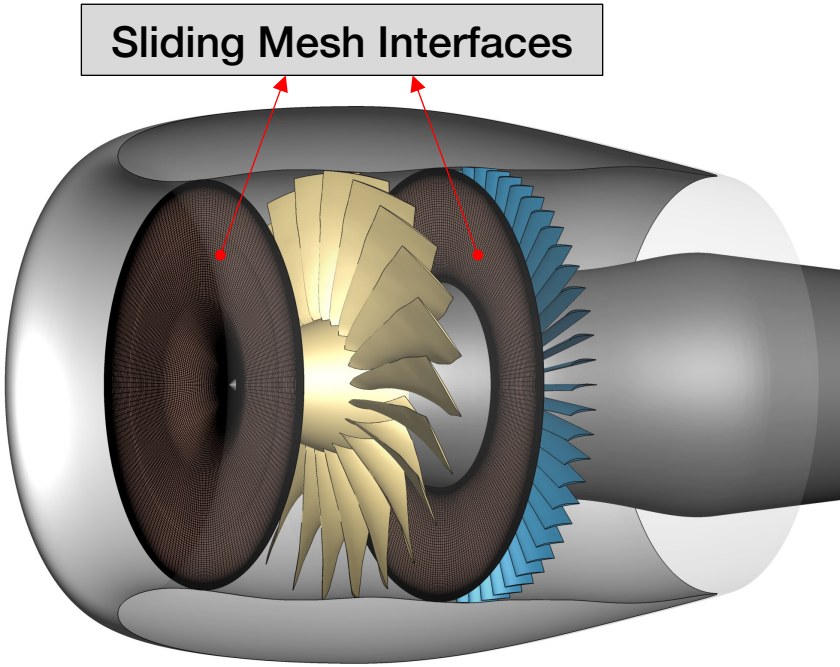
- No donor cell spatial search required at each time-step
- Simple linear interpolation from donor grid

$$\phi_{j,k} = \phi^d_{j,k} + (\theta_{j,k} - \theta^d_{j,k}) \left(\frac{\phi^d_{j+1,k} - \phi^d_{j,k}}{\theta^d_{j+1,k} - \theta^d_{j,k}} \right)$$



Initial grid configuration with grid points aligned

Grid misalignment at a general time-step t_i after rotation of the **red** grid (labelled as the donor grid)

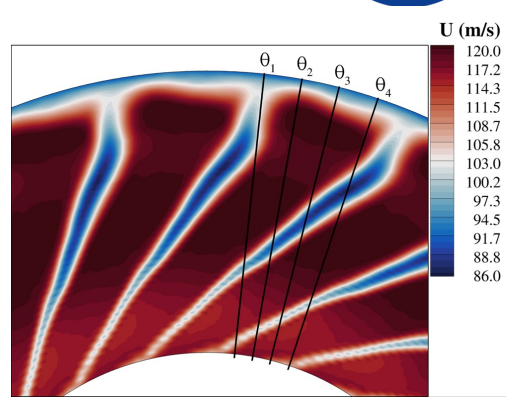


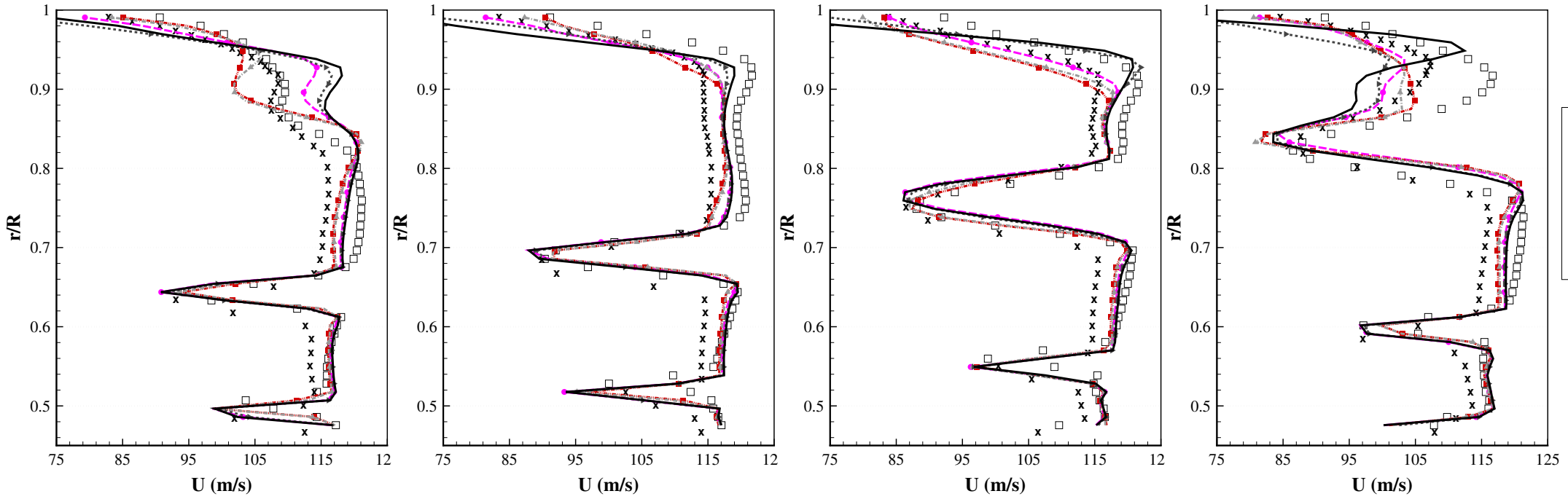
Sliding mesh interfaces used in the computational simulations

Turbulence Model Sensitivity

Radial line extractions of velocity profiles

- Different turbulence model variants show similar flow field features away from blade tip
- Blade tip region shows larger variability across different turbulence model variants tested, with Baseline SA showing the best agreement with experimental data profiles
- Other SA model variants appear to over-predict the boundary layer thickness in the blade tip region

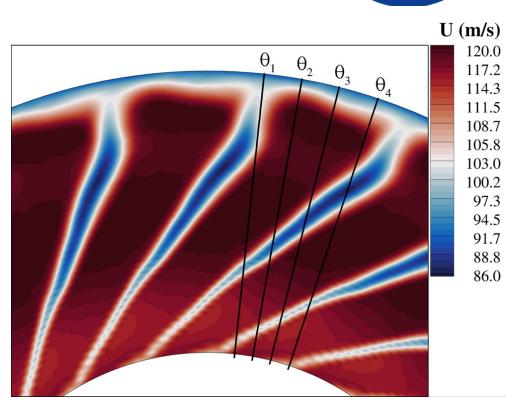


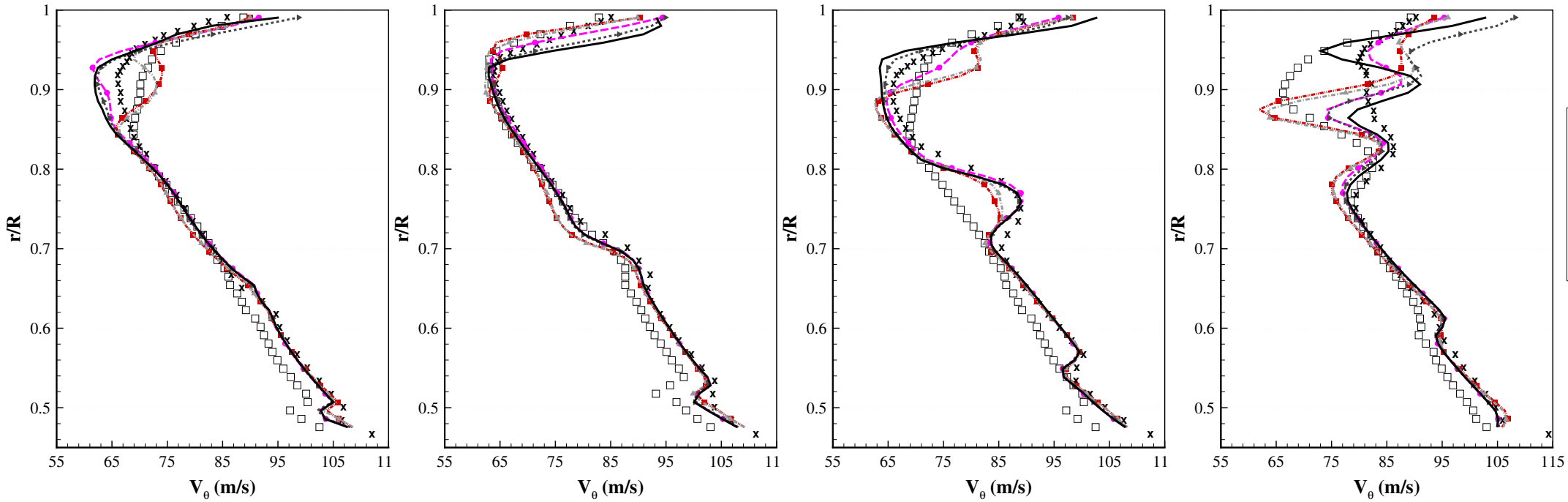


Turbulence Model Sensitivity

Radial line extractions of velocity profiles

- Different turbulence model variants show similar flow field features away from blade tip
- Blade tip region shows larger variability across different turbulence model variants tested, with Baseline SA showing the best agreement with experimental data profiles
- Other SA model variants appear to over-predict the boundary layer thickness in the blade tip region

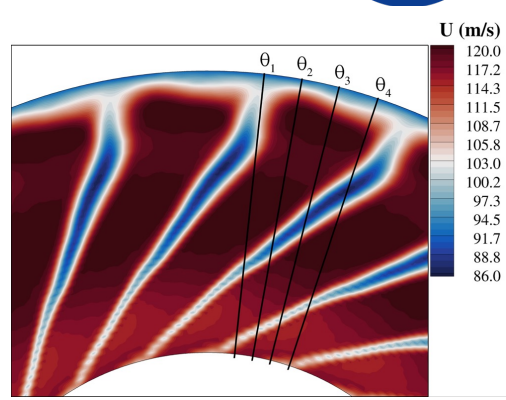


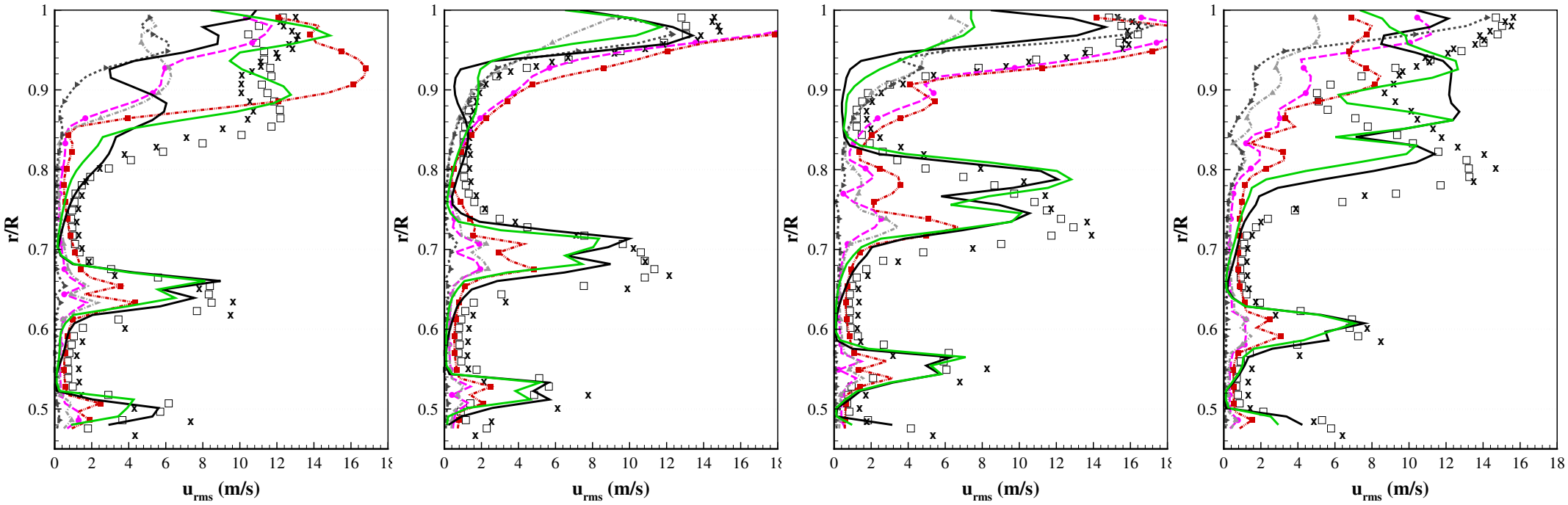


Turbulence Model Sensitivity

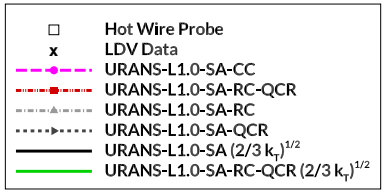
Radial line extractions of velocity profiles

- Different turbulence model variants show similar flow field features away from blade tip
- Blade tip region shows larger variability across different turbulence model variants tested, with Baseline SA showing the best agreement with experimental data profiles
- Other SA model variants appear to over-predict the boundary layer thickness in the blade tip region





RMS of Axial Velocity Fluctuations at hot-wire station 1



Turbulence Model Sensitivity

Radial line extractions of velocity profiles

- Different turbulence model variants show similar flow field features away from blade tip
- Blade tip region shows larger variability across different turbulence model variants tested, with Baseline SA showing the best agreement with experimental data profiles
- Other SA model variants appear to over-predict the boundary layer thickness in the blade tip region

